

École Doctorale Sciences pour l'Ingénieur et Microtechniques
Université de Technologie de Belfort-Montbéliard

THÈSE en co-tutelle internationale UTBM-NPU

Présentée pour obtenir le grade de :

**DOCTEUR DE L'UNIVERSITÉ DE TECHNOLOGIE DE BELFORT-
MONTBÉLIARD ET L'UNIVERSITÉ DE FRANCHE-COMTÉ**

Spécialité: **Sciences pour l'ingénieur**

**ANALYSIS AND OPTIMAL DESIGN OF LIGHTWEIGHT
SANDWICH STRUCTURES AND MATERIALS**

Par :

Kepeng QIU

Soutenue le 11 décembre 2008 devant le jury:

Rapporteurs : **Pierre DUYSINX**, Professeur, Université de Liège, Belgique
Ying Qiao GUO, Professeur des universités, Université de Reims,
France

Examineurs : **Dominique CHAMORET**, Maître de conférences, Université de
Technologie de Belfort Montbéliard, France
Matthieu DOMASZEWSKI, Professeur des universités, Université de
Technologie de Belfort Montbéliard, **co-directeur de thèse**, France
Xiao-Lu GONG, Professeur des universités, Université de Technologie
de Troyes, France
Weihong ZHANG, Professeur, Northwestern Polytechnical University,
co-directeur de thèse, Chine

Abstract

The present thesis deals with the performance analysis and the configuration design of lightweight cellular solids and sandwich structures. Special emphasis is devoted to the topological optimization of periodic cellular solids based on the superelement method and to the bending and dynamic analysis and the core design of sandwich panels considering the size effect of sandwich cores.

The multi-step homogenization is applied to calculate the effective elastic constants of multi-layered honeycomb sandwich on the basis of the 3D homogenization method. The effective results are credible by comparison with other methods including classical formula, energy method and engineering empirical method. Then, the inverse homogenization is applied to design the configuration of the microstructure. It concerns the maximization of uni-axial or multi-axial elastic moduli and thermal conductivities.

An integrated topology optimization procedure is developed for the global stiffness maximization of different cellular solids such as square, cyclic-symmetry, and cylinder structures. Each RVE (representative volume element) of periodic cellular solids is modeled by the SE (superelement). The technique of linking the design variables is adopted to ensure the periodicity of the optimal configuration over the whole structure after optimization. The various optimal configurations of RVE-SEs permit to illustrate the influence of size variation of RVE-SE on the optimal results. The computational efficiency is studied during the optimization process when the superelement method is adopted.

Special studies on the size effect are carried out in the bending and dynamic analysis and the core design of sandwich panels. A homogenization method is adopted to predict the effective properties of the material unit cell in its limit case. So it's unable to represent the scale effect of the unit cell. The bending and dynamic responses of sandwich panel with different size cores tend to ones with homogenized cores with decreasing the size and increasing the number of unit cells in sandwich cores. The size variation of unit cells also greatly influences the optimal configuration of sandwich cores. Special attention is devoted to the influence of size effect on the optimal results. The objective values are not monotonous when increasing the number of unit cells. From the static analysis and optimization results, the size effect is relevant with the boundary conditions. From the dynamic analysis and optimization results, the size effect has both sides.

Keywords: topology optimization, homogenization method, superelement method, sandwich structure, cellular solids, size effect

Résumé

Le travail présenté dans ce mémoire concerne les performances de l'analyse et de l'optimisation de structures composites légères du type « solides cellulaires et sandwichs ». Une étude spécifique est consacrée à l'optimisation topologique de solides cellulaires à périodicité. La méthode de super élément est développée et appliquée à l'analyse statique et dynamique de plaques composites en flexion considérant l'influence de la topologie et des dimensions de cellules périodiques constituant la structure.

La méthode multi-phase d'homogénéisation 3D est appliquée pour calculer les propriétés élastiques équivalentes de structures multi-couche nid d'abeille. Nos résultats sont conformes à ceux obtenus par des méthodes classiques basées sur l'approche énergétique ou sur les méthodes empiriques d'ingénieur. Ensuite, une méthode inverse d'homogénéisation est appliquée pour obtenir une configuration de la micro-structure. Elle concerne la maximisation de propriétés élastiques uni-axial ou multi-axial ainsi que de conductivités thermiques.

L'optimisation topologique est mise en œuvre pour maximiser la rigidité globale de différentes structures cellulaires comprenant les cellules carrées, à symétrie cyclique ou cylindrique. Tous les éléments volumiques représentatifs (RVE – representative volume element) d'une structure cellulaire périodique sont modélisés en utilisant la méthode de super-élément (SE). La technique de liaison de variables d'optimisation est utilisée afin de supposer la périodicité dans les structures optimales. Les différentes configurations optimales RVE-SE étudiées permettent d'illustrer l'influence du paramètre d'échelle entre RVE et SE sur le processus d'optimisation.

Pour finir, un travail particulier est consacré à l'influence de l'effet d'échelle dans le super-élément et dans la micro-structure dans le cadre de l'optimisation topologique des structures composites en statique et en dynamique. Des relations entre les dimensions d'une cellule et le nombre de cellules dans une plaque avec différentes conditions aux limites et leurs influences sur les solutions optimales en statique et en dynamique sont étudiées.

Keywords : structures composites, optimisation topologique, méthode d'homogénéisation, méthode de super-élément, effet de l'échelle de cellule

CONTENTS

ABSTRACT	III
RESUME	IV
1. INTRODUCTION	1
1.1 Structures and materials	2
1.1.1 Cellular solids	3
1.1.2 Sandwich structures	5
1.2 Design of structures and materials	7
1.2.1 Overview of topology optimization	8
1.2.2 Structural designs by topology optimization.....	10
1.2.3 Material designs by topology optimization.....	10
1.2.4 Integrated design of structures and materials.....	12
1.3 Objective.....	13
1.4 Outline of the thesis	14
2. CALCULATION OF EFFECTIVE ELASTIC CONSTANTS FOR HONEYCOMB SANDWICH STRUCTURES	17
2.1 Introduction.....	18
2.2 Homogenization method (HM).....	19
2.3 Effective calculation of 3D honeycomb core.....	22
2.3.1 Numerical solution of homogenized elastic constants of 3D honeycomb core based on HM	22
2.3.2 Other methods for the calculation of effective elastic constants of hexagonal honeycomb core	25
2.3.2.1 Gibson's formula.....	25
2.3.2.2 Modifications of Gibson's formula	26
2.3.2.3 Energy method	27
2.3.3 Comparison of the results of different methods.....	29
2.4 Effective calculation of 3D honeycomb sandwich.....	30
2.4.1 Multi-step homogenization of 3D honeycomb sandwich	30
2.4.2 Engineering empirical method	32
2.4.3 Comparisons of the results for honeycomb sandwich.....	33
2.5 Summary.....	35
3. TOPOLOGICAL DESIGN OF 3D MICROSTRUCTURE	37
3.1 Introduction.....	38
3.2 Formulation of topology optimization problem.....	39

3.3 Topological design of 3D material microstructure	45
3.3.1 Optimization algorithm.....	45
3.3.2 Optimal model	46
3.3.3 Sensitivity analysis	48
3.3.4 Microstructure design for maximum stiffness	50
3.3.4.1 Single objective design for the maximization of microstructure stiffness	50
3.3.4.2 Multi-objective design for the maximization of microstructure stiffness	51
3.3.5 Microstructure design for maximum thermal conductivity	53
3.3.5.1 Single objective design for the maximization of microstructure conductivity	53
3.3.5.2 Multi-objective design for the maximization of microstructure conductivity	53
3.4 Summary.....	54
4. TOPOLOGY OPTIMIZATION OF PERIODIC CELLULAR SOLIDS	57
4.1 Introduction	58
4.2 Representative volume element (RVE) and superelement (SE)	60
4.3 Optimal model and sensitivity analysis	62
4.4 Topology optimization of periodic cellular solids	65
4.4.1 Square structure	66
4.4.2 Cyclic-symmetry structure.....	69
4.4.2.1 Configuration design	69
4.4.2.2 Comparison of polar moments of inertia and torsional resistance.....	73
4.4.3 Cyclic-symmetry with non-designable domain	79
4.4.4 Cylinder structure	82
4.5 Summary.....	86
5. BENDING ANALYSIS OF SANDWICH PANELS AND TOPOLOGICAL DESIGN OF CORES	87
5.1 Introduction	88
5.2 Laminate plate theory	90
5.3 Analysis of bending responses of sandwich panels	92
5.3.1 Sandwich panels with the honeycomb cores	92
5.3.1.1 Hexagonal core	92
5.3.1.2 Square core	96
5.3.1.3 Discussion.....	99
5.3.2 Sandwich panels with the corrugated cores	99
5.3.2.1 Circle-core	100
5.3.2.2 X-core	102
5.4 Topology design of sandwich cores.....	105
5.4.1 Optimization model	105
5.4.2 Sensitivity analysis	106
5.4.3 Numerical examples	107

5.4.3.1 Optimal configurations	107
5.4.3.2 Discussion	113
5.5 Summary	114
6. DYNAMIC ANALYSIS OF SANDWICH PANELS AND OPTIMAL DESIGN OF CORES	115
6.1 Introduction.....	116
6.2 Dynamic analysis of sandwich panel	117
6.2.1 Dynamic analysis of laminate plate including transverse shear deformation	117
6.2.2 With hexagonal honeycomb cores	119
6.2.3 With square honeycomb cores	123
6.2.4 Discussion.....	128
6.3 Topology design of sandwich cores.....	129
6.3.1 Optimization model	129
6.3.2 Sensitivity analysis.....	129
6.3.3 Numerical examples.....	131
6.4 Summary.....	136
7. CONCLUSIONS AND FUTURE WORKS	137
7.1 Conclusions.....	138
7.2 Future works	140
REFERENCES.....	143
ACKNOWLEDGEMENTS	158

1. Introduction

How do you make a structure stronger?

The answer, it seems, is to fill it with thousands of holes.

It might be seem counterintuitive, but holes can add resilience to a material by absorbing stresses or the energy of an impact.

----- *Will Knight*

Microscopic holes are the secret of wood's resilience

New Scientist , 08 October 2005, issue 2520

1.1 Structures and materials

In this part, we describe the general relationship between structures and materials and introduce the research objects of this thesis and their research situation.

When the structures are mentioned in the engineering field, people naturally first bethink of building, civil engineering, mechanical structures, and so on. The human being has achieved creative and extraordinary successes in the structural engineering with the great developments of materials science and structural analysis. Eiffel tower and Chinese national stadium as seen in Fig.1.1 are the best evidences. All these structures are constituted of different types of elements such as columns, beams, plates, arches, shells and catenaries. At this level, we call them the macrostructures. Moreover, these structural elements also have various structural forms and they are made of materials with special properties.

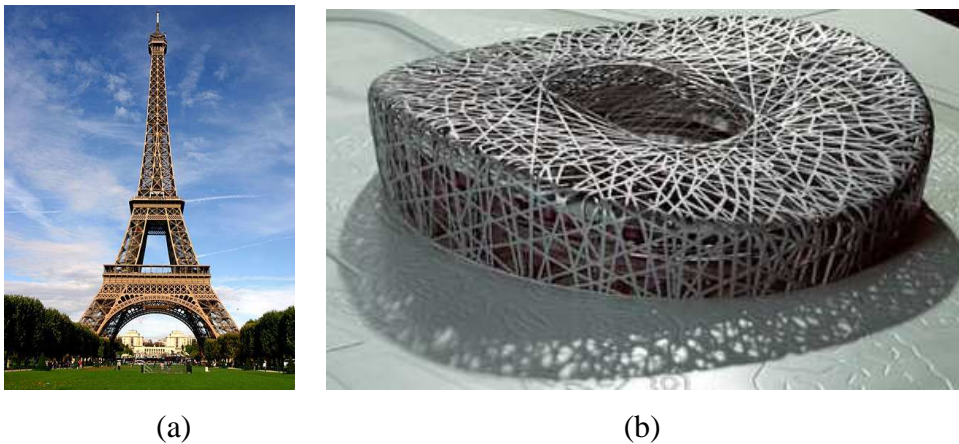


Fig.1.1 (a) Eiffel tower (b) Chinese national stadium

Actually, the material properties can be determined by their constituent elements and their forming way. It means that the desired properties of a material can be obtained by designing the form of its constituent elements. A material can be seen as a kind of structure and at this level; the material structure is named as microstructure.

Ashby (Ashby [2000]) ever said, “*When modern man builds large load-bearing structures, he uses dense solids; steel, concrete, glass. When nature does the same, she generally uses cellular materials; wood, bone, coral. There must be good reasons for it.*” Many natural and human-made materials exhibit structures on more than one length scale; in some

materials, the structural elements themselves have specific structures (Lakes [1993]). This structural hierarchy can influence the material properties. In fact, the difference between a structure and a material is not clearly defined. Many draw the lines between what you understand as a homogeneous material when you see it with your bare eyes, and the inhomogeneous material structure that you clearly see is made up of a fixed geometry or mixing of materials. For instance, a composite is by this definition a material even though it consists of two or more components, but a honeycomb core built up of two different components is a structure (Lukkassen and Meidell [2003]). Good understanding of the effects of innovative structure may guide the synthesis of new materials with physical properties, tailored for specific application. The cellular solids and sandwich structures embody perfectly this relationship between structure and material.

1.1.1 Cellular solids

A cellular solid is one made up of an interconnected network of solid struts or plates which form the edges and faces of cells. There exist three typical structures: the two-dimensional honeycomb, the three-dimensional open cell foam and the three-dimensional closed cell foam as shown in Fig.1.2 (Gibson [2005]; Gibson and Ashby [1997]). Man-made cellular solids have been widely utilized in the form of structural honeycombs in aircraft and as well in the form of foams for packing, cushioning, energy absorption applications, sandwich panel cores, structural purposes and thermal protection systems. Natural materials such as wood, cancellous bone, coral and leaves have a cellular structure. All these conventional cellular materials exhibit the usual properties.

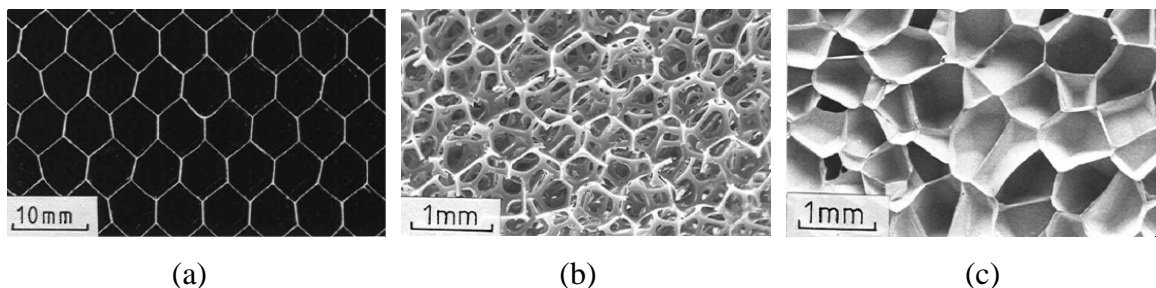


Fig.1.2 (a) Honeycomb (b) Open cell foam (c) Closed cell foam

Some theoretical attempts to understand the geometry and the fundamental principles of the mechanics of cellular solids have begun with the celebrated geometrician Leonard

Euler (De Boor [1998]). Since then, many scientists and researchers committed themselves to studying the geometric, mechanical, thermal and electrical characteristics of these solids. The most widely known of them is the attempt proposed by Gibson and Ashby (Gibson and Ashby [1997]) in which an extensive record on the structure and the properties of cellular solids is given. They are the pioneers this field. Grenestedt (Grenestedt [1998]; Grenestedt [1999a]; Grenestedt [1999b]) has investigated the influence of wavy distortions of cell walls and cell shape variations on elastic stiffness of cellular solids and calculated the effective elastic behavior of several cellular solids with the analytical and numerical methods. Li (Li [2005]) has studied the microstructure-property relations of two-dimensional cellular solids having irregular cell shapes and non-uniform cell wall thickness, and has found that the elastic moduli increase as cell shapes became more irregular, but decrease as cell wall thickness gets less uniform. Huang (Huang [2005]) has theoretically derived the elastic moduli and strengths of hexagonal honeycombs with non-straight cell edges from a curved cell edge model, and has concluded that the normalized elastic moduli and strengths of regular hexagonal honeycombs decreased with increasing cell curvature and waviness. Tekoğlu (Tekoğlu [2007]) has explored the physical mechanisms that were responsible for the size-dependent elastic behavior of cellular solids with a discrete microstructural model, and has assessed the capability of generalized continuum theories to capture size effects. Onck (Onck [2001]) and Andrews (Andrews [2001]) have studied theoretically and experimentally size effects for the modulus and strength of regular, hexagonal honeycombs under uni-axial and shear loadings.

The beforehand mentioned authors have accounted for the conventional properties of cellular solids. Lakes (Lakes [1987]) has presented a novel foam structure which exhibited a negative Poisson's ratio. Such a material expands laterally when stretched, conversely with ordinary materials. Foams with negative Poisson's ratios are made from conventional low-density open-cell polymer foams through causing the ribs of each cell to permanently protrude inward. An idealized reentrant unit is shown in Fig.1.3 (a). In the following twenty years, Lakes and his colleagues have carried out a series of studies on structures and materials with the negative Poisson's ratio (Chen and Lakes [1989]; Chen and Lakes [1996]; Choi and Lakes [1992]; Lakes [1991]; Lakes [2001]; Lakes and Witt [2002]) and positive or negative thermal expansion of unbounded magnitude (Lakes [1996]; Lakes

[2007]). As shown in Fig.1.3 (b) and (c), new materials with non-conventional and extreme properties are obtained by virtue of the designing of innovative structures. Therefore we call them structural materials.

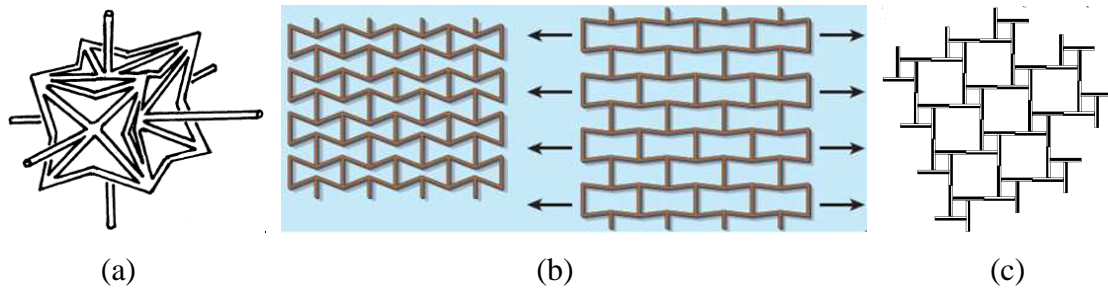


Fig.1.3 (a) Idealized reentrant unit produced by symmetrical collapse of a 24-sided polyhedron with cubic symmetry. (b) Artificial honeycomb with inverted cells, in which the structural elements unfolding causes the lateral expansion and a negative Poisson's ratio. (c) Cellular solid which undergoes thermal expansion via lateral bending displacement of ribs with an unusual connectivity.

1.1.2 Sandwich structures

Sandwich structures represent a special form of a laminated composite material or structural elements, which have a relatively thick, lightweight and compliant core material to separate thin, stiff and strong face sheets (Fig.1.4). The faces are usually made of aluminum alloys, stainless steels, titanium alloys and composite materials. And the typical cores can be a honeycomb or corrugated type material, a cellular foam, a truss type structure and so on. The faces and the core are joined by adhesive bonding, which ensures the load transfer between the sandwich constituent parts. Although these structures have a low weight, they have high flexural stiffness and buckling strength. Hence, sandwich structures are being used extensively in astronautic, aeronautic, marine, automotive, architectural and many other applications.

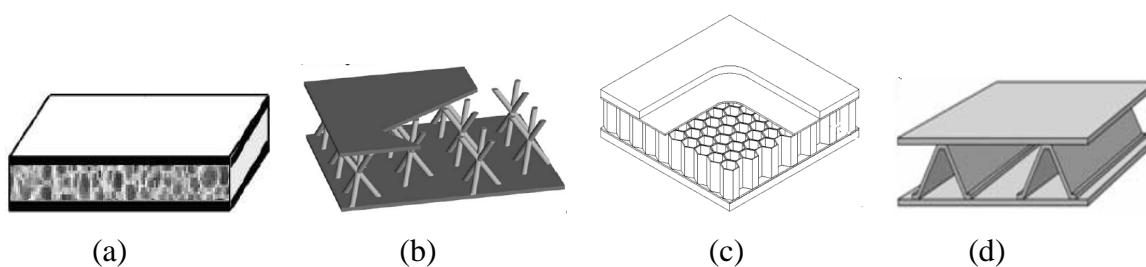


Fig.1.4 Sandwich structures with the different cores

(a) Foam cores (b) Truss cores (c) Honeycomb cores (d) Corrugated cores

The rising demand for new materials with higher specific stiffness and strength has stimulated a great development in the technology and theory of sandwich structures (Borsellino [2004]; Castanie [2002]; Mamalis [2007]; Rabczuk [2004]; etc.). Sandwich structures usually have three structural forms: sandwich beams, sandwich plates and sandwich shells with the various cores. Aiming at the following failure modes: wrinkle or bulking, yielding or fracture, fatigue, impact damage, the failure of the bond between the face and cores and so on, a great deal of studies are carried out on the basis of classical laminate theories about beam, plate and shell.

A sample of selected papers published in recent years are following which review the state of the art and provide numerous cross-references on this subject. Daniel and Abot (Daniel and Abot [2000]) experimentally determined the flexural behavior of composite sandwich beam and compared the results with predictions of theoretical models. In the reference (Banerjee [2007]), Banerjee has developed an accurate dynamic stiffness model for a three-layered sandwich beam of unequal thicknesses to investigate its free vibration characteristics. Birman (Birman [2004]) has analyzed the dynamic wrinkling of the facing for sandwich beams. Wang (Wang [2000]) has investigated the damping behavior of laminated honeycomb cantilever beams with fine solder balls enclosed in the cells as dampers. For sandwich panel, Besant (Besant [2001]) predicted the behavior under low velocity impact of sandwich panels by a finite element procedure and proposed a suitable yield criteria based on experimental observations; Grenestedt and Reany (Grenestedt and Reany [2007]) have investigated numerically, analytically and experimentally compression wrinkling of composite sandwich panels with corrugated skins. Valdevit (Valdevit [2006]) has studied experimentally and computationally the bending response of steel sandwich panels with corrugated cores in transverse and longitudinal loading orientations. In

references (Zenkour [2005a; 2005b]), Zenkour used the sinusoidal shear deformation plate theory to study the buckling and free vibration of the simply supported functionally graded sandwich plate. Much more studies on sandwich panel will be reviewed in chapter 5 and chapter 6. For sandwich shell, Hutchinson (Hutchinson [2000]) addressed buckling of cylindrical sandwich shells subject to axial compression for shells having foamed metal cores and obtained optimal face sheet thickness, core thickness and core density which minimized the weight of a shell with a specified load carrying capacity and imposed constraints by wrinkling and yielding of the face sheets and yielding of the core. Tanov (Tanov [2000]) came up with a third order shear deformable shell element for finite element analysis and behavior prediction of sandwich shells. Kalamkarov (Kalamkarov [2007]) applied himself to the analytical development of the method of two-scale asymptotic homogenization to determine the effective elastic stiffness of hexagonal honeycomb-cored structural sandwich composite shells. In addition, the optimal design of sandwich structures is also performed. Normally, the sandwich structures with the variables of cell sizes, the thickness of face and core, layer group fiber angles, core relative density and so on, are designed for the weight minimization subjected to the constraints of the deflection, the fundamental frequency, the buckling, the yielding and the wrinkling, or for the behavior maximization of heat transfer, resistance to bending and torsion or their combination, and the sound transmission loss. Concerning strictly speaking structural design for sandwich structures, we can evoke (Kam [1999]; Liu [2006; 2007]; Mai [2007]; Sciuva [2003]; Tan [2007]; Thamburaj [2002]; Tian [2005]; Wang [2003]; Zok [2003]). Designs of structures and materials and their relationship are narrated as follows.

1.2 Design of structures and materials

With higher performance requirements for innovative products being proposed, huge challenges appear in the designs of structures and materials. Conventional trial-and-error or empirical methods and single structural designs cannot satisfy these requirements. In recent years, integrated designs of structures and materials have been paid great attention to with the development of topology optimization technique due to their capability of attaining the desirable functions. Many achievements reviewed in section 1.2.4 have been obtained in this research field.

1.2.1 Overview of topology optimization

Structural design has experienced three phases: sizing, shape and topology optimizations (Bendsøe [2003]) that implements the designing procedure of a product from the preliminary configuration to the final refinement. However its innovative design is mainly completed in the phase of the topology optimization. Indeed, the choice of the appropriate topology of a structure in the conceptual phase is generally the most decisive factor for the efficiency of a novel product (Eschenauer [2001]).

The size and shape optimization does not allow changes of the structural topology during the solution process. So, topology optimization is most valuable as preprocessing tools for sizing and shape optimizations as seen in Fig.1.4 (Kim [2002]).

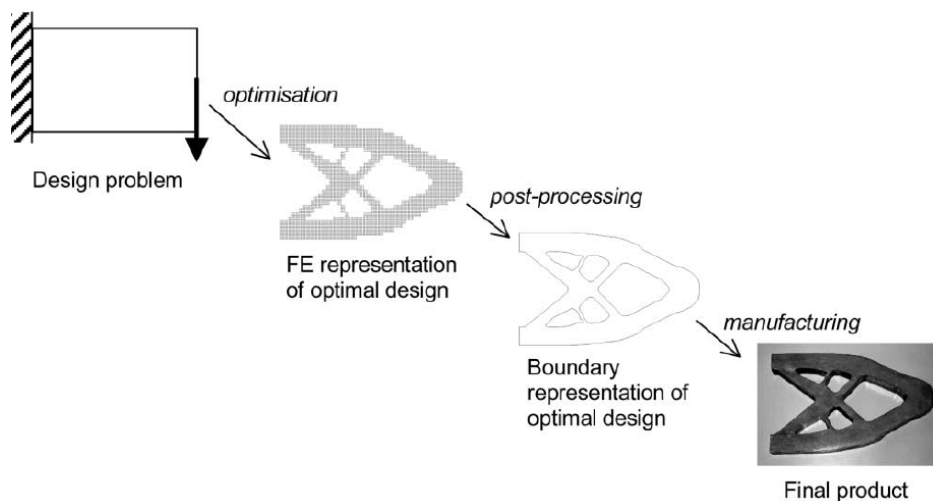


Fig.1.4 Design optimization of a short cantilever beam

Topology optimization is often referred to as the layout optimization or generalized shape optimization (Kita [1999]; Olhoff [1998]; Rozvany [1995]). Since Bendsøe and Kikuchi (Bendsøe [1988]) first implemented the topology optimization for continuum structures by using the homogenization method two decades ago, the research and development in this field have entered a new era. The classical methods to solve the topology optimization problem are as follows. At the beginning, the topology optimization problem was converted to a sizing problem with the introduction of a material density function. Assuming that the structural material consists of an infinite number of infinitely small periodic holes in the microscopic scale, the homogenization method was used to determine the macroscopic performance of the material (Hassani [1998b]). Next, artificial density

functions were employed to greatly reduce the computing complexity and boost the development of topology optimization. General artificial density functions include SIMP (Solid Isotropic Material with Penalization) (Rietz [2001]; Rozvany [1995]; Bendsøe [1999]) and RAMP (Rational Approximation of Material Properties) (Stolpe [2001]). They are also used as density penalization models to suppress the intermediate densities when topology optimization is transformed into a continuous optimization problem. In addition, many approaches have been studied to solve numerical instability in topology optimization: the perimeter method (Haber [1994; 1996]; Petersson [1999]; Jog [2002]; Zhang [2003]), the filtering technique (Sigmund [1994]), the local gradient constraint (Petersson [1998]), the minimum member size control (Zhou [2001]) and the MOLE (MONotonicity based minimum Length scale) method (Poulsen [2003]). Sigmund (Sigmund [1998]) and Fujii (Fujii [2000]) have executed a detailed survey on the procedures dealing with checkerboards, mesh-dependencies and local minima. In the iterative computation, two optimization algorithms (Kamat [1993]) were addressed: mathematical programming (MP) (Duyinx [1996]; Fleury [1989]; Pan [2000]; Bruyneel [2002]) and optimality criteria (OC) (Hassani [1998c]). Xie (Xie [1993]) proposed the evolutionary structural optimization (ESO) for topology design based on the gradient calculation and material removing, which has been extended as the bidirectional evolutionary structural optimization (BESO) (Querin [1998]; Young [1999]). Liu (Liu [2000]) developed a novel approach, called Metamorphic Development (MD), which can allow a structure to grow and degenerate towards an optimum topological layout. In this method, the optimization can start from the simplest possible geometry (layout) or any degree of development of the structure rather than from a complex ground mesh. Eschenauer (Eschenauer [1994]) proposed the bubbles method, in which the boundaries of the structure are considered to be variable and the shape optimizations of new bubbles and of the other variable boundaries of the component are carried out as a shape optimization problem. Recently, Level Set as an effective approach was applied in topology optimization (Wang [2003]; Allaire [2005]). In this method, the optimized structure is implicitly represented by a moving boundary embedded in a scalar function (the level set function) of a higher dimensionality. The optimum topology of a structure can be obtained by the alteration of the implicit moving boundary. The genetic algorithm (GA), an optimization technique based on the theory of natural selection (Jakiela [2000]; Nakanishi [2001]) and the wavelet method (Yoon [2005]) are

also applied to structural topology design problems. In a word, the theory and method of topology optimization have been tremendously developed and gradually perfected in past two decades. However, the study is still going on.

In practical applications, the topology optimization is mainly contributed to the structural designs in the macrostructure and the material designs in the microstructure (Kruijf [2007]).

1.2.2 Structural designs by topology optimization

Structural designs with topology optimization consist in finding the optimal structural layout by minimizing or maximizing structural responses under constraints of volume, stress, deflection and so on. Many kinds of examples can be evoked: compliance minimization of statically loaded structures (Sigmund [2001]) or due to the prestress (Pedersen [2002]), minimum weight with stress constraints (Duysinx and Bendsøe [1998]; Navarrina [2005]), maximization of the first eigenfrequency (Pedersen [2000]), maximization of the lowest buckling eigenvalue (Zhou [2004]), maximization of the overall geometric advantage or mechanical efficiency of the mechanism (Canfield [2000]), maximization of the magnetic energy with the volume constraint (Yoo [2004]), minimum resistance to heat dissipation (Kruijf [2007]). And it also has involved in multi-objective and multi-physics designs. Krog (Krog [1999]) used a max-min formulation based on a variable lower bound technique for the multi-objective topology optimization problem of statically loaded or freely vibrating disk and plate structures. Min (Min [2000]) proposed a unified topology design methodology to design a flexible structure which met both the static and vibration requirements with the multi-objective optimization approach. Sigmund (Sigmund [2001a; 2001b]) applied the topology optimization method to the design of multiphysics actuators and electrothermomechanical systems with one- and two-material structures. Yin (Yin [2002]) presented a new design parameterization scheme for the topology optimization problem involving three energy domains and multiple materials for the electro-thermal-compliant (ETC) design problem. Thus it can be seen that, structural designs with topology optimization focus on the structure behavior, not the material property.

1.2.3 Material designs by topology optimization

The material design with topology optimization consists in finding a reasonable material

distribution in the unit cell in order to obtain the prescribed properties. The development on material designs has begun ever since Sigmund (Sigmund [1994]) advocated an inverse homogenization method.

This structural material is made of periodic representative volume elements (RVE) which are designed as a kind of microstructure with the topology optimization technique to tailor the material properties. It is involved in multi-physics, multi-phase materials and multi-objective designs. Sigmund (Sigmund [1995]) modeled the microstructure as a truss or thin frame structure to tailor extreme materials, such as isotropic materials with Poisson's ratio close to -1, 0 and 0.5. Jung (Jung [2004]) designed the negative Poisson's ratio (-0.38) material with 15% volume constraint based on geometrically nonlinear analysis. Diaz and Benard (Diaz [2003]) extended the material design problem with prescribed elastic properties by using polygonal cells. Kikuchi (Kikuchi [1998]) and Nelli Silva (Nelli Silva [1999]) adopted the extended fixed grid method to solve a microstructure design problem of periodic composite materials with prescribed elastic properties and thermal expansion coefficients, shear-only and negative Poisson's ratio, as well as piezoelectric materials with maximizing hydrostatic coupling coefficient and figure of merit. Sigmund and Torquato (Sigmund [1997]) employed the three-phase topology optimization method to design materials with the maximum directional thermal expansion, the zero isotropic thermal expansion, and the negative isotropic thermal expansion. Gibiansky and Sigmund (Gibiansky [2000]) generated the optimal layouts of microstructure materials of two-dimensional three-phase composites with the maximization of bulk modulus in the Hashi-Shtrikman bounds. Kruijf (Kruijf [2007]) explored material designs with multiple conflicting objectives and tailored composite materials with the effective thermal conductivity and bulk modulus attaining their upper limits like Hashin-Shtrikman and Lurie-Cherkaev bounds. Guest and Prevost (Guest [2006; 2007]) maximized the bulk modulus and permeability in the multi-physics problem of periodic material designs according to the relative importance or weights assigned by the designer to the competing stiffness and flow terms in the objective function. From the above-mentioned works, it can be known that material designs with topology optimization demonstrate the broad capability of designing the new materials with the periodic microstructures.

1.2.4 Integrated design of structures and materials

There exists a natural and close relationship between structures and materials. Some researchers analyzed in detail performances and applications of structural materials and came up with the concept of simultaneous designs of structures and materials.

Evans (Evans [1999]) examined the thermomechanical properties of cellular metals that suggest their implementation in ultralight structures, and pointed out that there were substantial opportunities to greatly improve their thermal performance by tailoring cell size and density. Burgueno (Burgueno [2005]) concluded by experimental and analytical studies that hierarchical cellular designs can improve the performance of bio-composite beams and plates and that the further improvement in their mechanical efficiency can be achieved through optimized microstructures or hierarchical topological material arrangement. Soto (Soto [2000]) used the natural basis design model for designing simultaneously the global structural topology and the local material properties. Actually he solved two optimization problems: the global design of finding the optimum global material distribution for given local material properties and the local design of finding the optimum local material properties for the given global material distribution. Xia and Wang (Xia [2008]) proposed a level set based method for simultaneous optimization of material property (via material volume fraction) and topology of functionally graded structures for maximizing the structural performance. This optimization problem can be regarded as structural topology optimization with multi-phase materials.

Here we define integrated designs of structures and materials. The configuration and constituents of the microscopic periodic unit cell are designed in order to satisfy the requirements of the macro-structural performances and responses specified in section 1.2.2.

Structural designs and material designs with topology optimization have laid substantial foundation on the implementation of integrated designs of structures and materials. In the early foundational work of topology optimization (Bendsøe [1988]), structural topology designs are implemented by using the homogenization method to predict the material properties. They made a good preparation for integrated designs of structures and materials in theories and methods. Takano and Zako (Takano [2000]) proposed the integrated and computational design methodology of graded microstructures of heterogeneous materials for the emergence of macroscopic function. Rodrigues (Rodrigues [2002]) presented an

authentic model for simultaneous optimization of structures and materials. In this model, the general layout of structures was first obtained for the minimum compliance design, and then the finite elements with the intermediate density in the general layout are further designed as microstructures by the topology optimization technique. Sun (Sun [2006]) made a systematic investigation on the key theory and methods of topology optimization of materials and structures and implemented integrated designs of structures and materials for the global stiffness maximization of the overall structure and local design of material microstructures based on the homogenization method and scale-related computing. As a research hotspot and an efficient approach, integrated designs of structures and materials can fully and deeply dig the potential performances and properties of structures and materials. However, as a multidisciplinary task involved in structure, material and optimization, there exist some problems to be solved, e.g. size effects, computing efficiency, numerical stability in the optimization procedure and appropriate material interpolation models for multi-physics.

1.3 Objective

In the past, people have passively selected and used structures and materials that couldn't provide the desired performance for different industries, for instance, lightweight, high-performance, multi-function and so on. Nowadays, it appears necessary to actively seek new structures and materials. That explains the development of theories and methods for the analysis and design of structures and materials.

Many research works focus on sandwich structures and cellular solids which have the remarkable performances and characteristics, more precisely concerning computation of effective properties (Grenestedt [1999b]; Hohe [2001a]; Kim [2003]; Saha [2007a; 2007b]), analysis of structural responses (Cunningham [2003a, 2003b]) and optimal designs (Denli [2007]; Wen [2007]; Yu [2006]; Zok [2003]). With the development of numerical techniques such as the finite element method, homogenization method and topology optimization, the analysis and design of sandwich structures and cellular solids has entered a new phase.

In this context, predecessors' works above-mentioned and numerical tools, this thesis has three main goals:

- 1) To use the three-dimensional homogenization method to compute effective properties

of unit cells in multilayer structures and materials.

- 2) To attempt the superelement method to improve the computational efficiency in designs of periodic structures and materials.
- 3) To explore the size effect in static and dynamic response analysis and integrated designs of sandwich structures and materials.

1.4 Outline of the thesis

The aim of this thesis is to carry out the design of unit cell in periodic structures and materials on the basis of the computation of their effective properties by using three-dimensional homogenization method, and explore size effects in the analysis and designs of sandwich structures and materials and the method to improve the design efficiency.

In chapter 2, using the three-dimensional homogenization method and the finite element technique, we evaluate the effective elastic constants of the three-dimensional honeycomb sandwich panel. We consider the three-dimensional honeycomb core as a two-phase composite and model it with the finite element technique. We also use three variations of our three-dimensional homogenization method (one-step, two-step, and multi-step ones) to evaluate the overall effective elastic constants of the three-dimensional honeycomb sandwich with upper and lower skins. The computed results of the one-step, two-step, and multi-step homogenization methods are compared with those of the engineering empirical method.

Chapter 3 deals with the design of the stiffness and thermal conduction coefficient of three-dimensional microstructure unit cells with the given volume fraction by using the homogenization method and the finite element method.

In chapter 4, an integrated topology optimization procedure is implemented for the global stiffness maximization of square, cyclic-symmetry and cylindrical cellular solids. To retain the structural periodicity and reduce the computing time, superelement (SE) and design variable linking techniques are introduced to characterize the representative volume element (RVE) layout. Then, the formulated topology optimization problem is solved by the dual optimization algorithm. Besides, the quadratic perimeter constraint is employed to prevent checkerboards in the design process. To reveal the structural efficiency of the obtained topology designs, a comparative study of the equivalent torsional rigidity of

cyclic-symmetry structures is made between the obtained optimal configuration, the foam material and the specific configuration.

In chapter 5, bending responses of sandwich panels with periodic honeycomb and corrugated cores which have different sizes and the same structural forms are calculated numerically. Simultaneously, the theoretical solutions of sandwich panels with the effective core are also computed by using the Levy and Navier methods on the basis of the classical laminate plate theory. And then, considering the upper and lower skins as non-designable domains, the three-dimensional configurations of scale-related sandwich cores with the different sizes are designed for the global stiffness maximization of the sandwich panel. The topology optimization problem is solved by the dual optimization scheme. And the quadratic perimeter constraint is employed to eliminate checkerboards occurring in the design process.

In chapter 6, we firstly compute the natural frequencies for simply supported sandwich panels with homogenized cores by the dynamic analysis of laminate plate including transverse shear deformation and with periodic honeycomb cores with different sizes by the finite element analysis, respectively. And then, with the upper and lower skins as non-designable domains, three dimensional configurations of scale-related sandwich cores with different sizes are designed for the natural frequency maximization of the sandwich panel.

Finally, in chapter 7, we summarize the methods and rules in the computation of effective properties, analysis and designs of sandwich structures and materials. Then we draw the future work for the analysis and optimal design of lightweight sandwich structures and materials.

2. Calculation of effective elastic constants for honeycomb sandwich structures

In this chapter, the effective elastic properties of honeycomb sandwich structures are calculated using the homogenization method. Then they are compared with analytical methods.

The effective constants of 3D honeycomb core are computed by using Gibson's formula and its modification, energy method and homogenization method.

Finally, the 3D honeycomb sandwiches are studied and are considered as a multi-layered structure. Therefore, a multi-step homogenization procedure is applied to obtain their effective properties. The engineering empirical method is also used.

2.1 Introduction

It has been underlined in section 1.1.2, chapter 1 that sandwich structures have several different cores: the honeycomb core is one of them. They are extensively applied in many industries in the form of plates and shells because of their excellent strength-to-weight characteristics. For this reason, it appears very important to study their mechanical behavior including bending, vibration, buckling, impact, thermal insulation and so on.

However, the presence of thick cores means that the mechanical characteristics of sandwich shells are different from classical laminated shells or monolayer structures.

The classical laminated theory cannot be directly used to analyze the mechanical behavior of honeycomb sandwich structures. It needs to build up the micromechanical model or obtain the effective elastic constants of honeycomb sandwich structures. Then, their mechanical behavior can be analyzed numerically and theoretically. Currently, several approaches can be applied to compute effective elastic constants of the honeycomb sandwich structure: engineering empirical method (Wo [2000]), energy method (Hohe [2000]; Zhang [2007]), Gibson's formula and its modifications (Fu [1999]), general micromechanical method (Kalamkarov [2007]) and homogenization method (Sanchez-Palencia [1980]; Hassani [1996]). These methods have their own advantages to evaluate the effective elastic constants. However, some of them are restricted to two-dimensional sandwich beams and plates on the basis of the beam or thin plate theory. The homogenization method has strictly theoretical foundation. So it has been adopted to predict various equivalent properties of periodic composite structures, for instance, effective moduli (Peng [2002]), thermal conductivities (Laschet [2002]), piezoelectric coefficients (Berger [2005]), and so on.

In this chapter, we evaluate the effective elastic constants of the three-dimensional honeycomb sandwich structure by using the three-dimensional homogenization method and the finite element technique. All finite element models are built in the platform SAMCEF®. The different effective approaches and computing methods are utilized in order to deeply study the equivalent properties of honeycomb sandwich structures. As the theoretical foundation of computing effective properties of periodic cellular solids and designing structural materials with prescribed properties, the homogenization formulation and its finite element solution are firstly derived in detail in section 2.2. As Hassani

(Hassani [1996]), we consider, in section 2.3, the 3-D honeycomb core as a two-phase composite and we obtain the effective elastic constants with the 3D homogenization method and the finite element technique. Then, others methods (Gibson [1982]; Fu [1999]; Zhang [2007]; Hassani [1996]) are exploited to compute the effective elastic constants of the hexagonal honeycomb core. By comparison as shown in Table 2.3 and Fig.2.3, we validate the 3D homogenization method. In section 2.4, we use three variations of our 3D homogenization method (one-step, two-step, and multi-step ones explained with the aid of Fig.2.4) to evaluate the overall effective elastic constants of the 3D honeycomb sandwich with upper and lower skins; the evaluation results are given in Table 2.4. We exploit these three homogenization methods and the engineering empirical method of Wo (Wo [2000]) to calculate three kinds of effective elastic moduli of 3D honeycomb sandwich panel. The computed results are given and compared in Table 2.5. Finally in section 2.5, we give the final conclusions on calculating effective elastic constants of honeycomb sandwich structures with the homogenization method.

2.2 Homogenization method (HM)

Cellular materials, composed of periodically repetitive microstructure cells, can be analyzed by using averaging method such as homogenization to determine macroscopic material behavior. The homogenization method is based on a two-scale asymptotic expansion of material behaviors with periodic unit cells. The overall properties of an elastic body can be described with two different scales: the macroscopic or global level x , and the microscopic or local level y . The global level x is related to the local level y as $y = x/\varepsilon$, where ε is a very small positive number, which is a relative size of the periodic cell.

It is assumed that a physical quantity $\Phi(x, y)$ of a composite structure with periodic microstructures is given by:

$$\Phi(x, y) = \Phi(x, y + Y) \quad (2.1)$$

$$\frac{d\Phi}{dx} = \frac{\partial\Phi}{\partial x} + \frac{1}{\varepsilon} \frac{\partial\Phi}{\partial y} \quad (2.2)$$

where Y is the length of periodicity.

We introduce now the general elasticity problem of a composite structure with periodic

microstructures as seen in Fig. 2.1. The virtual displacement equation can be constructed as:

$$\int_{\Omega^\varepsilon} E_{ijkl}^\varepsilon \frac{\partial u_k^\varepsilon}{\partial x_i} \frac{\partial v_i}{\partial x_j} d\Omega = \int_{\Omega^\varepsilon} f_i^\varepsilon v_i d\Omega + \int_{\Gamma_f} t_i v_i d\Gamma + \int_{S^\varepsilon} p_i^\varepsilon v_i dS, \forall v \in V^\varepsilon \quad (2.3)$$

where f_i^ε are the body forces; t_i are the surface forces; p_i^ε are the hole boundary forces in unit cells (see Fig.2.1(c)); v_i is an arbitrary function that satisfies the boundary condition.

According to the symmetry of linear elasticity, we know $E_{ijkl}^\varepsilon = E_{jikl}^\varepsilon = E_{ijlk}^\varepsilon = E_{klji}^\varepsilon$. The stress-strain and strain-displacement relations are respectively $\sigma_{ij}^\varepsilon = E_{ijkl}^\varepsilon e_{kl}^\varepsilon$ and $e_{kl}^\varepsilon = (u_{k,l}^\varepsilon + u_{l,k}^\varepsilon)/2$. u^ε , e^ε and σ^ε depend on the macroscopic level x and microscopic level y . Using a double-scale asymptotic expansion, the displacement field can be written as:

$$u^\varepsilon(x) = u^0(x, y) + \varepsilon^1 u^1(x, y) + \varepsilon^2 u^2(x, y) + \dots \quad (2.4)$$

where $u^i(x, y)$ defined in $(x, y) \in \Omega \times Y$ is the Y -periodic function.

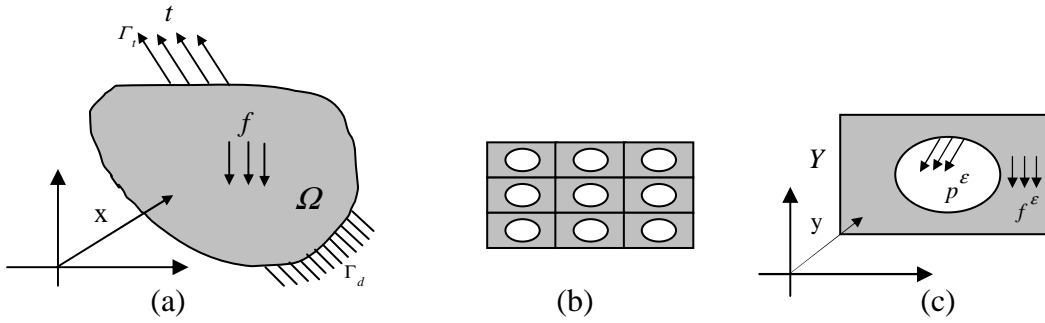


Fig.2.1 Elastic problem with periodic microstructures

(a) General elasticity problem (b) Cellular structure (c) Unit cell

For a Y -periodic function $\varphi(y)$, we have

$$\lim_{\varepsilon \rightarrow 0^+} \int_{\Omega^\varepsilon} \varphi\left(\frac{x}{\varepsilon}\right) d\Omega = \frac{1}{|Y|} \int_{\Omega} \int_Y \varphi(y) dY d\Omega \quad (2.5)$$

where $|Y|$ is the volume of unit cell.

Substituting Eqs. (2.2) and (2.4) into Eq. (2.3), we obtain

$$\begin{aligned}
& \int_{\Omega^\varepsilon} E_{ijkl}^\varepsilon \left\{ \frac{1}{\varepsilon^2} \frac{\partial u_k^0}{\partial y_l} \frac{\partial v_i}{\partial y_j} + \frac{1}{\varepsilon} \left[\left(\frac{\partial u_k^0}{\partial x_l} + \frac{\partial u_k^1}{\partial y_l} \right) \frac{\partial v_i}{\partial y_j} + \frac{\partial u_k^0}{\partial y_l} \frac{\partial v_i}{\partial x_j} \right] \right. \\
& \quad \left. + \left[\left(\frac{\partial u_k^0}{\partial x_l} + \frac{\partial u_k^1}{\partial y_l} \right) \frac{\partial v_i}{\partial y_j} + \left(\frac{\partial u_k^1}{\partial x_l} + \frac{\partial u_k^2}{\partial y_l} \right) \frac{\partial v_i}{\partial y_j} \right] + \varepsilon(\dots) \right\} d\Omega \\
& = \int_{\Omega^\varepsilon} f_i^\varepsilon v_i d\Omega + \int_{\Gamma_i} t_i v_i d\Gamma + \int_{S^\varepsilon} p_i^\varepsilon v_i dS, \quad \forall v \in V_{\Omega \times Y}
\end{aligned} \tag{2.6}$$

where $V_{\Omega \times Y} = \{ v(x, y) \text{ defined for } (x, y) \in \Omega \times Y \mid v(\square, y) \text{ } Y\text{-periodic; } v \text{ smooth enough; } v|_{\Gamma_d} = 0 \}$. All the functions are assumed sufficiently smooth so when $\varepsilon \rightarrow 0^+$, all integrals exist. By equating the terms with the same power of ε , using the divergence theorem and applying the periodicity conditions on the opposite faces of Y , the general elasticity problem of Eq. (2.3) with the periodic base cells in a cellular body is decomposed into two parts: one solves the equilibrium problem of Eq. (2.7) in the microscopic level; the other solves the equilibrium problem of Eq. (2.8) in the macroscopic level. The detailed derivations can be found in Refs. (Guedes [1990], Hassani [1996; 1998a]). It is also concluded that the first term of the expansion of u^ε only depends on the macroscopic scale x .

$$\int_Y E_{ijkl} \left(\frac{\partial u_k^1}{\partial x_l} + \frac{\partial u_k^2}{\partial y_l} \right) \frac{\partial v_i(y)}{\partial y_j} dY = \int_Y f_i v_i(y) dY, \quad \forall v \in V_Y \tag{2.7}$$

$$\begin{aligned}
& \int_{\Omega} E_{ijkl}^H(x) \frac{\partial u_k^0(x)}{\partial x_l} \frac{\partial v_i(x)}{\partial x_j} d\Omega \\
& = \int_{\Omega} \tau_{ij}(x) \frac{\partial v_i(x)}{\partial x_j} d\Omega + \int_{\Omega} b_i(x) v_i(x) d\Omega + \int_{\Gamma_i} t_i(x) v_i(x) d\Gamma, \quad \forall v \in V_{\Omega}
\end{aligned} \tag{2.8}$$

E_{ijkl}^H is the homogenized elastic tensor, and

$$E_{ijkl}^H(x) = \frac{1}{|Y|} \int_Y \left(E_{ijkl} - E_{ijpm} \frac{\partial \chi_p^{kl}}{\partial y_m} \right) dY \tag{2.9}$$

$\tau_{ij}(x)$ are the average residual stresses within the cell due to the tractions p^ε inside the holes, and

$$\tau_{ij}(x) = \frac{1}{|Y|} \int_Y E_{ijkl} \frac{\partial \psi_k}{\partial y_l} dY \tag{2.10}$$

$b_i(x)$ are the average body forces, and

$$b_i(x) = \frac{1}{|Y|} \int_Y f_i dY \quad (2.11)$$

ψ_k is the displacement field due to the tractions p^ε . χ^{kl} are the microscopic displacement fields within unit cells under the periodic boundary condition, and then

$$\int_Y E_{ijpm} \frac{\partial \chi_p^{kl}}{\partial y_m} \frac{\partial v_i(y)}{\partial y_j} dY = \int_Y E_{ijkl} \frac{\partial v_i(y)}{\partial y_j} dY \quad (2.12)$$

$$\int_Y E_{ijkl} \frac{\partial \psi_k}{\partial y_l} \frac{\partial v_i(y)}{\partial y_j} dY = \int_S p_i v_i(y) dY \quad (2.13)$$

As shown above, the microscopic and macroscopic problems are not coupled when $\varepsilon \rightarrow 0$. The homogenized elastic constants can be computed within the base cell by solving Eqs. (2.12) and (2.13) with the finite element analysis for χ^{kl} and ψ_k . The mechanical response of the general elasticity problem with the periodic microstructures can be analyzed under the consideration of homogenous structures.

2.3 Effective calculation of 3D honeycomb core

2.3.1 Numerical solution of homogenized elastic constants of 3D honeycomb core based on HM

To calculate the effective elastic tensor E_{ijkl}^H , as defined in Eq. (2.9), it is necessary to determine the microscopic displacement field χ^{kl} , which is the Y -periodic solution of Eq. (2.12). For the 3D problem, Eq. (2.9) and Eq. (2.12) with different values of kl ($kl = 11, 22, 33, 12, 23, 13$) provide essential equations to find the elements of the homogenized matrix.

From Eq. (2.9), it follows that:

$$\begin{aligned} E_{ijkl}^H &= \frac{1}{|Y|} \int_Y [E_{ijkl}(y) - E_{ijrs}(y) e_{rs}(\chi^{kl})] dy \\ &= \frac{1}{|Y|} \int_Y [E_{ijkl}(y) - \sigma_{ij}(\chi^{kl})] dy \\ &= \frac{1}{\sum_{m=1}^{nele} |Y_m|} \sum_{m=1}^{nele} \int_{Y_m} [E_{ijkl}(y) - \sigma_{ij}(\chi^{kl})] dy_m \end{aligned} \quad (2.14)$$

where $|Y|$ is the volume of unit cell; $|Y_m|$ is the volume of each element in the unit cell; $nele$ is the number of finite elements in the unit cell; $e_{rs}(\chi^{kl})$ and $\sigma_{ij}(\chi^{kl})$ are respectively strain and stress tensors corresponding the characteristic displacement χ^{kl} of unit cell, obtained by solving the following Eq. (2.15).

From Eq. (2.12), the conventional stiffness equation of microscopic base cell is:

$$K \chi^{kl} = F^{kl} \quad (2.15)$$

Here, the stiffness matrix of the microscopic base cell and the initial strain loads are:

$$K = \sum_{e=1}^{nele} k_e = \sum_{e=1}^{nele} \int_{Y_e} B_e^T E_e B_e dy \quad (2.16)$$

$$F^{kl} = \sum_{e=1}^{nele} F_e^{kl} = \sum_{e=1}^{nele} \int_{Y_e} B_e^T E_e \varepsilon_0^{kl} dy \quad (2.17)$$

where ε_0^{kl} are the unit initial strains in the microscopic base cell. For 3D microstructure homogenization, ε_0^{kl} have six different cases corresponding to six load cases.

The finite element model of unit cell of the honeycomb core can be seen in Fig.2.2. We assume that the cell wall is made of the isotropic materials with $E_1 = 0.91\text{GPa}$, and the hole is replaced by weak materials, $E_2 = 0.00001\text{GPa}$. Both Poisson's ratios are 0.3. The ratio of wall thickness to side length of unit cell is $t/a = \sqrt{3}/6$.

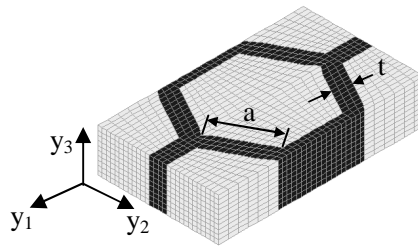


Fig.2.2 Finite element model of 3D honeycomb core

According to Hooke's Law relating stress and strain Eq. (2.18) for orthotropic materials, the overall general equations in term of the principal materials directions are following as in Eq. (2.19):

$$\begin{Bmatrix} \sigma_1 \\ \sigma_2 \\ \sigma_3 \\ \sigma_4 \\ \sigma_5 \\ \sigma_6 \end{Bmatrix} = \begin{bmatrix} C_{11} & C_{12} & C_{13} & 0 & 0 & 0 \\ C_{12} & C_{22} & C_{23} & 0 & 0 & 0 \\ C_{13} & C_{23} & C_{33} & 0 & 0 & 0 \\ & & & C_{44} & 0 & 0 \\ & sym & & & C_{55} & 0 \\ & & & & & C_{66} \end{bmatrix} \begin{Bmatrix} \epsilon_1 \\ \epsilon_2 \\ \epsilon_3 \\ \epsilon_4 \\ \epsilon_5 \\ \epsilon_6 \end{Bmatrix} \quad (2.18)$$

$$\begin{aligned} C_{11} &= E_{11}(1 - \nu_{23}\nu_{32})/\Delta \\ C_{22} &= E_{22}(1 - \nu_{13}\nu_{31})/\Delta \\ C_{33} &= E_{33}(1 - \nu_{12}\nu_{21})/\Delta \\ C_{12} &= (\nu_{21} + \nu_{31}\nu_{23})E_{11}/\Delta = (\nu_{12} + \nu_{32}\nu_{13})E_{22}/\Delta \\ C_{13} &= (\nu_{31} + \nu_{21}\nu_{32})E_{11}/\Delta = (\nu_{13} + \nu_{12}\nu_{23})E_{22}/\Delta \\ C_{23} &= (\nu_{32} + \nu_{12}\nu_{31})E_{22}/\Delta = (\nu_{23} + \nu_{21}\nu_{13})E_{33}/\Delta \\ C_{44} &= G_{23} \\ C_{55} &= G_{13} \\ C_{66} &= G_{12} \\ \Delta &= 1 - \nu_{12}\nu_{21} - \nu_{23}\nu_{32} - \nu_{31}\nu_{13} - 2\nu_{21}\nu_{32}\nu_{13} \end{aligned} \quad (2.19)$$

where E_{11} , E_{22} , E_{22} , G_{12} , G_{23} , G_{13} , ν_{12} , ν_{23} and ν_{13} are elastic constants in the principal materials directions. We obtain effective elastic constants as seen in Table 2.1 and the corresponding effective elastic matrix of the honeycomb core as seen in Eq. (2.20) by the finite element analysis and the code program.

Table 2.1 Effective elastic constants

E_{11}/GPa	0.03229932	G_{12}/GPa	0.009252872	ν_{12}	0.7777879
E_{22}/GPa	0.03213468	G_{23}/GPa	0.05289672	ν_{23}	0.03993055
E_{33}/GPa	0.2414293	G_{13}/GPa	0.05303416	ν_{13}	0.04013513

$$E_{ijkl}^H = \begin{bmatrix} 0.08977385 & & & & & \\ 0.07139982 & 0.08931070 & & & & \\ 0.04835210 & 0.04821316 & 0.2703989 & & & \\ & & & 0.009252872 & & \\ & & 0 & & 0.05289672 & \\ & & & & & 0.05303416 \end{bmatrix} \quad (2.20)$$

From Table 2.1, the effective elastic moduli along y_1 and y_2 directions are less than one along y_3 direction. Moreover the effective shear moduli in y_1 - y_3 and y_2 - y_3 planes are greater than one in y_1 - y_2 plane. These facts demonstrate that the core in the honeycomb sandwich structure mainly carry the transverse shear loads. In addition, the effective elastic moduli along y_1 and y_2 directions are not equal. This shows the honeycomb structure has weakly anisotropic characteristics in y_1 - y_2 plane and the elastic modulus along y_1 direction is bigger than along y_2 direction. This conclusion is the same as the one proposed by Fu (Fu [1999]).

2.3.2 Other methods for the calculation of effective elastic constants of hexagonal honeycomb core

The hexagonal honeycomb core is the most popular cellular solid used as the sandwich core. Besides the homogenization method, there exist several methods to compute effective elastic constants of hexagonal honeycomb core: Gibson's formula (Gibson [1982]) and its modification (Fu [1999]), energy method (Zhang [2007]). In the following we will adopt respectively these methods to calculate the effective properties of the 2D hexagonal honeycomb core.

For preliminary calculation in design or where a great accuracy is not needed, one uses simpler forms for some of the expressions in Eq. (2.19):

$$\begin{aligned} C_{11} &= E_{11} / (1 - \nu_{12}\nu_{21}) \\ C_{22} &= E_{22} / (1 - \nu_{12}\nu_{21}) \\ C_{12} = C_{21} &= \nu_{21}E_{11} / (1 - \nu_{12}\nu_{21}) = \nu_{12}E_{22} / (1 - \nu_{12}\nu_{21}) \\ C_{66} &= G_{12} \end{aligned} \quad (2.21)$$

2.3.2.1 Gibson's formula

Because the thickness of sandwich core is much bigger than upper and lower skins, the in-plane stiffness and bending stiffness cannot be ignored. Gibson (Gibson [1982]) gave the analytical formulation of Eq. (2.22) - Eq. (2.26) to calculate the effective properties of the hexagonal honeycomb core considering the sandwich core as an orthotropic layer.

$$E_{11} = E \frac{t^3}{a^3} \frac{\cos \theta}{(\beta + \sin \theta) \sin^2 \theta} = 0.050556 \text{ GPa} \quad (2.22)$$

$$\nu_{12} = \frac{\cos^2 \theta}{(\beta + \sin \theta) \sin \theta} = 1 \quad (2.23)$$

$$E_{22} = E \frac{t^3 (\beta + \sin \theta)}{a^3 \cos^3 \theta} = 0.050556 \text{ GPa} \quad (2.24)$$

$$\nu_{21} = \frac{(\beta + \sin \theta) \sin \theta}{\cos^2 \theta} = 1 \quad (2.25)$$

$$G_{12} = E \frac{t^3 (\beta + \sin \theta)}{a^3 \beta^2 (2\beta + 1) \cos \theta} = 0.0126389 \text{ GPa} \quad (2.26)$$

where $\beta = 1$ for the hexagonal honeycomb core; $\theta = \pi/6$; $E = 0.91 \text{ GPa}$ is the elastic modulus of the cell wall made. The ratio of wall thickness to side length of unit cell is $t/a = \sqrt{3}/6$.

2.3.2.2 Modifications of Gibson's formula

For the uni-axial elongation case, the Gibson's formula coincides with the experimental results. However the stiffness matrix cannot be obtained through the Gibson's formula because the stretching deformation of the cell wall is ignored. Thus Fu (Fu [1999]) modified the Gibson's formula as follows:

$$E_{11} = \frac{4}{\sqrt{3}} E \left(1 - 3 \frac{t^2}{l^2} \right) \frac{t^3}{l^3} = 0.037916666 \text{ GPa} \quad (2.27)$$

$$\nu_{12} = 1 - 4 \frac{t^2}{l^2} = 0.66667 \quad (2.28)$$

$$E_{22} = \frac{4}{\sqrt{3}} E \left(1 - \frac{5}{3} \frac{t^2}{l^2} \right) \frac{t^3}{l^3} = 0.04353395 \text{ GPa} \quad (2.29)$$

$$\nu_{21} = 1 - \frac{8}{3} \frac{t^2}{l^2} = 0.77778 \quad (2.30)$$

The stretch deformation has little influence on the transverse shear modulus $G_{12} = 0.01263888 \text{ GPa}$.

According to Eq. (2.21), the in-plane effective elastic matrix of the hexagonal honeycomb core is obtained as follows:

$$E^H = \begin{bmatrix} \frac{E_{11}}{1-\nu_{12}\nu_{21}} & \frac{\nu_{21}E_{11}}{1-\nu_{12}\nu_{21}} \\ \frac{\nu_{12}E_{22}}{1-\nu_{12}\nu_{21}} & \frac{E_{22}}{1-\nu_{12}\nu_{21}} \\ & & G_{12} \end{bmatrix} = \begin{bmatrix} 0.07875 & 0.06028 & \\ 0.06028 & 0.09042 & \\ & & 0.01264 \end{bmatrix} \quad (2.31)$$

2.3.2.3 Energy method

According to the average-field theory (Hori [1999]), the strains and stresses of effective honeycomb cores are the volume average of the corresponding strains and stresses within the microstructure unit cell of the honeycomb core:

$$\bar{\sigma} = \frac{1}{V} \int_{\Omega} \sigma d\Omega \quad (2.32)$$

$$\bar{\varepsilon} = \frac{1}{V} \int_{\Omega} \varepsilon d\Omega \quad (2.33)$$

From Hooke's Law relating stress and strain Eq. (2.18), the effective elastic matrix for the 2D honeycomb core is given as the following Eq. (2.34) which reflects the relations between the average strains and stresses.

$$\begin{bmatrix} \bar{\sigma}_1 \\ \bar{\sigma}_2 \\ \bar{\sigma}_3 \end{bmatrix} = \begin{bmatrix} E_{1111}^H & E_{1122}^H & 0 \\ E_{2211}^H & E_{2222}^H & 0 \\ 0 & 0 & E_{1212}^H \end{bmatrix} \begin{bmatrix} \bar{\varepsilon}_1 \\ \bar{\varepsilon}_2 \\ \bar{\varepsilon}_3 \end{bmatrix} \quad (2.34)$$

The strain energy per unit volume of unit cell is expressed as:

$$\begin{aligned} E &= \frac{1}{2V} \int_{\Omega} (\sigma_1 \varepsilon_1 + \sigma_2 \varepsilon_2 + \sigma_3 \varepsilon_3) d\Omega \\ &= \frac{1}{2} (\bar{\sigma}_1 \bar{\varepsilon}_1 + \bar{\sigma}_2 \bar{\varepsilon}_2 + \bar{\sigma}_3 \bar{\varepsilon}_3) \end{aligned} \quad (2.35)$$

For the 2D honeycomb core, we can obtain the effective elastic matrix through the finite element analysis with the four displacement load cases in Table 2.2. The displacement load u equals $3a/2$; v equals $\sqrt{3}a/2$. Here a is the side length of cell wall. Of course, the effective properties of 3D honeycomb core can also be achieved by the energy method when sufficient boundary conditions are given. The effective results are seen as Table 2.3. Actually, the strain energy-based method and homogenization method are just two variants of the same definition of effective material properties (Sigmund [1994; 1997]) and they are physically identical (Zhang [2007]).

The effective elastic properties can be written in its energy form as:

$$E_{pqrs}^H \boldsymbol{\varepsilon}_{pq}^{0(kl)} \boldsymbol{\varepsilon}_{rs}^{0(ij)} = \frac{1}{|Y|} \int_Y E_{pqrs} (\boldsymbol{\varepsilon}_{pq}^{0(kl)} - \boldsymbol{\varepsilon}_{pq}^{(kl)}) (\boldsymbol{\varepsilon}_{rs}^{0(ij)} - \boldsymbol{\varepsilon}_{rs}^{(ij)}) dY \quad (2.36)$$

From Eqs. (2.34) and (2.35), the relationship between the effective elastic properties and the strain energy of microstructure in the strain energy-based method can be stated as

$$E(\boldsymbol{\varepsilon}^0) = E_{pqrs}^H \boldsymbol{\varepsilon}_{pq}^{0(kl)} \boldsymbol{\varepsilon}_{rs}^{0(ij)} \quad (2.37)$$

By comparing Eq. (2.36) with Eq. (2.37), one can see that they are equivalent in fact.

Table 2.2 Boundary conditions and corresponding strain energy

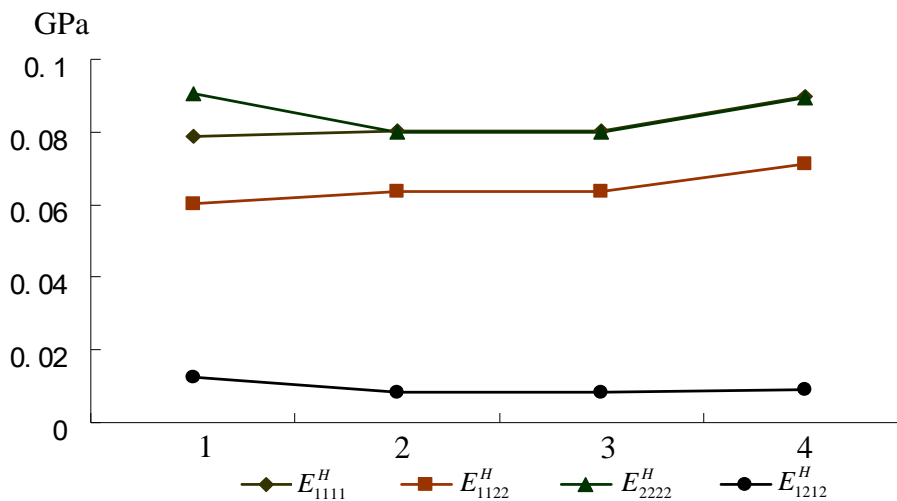
Boundary conditions	Strain fields	Strain energy	Energy value
	$\bar{\boldsymbol{\varepsilon}}^{(1)} = \begin{pmatrix} 1 \\ 0 \\ 0 \end{pmatrix}$	$E^{(1)} = \frac{1}{2} E_{1111}^H$	0.0401
	$\bar{\boldsymbol{\varepsilon}}^{(2)} = \begin{pmatrix} 0 \\ 1 \\ 0 \end{pmatrix}$	$E^{(2)} = \frac{1}{2} E_{2222}^H$	0.039852
	$\bar{\boldsymbol{\varepsilon}}^{(3)} = \begin{pmatrix} 0 \\ 0 \\ 1 \end{pmatrix}$	$E^{(3)} = \frac{1}{2} E_{1212}^H$	0.005584
	$\bar{\boldsymbol{\varepsilon}}^{(4)} = \begin{pmatrix} 1 \\ 1 \\ 0 \end{pmatrix}$	$E^{(4)} = \frac{1}{2} (2E_{1122}^H + E_{1111}^H + E_{2222}^H)$	0.1434

2.3.3 Comparison of the results of different methods

From Gibson’s formula, obviously the effective elastic matrix can’t be determined because of $\nu_{12}\nu_{21} = 1$. So we give the comparison of effective elastic constants of honeycomb core according to modifications of Gibson’s formula, energy method and homogenization method as seen in Table 2.3 and Fig. 2.3.

Table 2.3 Comparison of effective elastic constants of honeycomb core

Components	E_{1111}^H /GPa	E_{1122}^H /GPa	E_{2222}^H /GPa	E_{1212}^H /GPa
Modifications of Gibson’s formula (Fu and Yin [1999])	0.07875	0.06028	0.09042	0.01264
Energy method (Zhang [2007])	0.080334	0.063458	0.07984	0.008501
2D homogenization (Hassani [1996])	0.080334	0.063458	0.07984	0.008501
3D homogenization	0.089774	0.0713998	0.089311	0.009253



1—Modifications of Gibson’s formula; 2—Energy method;
3—2D homogenization; 4—3D homogenization

Fig.2.3 Comparison of effective elastic constants of honeycomb core

Comparing the elastic moduli in Table 2.3, we can notice that computing results with

different methods coincide approximately. The flatness of each curve in Fig.2.3 reflects this fact. The comparison results also indicate the validity of each effective method. However, we can obtain all elastic constants of the honeycomb core using 3D homogenization that provides the complete data for the analysis and evaluation of the mechanical responses of honeycomb structures.

2.4 Effective calculation of 3D honeycomb sandwich

2.4.1 Multi-step homogenization of 3D honeycomb sandwich

The 3D honeycomb sandwich can be considered as a type of multilayered structure composed of upper and lower skins and a core.

Hohe (Hohe [2003]) directly determined the in-plane, bending and transverse shear stiffness components of structural sandwich panels by means of a strain energy based procedure which assumed equivalence of a representative plate element for the given microstructure and a similar homogeneous plate element if the strain energy of both elements is equal. Considering the skin effect, Xu (Xu [2002]) proposed a multi-pass homogenization method to derive elastic tensors for general honeycomb sandwiches. In this method, firstly a spatial heterogeneous problem was transferred into a material heterogeneous problem with consequent intermediate equivalent properties. Secondly the 2D heterogeneous problem was analytically homogenized in a unit cell by the variational approximations of displacement field. Finally the effective elastic tensors of honeycomb sandwiches were obtained. Both of the two methods homogenized the 3D honeycomb sandwich structure based on the analysis of 2D plate structures. Here, we directly adopt the 3D homogenization method to evaluate the overall effective elastic constants of the honeycomb sandwich with upper and lower skins. As seen in Fig.2.4, there are three variations: (1) direct equivalent (one-step); (2) firstly homogenizing the honeycomb core, and then combining with the lower and upper skins (two-step); (3) firstly homogenizing the honeycomb core, and then, in turn combining with the lower and upper skins (multi-step).

Although these three methods are based on the homogenization method, the substantial difference lies in that the former method simultaneously homogenizes three variations of isotropic materials; the latter two methods firstly obtain the orthotropic equivalent core,

and then simultaneously or in turn combine with the lower and upper skins.

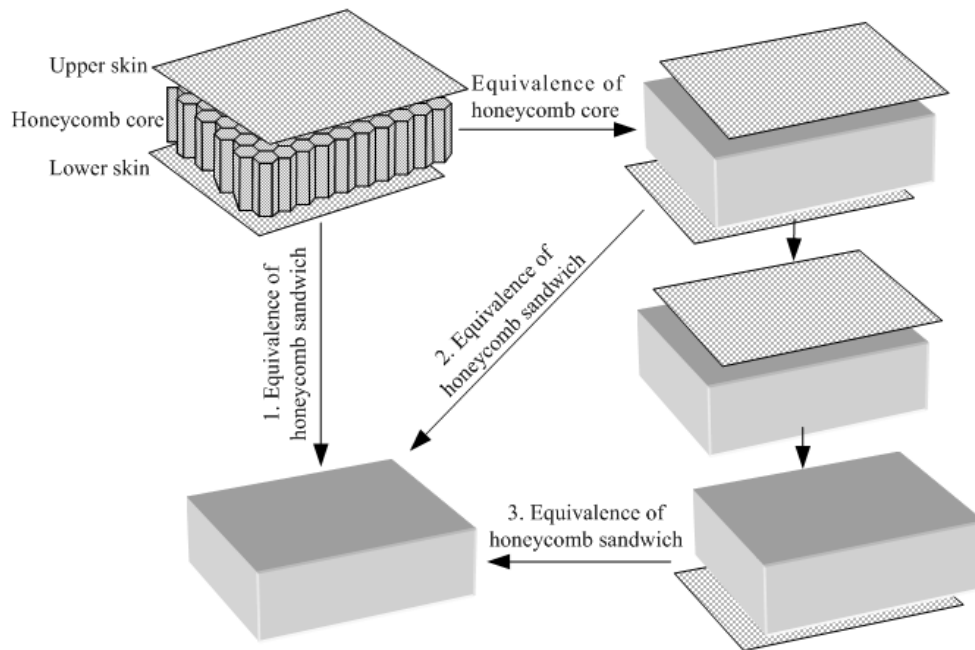


Fig.2.4 Equivalence of honeycomb sandwich structure by one, two and multi-step homogenization schemes

Now we build the finite element model of the honeycomb sandwich structure with one unit cell as seen in Fig.2.5. We assume that the lower and upper skins are made of the isotropic material and have elastic modulus $E = 2.0\text{GPa}$, Poisson’s ratio $\nu = 0.3$ and thickness $h_f = 1.25\text{mm}$. The honeycomb core has the same material as in Fig.2.2 and thickness $h_c = 16.25\text{mm}$. So the total thickness of the honeycomb sandwich structure is $h = h_c + 2h_f = 18.75$ (f -face, c -core). The computing results with the three methods are listed in Table 2.4.

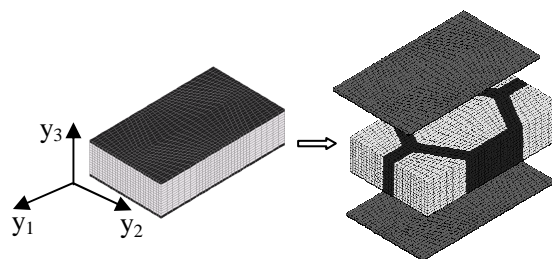


Fig.2.5 Finite element model of honeycomb sandwich structure with one unit cell

Table 2.4 Comparison of effective elastic constants with three methods

Elastic constants	One-step	Two-step	Multi-step	
			first	second
E_{11}/GPa	0.3471983	0.3075509	0.1844299	0.3075508
E_{22}/GPa	0.3469135	0.3072475	0.1841251	0.3075508
E_{33}/GPa	0.2802617	0.2913491	0.2710600	0.2913491
G_{12}/GPa	0.1301219	0.1105833	0.0635370	0.1105833
G_{23}/GPa	0.0592139	0.0603957	0.0566659	0.0603957
G_{13}/GPa	0.0593021	0.0605510	0.0568124	0.0605510
ν_{12}	0.3335783	0.3920744	0.4543954	0.3920745
ν_{23}	0.1510265	0.1287283	0.1071237	0.1289385
ν_{13}	0.1516072	0.1289882	0.1073589	0.1287782

From Table 2.4, we can see that computing results with different methods nearly identical, especially for two-step and multi-step method. This fact demonstrates that the homogenization sequence has little influence on equivalent moduli values of the honeycomb sandwich structure obtained by the homogenization method.

2.4.2 Engineering empirical method

In the engineering design, tension or shear loads are applied in three directions of the honeycomb sandwich structure. And then according to the equilibrium condition and strain compatibility, the tension and shear moduli along three directions can be calculated. In this section, we use the engineering empirical method (Wo [2000]) to compute the equivalent elastic moduli of the honeycomb sandwich structure. We compare this approach with the homogenization method. Here the elastic moduli of honeycomb cores are the same as Table 2.1. In the following formula (2.38)~(2.43), E_{11} , E_{22} , E_{33} , G_{12} , G_{23} and G_{13} are the equivalent elastic moduli of the honeycomb sandwich; E_{f11} , E_{f22} , E_{f33} , G_{f12} , G_{f23} and G_{f13} are the elastic moduli of the lower and upper skins; E_{c11} , E_{c22} , E_{c33} , G_{c12} , G_{c23} and G_{c13} are the elastic moduli of honeycomb cores.

(1) Tension moduli in plane

$$\begin{aligned} E_{11} &= E_{f11} \frac{2t_f}{h} + E_{c11} \frac{h_c}{h} \\ &= 2.0 \times \frac{2 \times 1.25}{18.75} + 0.0323 \times \frac{16.25}{18.75} = 0.29466 \text{GPa} \end{aligned} \quad (2.38)$$

$$\begin{aligned} E_{22} &= E_{f22} \frac{2t_f}{h} + E_{c22} \frac{h_c}{h} \\ &= 2.0 \times \frac{2 \times 1.25}{18.75} + 0.032135 \times \frac{16.25}{18.75} = 0.294517 \text{GPa} \end{aligned} \quad (2.39)$$

(2) Shear moduli

$$\begin{aligned} \frac{1}{G_{13}} &= \frac{2t_f}{G_{f13}h} + \frac{h_c}{G_{c13}h} \\ &= \frac{2 \times 1.25}{0.76923 \times 18.75} + \frac{16.25}{0.053034 \times 18.75} = 16.5150514 \\ \Rightarrow G_{13} &= 0.060551 \text{GPa} \end{aligned} \quad (2.40)$$

$$\begin{aligned} \frac{1}{G_{23}} &= \frac{2t_f}{G_{f23}h} + \frac{h_c}{G_{c23}h} \\ &= \frac{2 \times 1.25}{0.76923 \times 18.75} + \frac{16.25}{0.05289672 \times 18.75} = 16.55746217 \\ \Rightarrow G_{23} &= 0.06039573 \text{GPa} \end{aligned} \quad (2.41)$$

$$\begin{aligned} G_{12} &= G_{12} \frac{2t_f}{h} + G_{c12} \frac{h_c}{h} \\ &= 0.76923 \times \frac{2 \times 1.25}{18.75} + 0.009252872 \times \frac{16.25}{18.75} = 0.11058 \text{GPa} \end{aligned} \quad (2.42)$$

(3) Transverse tension moduli

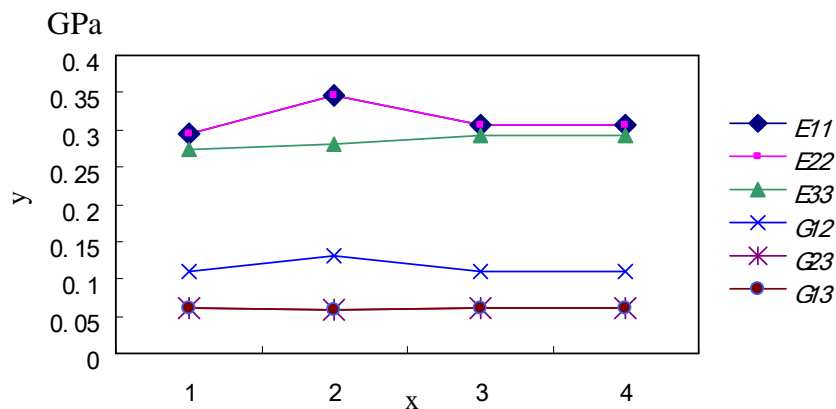
$$\begin{aligned} \frac{1}{E_{33}} &= \frac{2t_f}{E_{f33}h} + \frac{h_c}{E_{c33}h} = \frac{2 \times 1.25}{2.0 \times 18.75} + \frac{16.25}{0.2414293 \times 18.75} = 3.6564 \\ \Rightarrow E_{33} &= 0.2734931 \text{GPa} \end{aligned} \quad (2.43)$$

2.4.3 Comparisons of the results for honeycomb sandwich

We obtain the main elastic moduli of the honeycomb sandwich using the engineering empirical method. The resultant comparisons with the homogenization method can be seen in Table 2.5 and Fig.2.5.

Table 2.5 Comparison of main elastic moduli

	Tension moduli in plane		Shear moduli			Transverse tension moduli
	E_{11} /GPa	E_{22} /GPa	G_{13} /GPa	G_{23} /GPa	G_{12} /GPa	E_{33} /GPa
Engineering empirical method (Wo [2000])	0.29466	0.29452	0.06055	0.0604	0.1105831	0.2735
one-step homogenization	0.3472	0.3469	0.0593	0.0592	0.130122	0.2803
two-step homogenization	0.30755	0.30725	0.06055	0.0604	0.1105833	0.29135
multi-step homogenization	0.30755	0.30755	0.06055	0.0604	0.1105833	0.29135



1—Engineering empirical method; 2—One-step homogenization;

3—Two-step homogenization; 4—Multi-step homogenization

Fig. 2.5 Comparison of equivalent elastic moduli

As we can notice from Table 2.5, the equivalent elastic moduli of the honeycomb sandwich respectively calculated with 3D homogenization and engineering empirical methods are

basically identical. The flatness of each curve in Fig.2.5 reflects the consistency of computing results with different methods. In addition, observing the expressions in the engineering empirical method, we find that each elastic modulus only depends on the ratio between the thickness of the honeycomb core h_c and the thickness of lower and upper skins t_f . Therefore, the engineering empirical method just like the homogenization method cannot embody the influence of the unit cell scale on equivalent elastic moduli. This approximate computation is valid only when the unit cell is very small relative to the whole structure.

2.5 Summary

Firstly, by calculating and comparing the effective elastic constants of honeycomb core with different methods, we have confirmed the rightness and validity of 3D homogenization method and provide the background for the computation of effective elastic constants of honeycomb sandwich structures.

Secondly, combining 3D homogenization method with the finite element technique, one can obtain all effective elastic constants of honeycomb sandwich structures. Fairly good agreement with the engineering empirical method demonstrates that the multi-step homogenization method is valid and that the equivalent sequence has no influence on the equivalent results.

Although the present study is directed to an analysis of sandwich structures with honeycomb cores, the multi-step homogenization method can be applied to a much broader class of layered structures that consist of a heterogeneous medium such as hybrid composites and braided structures. Moreover we can also employ this method to design the 3D configuration of unit cells of cellular structures with the specific properties.

3. Topological design of 3D microstructure

In this chapter, maximization of elastic moduli and thermal conductivities is used to design the material microstructure. This is based on the homogenization method and topology optimization.

The single objective and multi-objective designs are employed to maximize uni-axial and multi-axial properties. Actually the multi-objective design is transformed into the single objective through the vector aggregation. Different initial structures have been used in the optimization process.

3.1 Introduction

In the previous chapter, we have used the homogenization method with the asymptotic expansion to passively predict effective properties of periodic unit cells of honeycomb sandwich structures within the finite element framework.

In fact, we would like to achieve the desired properties of material microstructures by using the topology optimization in conjunction with the homogenization method and the finite element technique. Usually cellular materials and solids, which are constituted of ordered microstructures and formed by the periodic repetition of unit cells, possess excellent properties which are sensitive to the configuration of the microstructure cells. Therefore new types of cellular materials and solids with the specific properties can be designed by establishing relationships between topology and performance to satisfy the special requirement for structural performance.

In the mid 1990ies, Sigmund (Sigmund [1994; 1995; 1997]) proposed the topological optimization method to design periodic microstructures of a material to obtain prescribed constitutive properties.

The microstructure was modeled as a truss or thin frame structure in two and three dimensions. He also used a topology optimization procedure to determine the distribution of three phases in order to design composites with extreme or unusual thermal expansion behaviors. Neves (Neves [2000]) presented 2D computational models which addressed the problem of finding the optimal representative microstructural element for periodic media that maximized either a weighted sum of equivalent strain energy densities for specified multiple macroscopic strain fields, or a linear combination of the equivalent material properties.

All these works have pursued the optimal layout under given constraints based on the inverse homogenization method which was required to update the evaluation of effective elastic tensor during the optimization process. More works have been reviewed in chapter 1. Continuing along previous works, we explore the topological design of 3D microstructure cell combining the finite element analysis with the optimal algorithm.

In this chapter, we first introduce the general problem of topology optimization and the optimal scheme that are adopted in our works. Then we establish the optimal models. Single equivalent constant and a linear combination of the equivalent material properties with regard to elastic constants and thermal conductivity coefficients are maximized under

the constraint of specific volume fraction. Numerically, 3D microstructures with the maximum stiffness and thermal conductivity in single and multiple directions are designed and satisfactory results are obtained. Lastly, we also point out that the initial values of design variables have great influence on the optimal configuration of 3D microstructures and several test examples are given to show the difference between optimal layouts.

3.2 Formulation of topology optimization problem

The topology optimization problem can be formulated as follows: to determine an optimal distribution of material within the given design domain. The amount of material is bounded to a given percentage of the design domain.

Let us consider the general linear elasticity problem subject to the applied body force f in a bounded open domain Ω and the surface traction forces t on Γ_t . Assume that Ω has a smooth boundary Γ comprising the free boundary Γ_f , Γ_d , where displacements are prescribed and Γ_t where traction forces are applied. It is also assumed that $\Gamma = \partial\Omega = \Gamma_f \cup \Gamma_d \cup \Gamma_t$ and $\Gamma_f \cap \Gamma_d \cap \Gamma_t = \emptyset$. The boundary value condition and the stress-strain and strain-displacement relationships are described as following:

$$\begin{aligned} -\operatorname{div}\sigma(u) &= f & \text{in } \Omega \\ u &= u_0 & \text{on } \Gamma_d \\ \sigma(u) \cdot n &= \sigma_0 & \text{on } \Gamma_t \end{aligned} \quad (3.1)$$

$$\begin{aligned} \forall x \in \Omega, \sigma(u) &= E \cdot \varepsilon(u) \\ \varepsilon(u) &= \frac{1}{2} \left(\nabla u + (\nabla u)^T \right) \end{aligned} \quad (3.2)$$

The material distribution problem, is controlled by a design variable that can be expressed by a switch function defined as

$$\rho(x) = \begin{cases} 1 & \text{if } x \in \Omega_s \\ 0 & \text{if } x \in \Omega / \Omega_s \end{cases} \quad (3.3)$$

where Ω denotes the entire design domain and Ω_s denotes the domain occupied by solid elastic materials.

The general mathematical model of topology optimization for minimizing the objective function, subjected to the volume constraints, is formulated with a discrete valued design (0 for void and 1 for solid):

$$\begin{aligned}
& \underset{\rho}{\text{Min}} f(\rho) \\
& \text{s.t.} \quad \int_{\Omega} \rho d\Omega \leq \bar{V} \\
& \quad \rho(x) = 0 \text{ or } 1, \forall x \in \Omega
\end{aligned} \tag{3.4}$$

where \bar{V} is the upper bound of volume constraint, ρ is the volume density and $f(\rho)$ is a performance criterion.

This topology optimization problem is generally solved numerically using the finite element discretization approach. The design domain Ω is divided into n finite elements and the density function ρ is discretized correspondingly into element wise constant density functions. The formulation of topology optimization is expressed as:

$$\begin{aligned}
& \underset{X}{\text{Min}} f(X) \\
& \text{s.t.} \quad V(X) = \sum_{i=1}^n x_i v_i \leq \bar{V} \\
& \quad x_i = 0 \text{ or } 1, i = 1, \dots, n
\end{aligned} \tag{3.5}$$

This discrete problem is difficult to solve because of its highly combinational nature (Bendsøe [1989]; Duysinx [2007]). Beckers (Beckers [1999; 2000]) developed a mathematical programming method combining the dual method and convex separable approximate scheme to directly solve structural optimization problems involving discrete variables. However the solution procedure is rather complicated. Normally we consider an alternative formulation to allow the density variables varying continuously from 0 to 1 via all intermediate densities. The optimal model on the material distribution problem can be written as follows:

$$\begin{aligned}
& \underset{X}{\text{Min}} f(X) \\
& \text{s.t.} \quad V(X) = \sum_{i=1}^n x_i v_i \leq \bar{V} \\
& \quad 0 < \delta \leq x_i \leq 1, i = 1, \dots, n
\end{aligned} \tag{3.6}$$

where δ is a positively small quantity to avoid the singularity of the stiffness matrix.

Now we can employ the sensitivity analysis and mathematical programming algorithms to efficiently solve the material distribution problem. Unfortunately numerical instabilities may occur: checkerboards and mesh-dependency. In fact, the discrete topology optimization problem without additional constraints is ill-posed.

To suppress the intermediate densities, two density penalization models are generally employed: the SIMP method (Solid Isotropic Microstructure with Penalization) proposed

by Bendsøe and Sigmund (Bendsøe [1999]; Rozvany [1992]) and the RAMP (Rational Approximation of Material Properties) scheme proposed by Stolpe and Svanberg (Stolpe [2001]). These approaches assume that the following relationships exist between the elastic modulus E_i of the i -th element with the density value x_i and the solid elastic modulus E_0 :

$$E_i = x_i^p E_0 \quad (\text{for SIMP}) \quad (3.7)$$

$$E_i = \frac{x_i E_0}{1 + q(1 - x_i)} \quad (\text{for RAMP}) \quad (3.8)$$

where $p \geq 1$ and $q \geq 1$ are penalization factors. From Fig.3.1 and Fig.3.2, the use of SIMP and RAMP material models will force the topology optimization towards limiting values $x_i=0$ (void) and $x_i=1$ (solid).

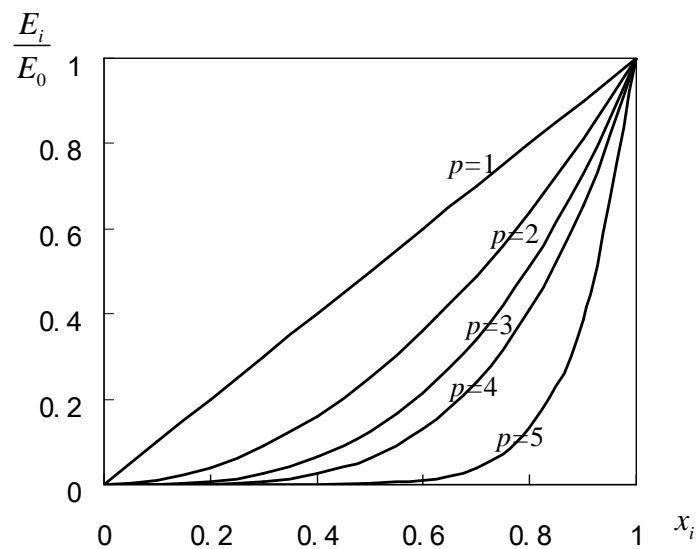


Fig.3.1 Relative stiffness with respect to density variable for the SIMP material model for the different penalization factors p

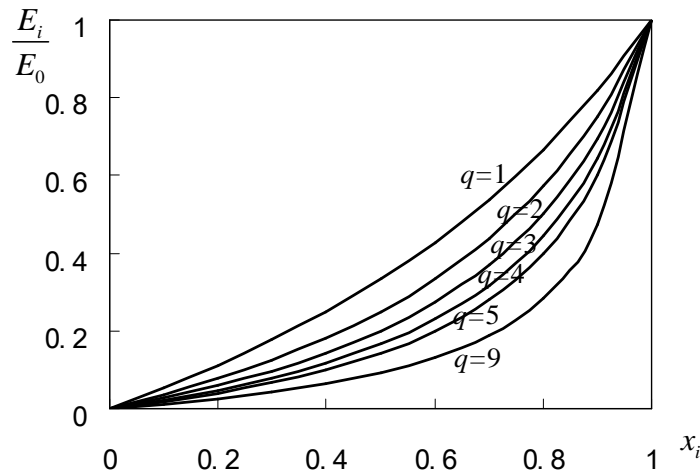
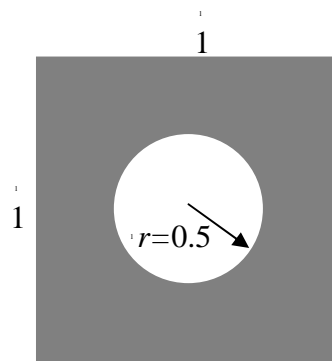


Fig.3.2 Relative stiffness with respect to density variable for the RAMP material model for the different penalization factors q

In a finite element context, the use of SIMP and RAMP material model leads to a mesh-dependence. To prevent numerical instabilities of the iterative procedure, a few of control methods reviewed in chapter 1 are proposed. We have mainly adopted two of them in our work: the perimeter control and the sensitivity filtering.

(1) Perimeter control

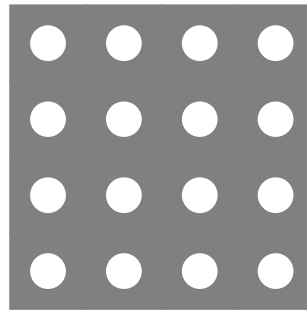
In the perimeter control scheme, a global constraint on the perimeter of structural boundaries is imposed. The perimeter of boundaries of a structure is the summation of length of boundaries between solid and void in the 0-1 topology optimization problem. It is obvious from an example as seen in Fig. 3.3 that the perimeter constraint can limit the number of holes in the domain (Bendsøe [2003]). Assuming the unit thickness of the domain, V is the volume and P is the perimeter of the internal holes. For the fixed volume, the number of holes decreases with the perimeter becoming small.



$$V = 1 - \pi \cdot 0.5^2 = 0.2146$$

$$P = 2\pi \cdot 0.5 = 3.1416$$

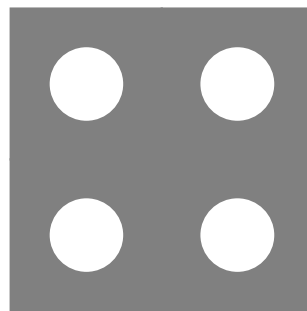
(a)



$$V = 1 - 4 \cdot \pi \cdot \left(\frac{0.5}{2}\right)^2 = 0.2146$$

$$P = 4 \cdot 2\pi \cdot \frac{0.5}{2} = 6.2832$$

(b)



$$V = 1 - 16 \cdot \pi \cdot \left(\frac{0.5}{4}\right)^2 = 0.2146$$

$$P = 16 \cdot 2\pi \cdot \frac{0.5}{4} = 12.5664$$

(c)

Figure 3.3 An example for explaining the perimeter control

Suppose that x_i and x_j are the values of the density variable on the each side of an element edge or interface in the discretized structure, and then the total perimeter is given by

$$P(X) = \sum_{k=1}^K l_k |x_i - x_j| \quad (3.9)$$

When $x_i=x_j$, the perimeter function is non-differentiable, the approximate expression of Eq. (3.9) can be formulated as:

$$P(X) = \sum_{k=1}^K l_k \left(\sqrt{(x_i^2 - x_j^2) + \varepsilon^2} - \varepsilon \right) \quad (3.10)$$

where K is the total number of element interfaces. l_k denotes the edge length for 2D or the interface area for 3D of the k -th interface between adjacent elements i and j . The symbol ε is an artificial smoothing parameter with positive small value that guarantees the differentiability of the perimeter function. In the optimization problem, the constraint $P(X) \leq \bar{P}$ is treated with an interior penalty method. The upper bound \bar{P} with the gradual relaxation controls jumps of material density variations at all adjacent elements.

The sensitivity in Eq. (3.10) is expressed as follows:

$$\frac{\partial P}{\partial x_i} = \sum_{k=1}^K l_k \frac{x_i - x_j}{\sqrt{(x_i - x_j)^2 + \varepsilon^2}} \quad (3.11)$$

Obviously, the perimeter function is non-monotonous because its first-order partial derivative may be either positive or negative depending upon values of design variables. A variant perimeter constraint of quadratic form is proposed here to restrict variations of element densities over the whole design domain (Zhang [2003]).

$$P(X) = \sum_k l_k (x_i - x_j)^2 \leq \bar{P} \quad (3.12)$$

Sun (Sun [2006]) implemented this approach and proposed a generalized perimeter control method for irregular finite elements.

(2) Sensitivity filtering

Getting inspiration from filtering technique in image processing, filtering of design sensitivities in the each iteration of topology optimization process can efficiently control the checkerboard phenomenon and ensure mesh-independency. This approach is to modify the design sensitivity of a specific element, based on a weighted average of the element sensitivities in a fixed neighborhood. Such a filter is purely heuristic. The scheme works by

modifying the element sensitivities of the objective function as follows (Bendsøe [2003]):

$$\frac{\partial \widehat{f}}{\partial \rho_k} = (\rho_k)^{-1} \frac{1}{\sum_{i=1}^N \widehat{H}_i} \sum_{i=1}^N \widehat{H}_i \rho_i \frac{\partial f}{\partial \rho_i} \quad (3.13)$$

The convolution operator (weight factor) \widehat{H}_i is written as:

$$\widehat{H}_i = r_{\min} - \text{disk}(k, i), \quad \{i \in N \mid \text{dist}(k, i) \leq r_{\min}\}, k = 1, \dots, N \quad (3.14)$$

The operator $\text{dist}(k, i)$ is defined as the distance between the center of element k and the center of element i . The convolution operator \widehat{H}_i is zero outside the filter area. The convolution operator for element i is seen to decay linearly with the distance from element k . In this fashion, an element with low sensitivity obtains a much higher sensitivity after the modification if the sensitivities of elements within the zone of radius r_{\min} of this element have higher values. This guarantees that wherever a member is formed during the optimization process, the radius of the member is in general not below r_{\min} . It is worthwhile noting that the filtering sensitivity converges to the original sensitivity when r_{\min} approaches zero and that all sensitivities will be equal (resulting in an even distribution of material) when r_{\min} approaches infinity.

3.3 Topological design of 3D material microstructure

3.3.1 Optimization algorithm

A general optimization problem with constraints is stated as follows:

$$\begin{aligned} & \text{Find } X = (x_1, x_2, \dots, x_n) \\ & \text{Min}_X g_0(X) \\ & \text{s.t. } g_j(X) \leq g_j^{\max} \quad j = 1, \dots, m \\ & \quad \underline{x}_i \leq x_i \leq \bar{x}_i \quad i = 1, \dots, n \end{aligned} \quad (3.15)$$

Most of the time, this optimization problem is non-linear and non-explicit with respect to the design variables. In order to efficiently solve this problem, explicit approximations of the actual functions, that are, explicit sub-problems are built to replace the real optimization problem. These sub-problems are obtained by expanding the objective function and the constraints in the neighborhood of a given design point. In our work, we adopt the optimal solver CONLIN (CONvex LINEarization) (Fleury [1989]) with a dual sub-iteration scheme developed by Fleury (Fleury [1989]) and Zhang (Zhang [1997];

2003]). The convex linear approximation is based on first order derivatives as follows.

$$\bar{g}_j(X) \approx g_j(X^k) + \sum_i^+ \frac{\partial g_j(X^k)}{\partial x_i} (x_i - x_i^k) - \sum_i^- \frac{\partial g_j(X^k)}{\partial x_i} (x_i^k)^2 \left(\frac{1}{x_i} - \frac{1}{x_i^k} \right) \quad (3.16)$$

where $\bar{g}_j(X)$ ($j=0,1,\dots,m$) are the explicit form of original functions, symbols \sum_i^+ and \sum_i^- denote the summation over the terms with positive and negative first order derivatives, respectively. X^k designate the developing point.

To prevent numerical instabilities in topology optimization, a variant perimeter constraint of quadratic form, see Eq. (3.12), is used in the construction of each explicit optimization sub-problem.

3.3.2 Optimal model

Here, topology optimization of the material microstructure is performed to find the maximum stiffness and the optimal heat transfer path along desired directions. Homogenization method is firstly applied to achieve the effective elastic matrix and thermal conductivity matrix of 3D unit cells. The formulation of calculating homogenized elastic constants shown as follows has been derived in chapter 2:

$$E_{ijkl}^H(x) = \frac{1}{|Y|} \int_Y \left(E_{ijkl} - E_{ijpm} \frac{\partial \chi_p^{kl}}{\partial y_m} \right) dY \quad (3.17)$$

In order to solve the thermal conductivity problem of cellular materials composed of periodically repetitive microstructure cells, the temperature field with the double scale asymptotic expansion can also be written as:

$$T^\varepsilon = T^0(x, y) + \varepsilon T^1(x, y) + \varepsilon^2 T^2(x, y) + \dots \quad (3.18)$$

The heat conduction is similar to the elasticity problem. Starting from the equation of heat conduction in the general 3D case, the equation of heat balance is obtained.

$$-\frac{\partial}{\partial x_i} \left[K_{ij}^H \frac{\partial T(x)}{\partial x_j} \right] = f_i \quad (3.19)$$

where K_{ij}^H are the effective thermal conductivities depending on the following equation.

$$K_{ij}^H = \frac{1}{|Y|} \int_Y \left(K_{ij} - K_{ip} \frac{\partial \phi^j}{\partial y_p} \right) dY \quad (3.20)$$

wherein ϕ^j is the solution of the partial differential equation with the periodic boundary

conditions as follows:

$$\frac{\partial}{\partial y_p} \left[K_{ij} - K_{ip} \frac{\partial \phi^j}{\partial y_p} \right] = 0 \quad \text{on } Y \quad (3.21)$$

The objective functions are selected to be the primary diagonal quantities or a weighted combination of them. Making use of the abbreviation $ij \rightarrow I$ for the 3D problem defined by $11 \rightarrow 1$, $22 \rightarrow 2$, $33 \rightarrow 3$, $12 \rightarrow 4$, $23 \rightarrow 5$ and $31 \rightarrow 6$.

The optimization model for the maximum stiffness is stated as follows:

$$\begin{aligned} \max \quad & f = \sum_{k=1}^6 w_k E_{kk}^H(x_t) \\ \text{subject to: } & V(x) = \sum_{t=1}^n x_t v_t \leq \bar{V}, \\ & TV_2(x) = \sum_{k=1}^M l_k (x_i - x_j)^2 \leq \bar{P} \\ & 0 < \delta \leq x_t \leq 1 \quad t = 1, n \end{aligned} \quad (3.22)$$

The optimization model for the optimal heat conduction path is similarly written as:

$$\begin{aligned} \max \quad & f = \sum_{k=1}^3 w_k K_k^H(x_t) \\ \text{subject to: } & V(x) = \sum_{t=1}^n x_t v_t \leq \bar{V}, \\ & TV_2(x) = \sum_{k=1}^M l_k (x_i - x_j)^2 \leq \bar{P} \\ & 0 < \delta \leq x_t \leq 1 \quad t = 1, n \end{aligned} \quad (3.23)$$

where E_{kk}^H are the effective elastic constants and K_k^H are the effective thermal conductivities. w_k is the weighted coefficient ($\sum w_k = 1$). Suppose a unit cell is discretized into a finite element model. Design variables x_t ($t = 1, n$) are assigned to each element as pseudo-densities. Following the SIMP law, the element thermo-mechanical properties depend upon the density variable in an exponential form.

$$E_t = x_t^p \bar{E}_t \quad (3.24)$$

$$K_t = x_t^p \bar{K}_t \quad (3.25)$$

where \bar{E}_t and \bar{K}_t respectively designate the nominal stiffness matrix and thermal conductivity matrix of element t with solid material, the exponent p in the SIMP law is

often chosen to be $p=3$ or 4 for the penalty. $V(x)$ is the total material volume limited by its upper bound \bar{V} over the unit cell. A small value of $\delta=10^{-5}$ is used to avoid the singularity of the elementary stiffness matrix during optimization. TV_2 denotes the total variation (TV) control used to regularize the solid-void pattern and the checkerboard control of the material layout.

3.3.3 Sensitivity analysis

After evaluation of the elastic properties of microstructure cells by finite element computation of homogenization problem, the sensitivity of objective functions with respect to the pseudo-density design variables x_t ($t=1, n$) have to be solved before carrying out the optimization step. From Eq. (3.22) and Eq. (3.23), the sensitivity of objective function is actually the sensitivity of effective properties with respect to design variables.

Starting from Eq. (3.17), the sensitivity of effective elasticity tensor components with respect to the design variables can be calculated as:

$$\frac{\partial E_{ijkl}^H}{\partial X} = \frac{1}{|Y|} \int_Y \left(\frac{\partial E_{ijkl}}{\partial X} - \frac{\partial}{\partial X} \left(E_{ijpm}^e \frac{\partial \chi_p^{kl}}{\partial y_m} \right) \right) dY \quad (3.26)$$

After the finite element discretization, the above equation can be rewritten in the following form:

$$\begin{aligned} \frac{\partial E_{ijkl}^H}{\partial x_t} &= \frac{1}{V} \sum_{e=1}^n \left(\frac{\partial E_{ijkl}^e}{\partial x_t} - \frac{\partial}{\partial x_t} \left(E_{ijpm}^e \boldsymbol{\varepsilon}_{pm}^{ekl} \right) \right) \nu_e \\ &= \frac{\nu_t}{V} \frac{\partial E_{ijkl}^t}{\partial x_t} - \frac{1}{V} \sum_{e=1}^n \left(\frac{\partial E_{ijpm}^e}{\partial x_t} \boldsymbol{\varepsilon}_{pm}^{ekl} + E_{ijpm}^e \frac{\partial \boldsymbol{\varepsilon}_{pm}^{ekl}}{\partial x_t} \right) \nu_e \\ &= \frac{\nu_t}{V} \left(\frac{\partial E_{ijkl}^t}{\partial x_t} - \frac{\partial E_{ijpm}^t}{\partial x_t} \boldsymbol{\varepsilon}_{pm}^{tkl} \right) - \frac{1}{V} \sum_{e=1}^n E_{ijpm}^e \frac{\partial \boldsymbol{\varepsilon}_{pm}^{ekl}}{\partial x_t} \nu_e \end{aligned} \quad (3.27)$$

From Eq. (3.24),

$$\frac{\partial E_t}{\partial x_t} = \frac{p}{x_t} E_t \quad (3.28)$$

So the sensitivity formulation can be expressed as:

$$\begin{aligned} \frac{\partial E_{ijkl}^H}{\partial x_t} &= \frac{\nu_t}{V} \frac{p}{x_t} \left(E_{ijkl}^t - E_{ijpm}^t \boldsymbol{\varepsilon}_{pm}^{tkl} \right) - \frac{1}{V} \sum_{e=1}^n E_{ijpm}^e \frac{\partial \boldsymbol{\varepsilon}_{pm}^{ekl}}{\partial x_t} \nu_e \\ &= \frac{\nu_t}{V} \frac{p}{x_t} \left(E_{ijkl}^t - \boldsymbol{\sigma}_{pm}^{tkl} \right) - \frac{1}{V} \sum_{e=1}^n E_{ijpm}^e \frac{\partial \boldsymbol{\varepsilon}_{pm}^{ekl}}{\partial x_t} \nu_e \end{aligned} \quad (3.29)$$

Similarly from Eq. (3.20) and Eq. (3.25), the sensitivity of effective thermal conductivity with respect to the design variables after the finite element discretization can be calculated as:

$$\begin{aligned}
\frac{\partial K_{ij}^H}{\partial x_t} &= \frac{1}{|Y|} \int_Y \left(\frac{\partial K_{ij}}{\partial x_t} - \frac{\partial}{\partial x_t} \left(K_{ip} \frac{\partial \phi^j}{\partial y_p} \right) \right) dY \\
&= \frac{1}{V} \sum_{e=1}^n \left(\frac{\partial K_{ij}^e}{\partial x_t} - \frac{\partial}{\partial x_t} \left(K_{ip}^e \frac{\partial \phi^j}{\partial y_p} \right) \right) \cdot v^e \\
&= \frac{v_t}{V} \left(\frac{\partial K_{ij}^t}{\partial x_t} - \frac{\partial K_{ip}^t}{\partial x_t} \cdot \frac{\partial \phi^j}{\partial y_p} \right) - \frac{1}{V} \sum_{e=1}^n K_{ij}^e \frac{\partial}{\partial x_t} \left(\frac{\partial \phi^j}{\partial y_p} \right) \cdot v^e \\
&= \frac{v_t}{V} \frac{P}{x_t} \left(K_{ij}^t - K_{ip}^t \frac{\partial \phi^j}{\partial y_p} \right) - \frac{1}{V} \sum_{e=1}^N K_{ij}^e \frac{\partial}{\partial x_t} \left(\frac{\partial \phi^j}{\partial y_p} \right) \cdot v^e
\end{aligned} \tag{3.30}$$

In the above formulations, V is the volume of microstructure cell and v_t is the volume of each element in the microstructure cell. The detailed microstructure design procedure is given as seen in Fig.3.4.

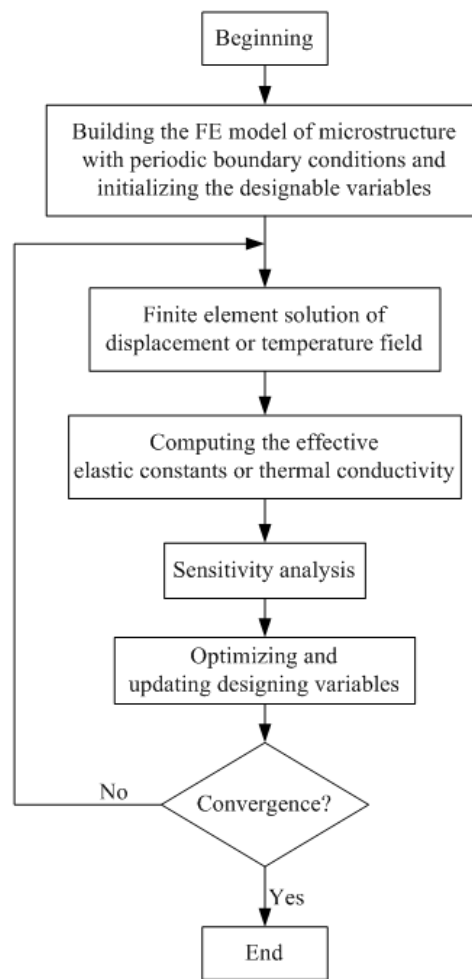


Fig.3.4 Flow chart of microstructure design procedure

3.3.4 Microstructure design for maximum stiffness

In this section, the microstructure of cellular solids will be designed with isotropic materials (elastic modulus $E=0.91GPa$ and Poisson's ratio $\mu=0.3$). The unit cell is meshed with $8 \times 8 \times 8 = 512$ elements. Suppose the volume fraction of the solid is of 50%. In the optimization procedure, the iteration begins with different distributions of element density values that satisfy the volume constraint over the unit cell.

3.3.4.1 Single objective design for the maximization of microstructure stiffness

Here, two FE models with different initial values are given. In the first model, the distribution of element density is layered symmetrically. In another model, the density variable values of eight central elements are 0.4, while others are 0.5. The distribution of element density values satisfies the volume constraint. Two completely different

configurations are obtained as shown in the Table 3.1, and the effective elastic constants of optimal microstructure with maximizing the uniaxial stiffness are seen in the Table 3.2. Obviously, the latter result is better for maximizing the uniaxial stiffness because the latter materials located along direction 1 are stiffer than the former one.

Table 3.1 Optimal configuration with maximization of uniaxial stiffness

Max E_{11}^H			
	Initial model	Optimal configuration	Optimal configuration (only with solids)
The first model			
The second model			

Table 3.2 Effective elastic constants of optimal microstructure

The first model	$E_{11}^H = 0.499499 \text{ GPa}$ $E_{22}^H = 0.499499 \text{ GPa}$ $E_{33}^H = 0.000136 \text{ GPa}$ $E_{12}^H = 0.174815 \text{ GPa}$ $E_{23}^H = 0.000039 \text{ GPa}$ $E_{13}^H = 0.000039 \text{ GPa}$
The second model	$E_{11}^H = 0.522146 \text{ GPa}$ $E_{22}^H = 0.310918 \text{ GPa}$ $E_{33}^H = 0.310918 \text{ GPa}$ $E_{12}^H = 0.113786 \text{ GPa}$ $E_{23}^H = 0.028148 \text{ GPa}$ $E_{13}^H = 0.113786 \text{ GPa}$

3.3.4.2 Multi-objective design for the maximization of microstructure stiffness

Two FE models with the same initial density distribution are also given as the above example. As we can see in the Table 3.3 and Table 3.4, both kinds of material layouts are

mainly located along diagonal directions in the design space. This illustrates that optimal results are reasonable. Note that the central part in the optimal microstructure of the second model is void. In addition the first optimal microstructure is not symmetric because of the asymmetric initial model. But, its object values are greater than the second one because the former materials distributed along diagonal directions are more. That is the reason why the former uni-axial stiffness is smaller than the latter.

Table 3.3 Optimal configuration with maximization of three shear stiffness terms

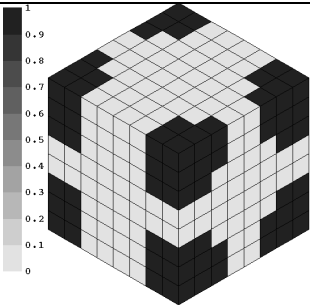
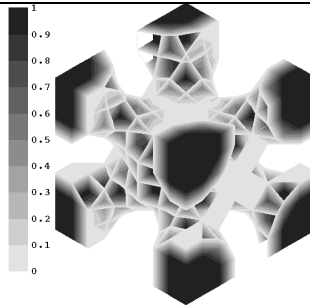
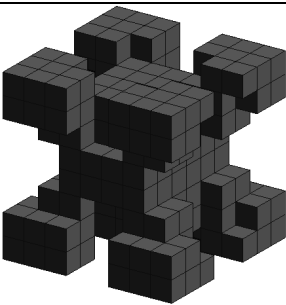
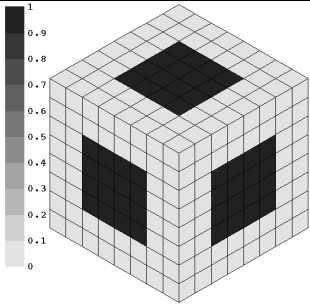
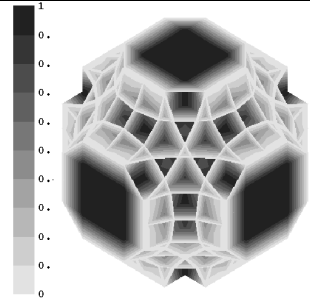
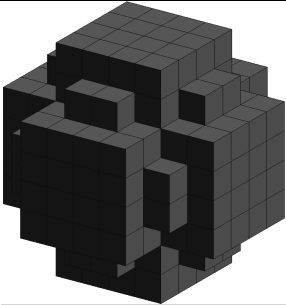
Max $E_{12}^H + E_{23}^H + E_{31}^H$			
Cases	Optimal configuration	Isoline figure	Optimal configuration (only with solids)
The first model			
The second model			

Table 3.4 Effective elastic constants of optimal microstructure

The first model	$E_{11}^H = 0.206832 \text{ GPa}$ $E_{22}^H = 0.230021 \text{ GPa}$ $E_{33}^H = 0.187013 \text{ GPa}$
	$E_{12}^H = 0.091302 \text{ GPa}$ $E_{23}^H = 0.092418 \text{ GPa}$ $E_{13}^H = 0.088311 \text{ GPa}$
The second model	$E_{11}^H = 0.264399 \text{ GPa}$ $E_{22}^H = 0.264399 \text{ GPa}$ $E_{33}^H = 0.264399 \text{ GPa}$
	$E_{12}^H = 0.079924 \text{ GPa}$ $E_{23}^H = 0.079924 \text{ GPa}$ $E_{13}^H = 0.079924 \text{ GPa}$

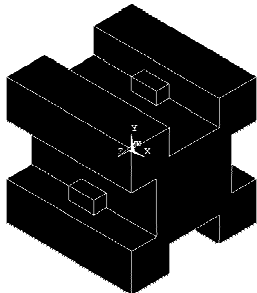
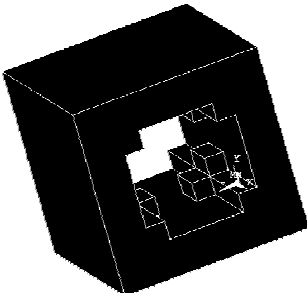
3.3.5 Microstructure design for maximum thermal conductivity

In this section, the microstructure of cellular solids will still be designed with isotropic materials (thermal conductivity of the solid part $K=1000\text{W}/(\text{m}\cdot\text{K})$). The unit cell is meshed with $10\times 10\times 10=1000$ elements.

3.3.5.1 Single objective design for the maximization of microstructure conductivity

Here, two models are given with the volume fraction 70% which have the opposite initial density distribution. That is, in the first model, density values of central elements are greater than outside elements. The second model is reversed. Therefore optimal microstructures are too completely different corresponding to the initial values. But their thermal conductivity values are close. Optimal results are shown in the Table 3.5.

Table 3.5 Maximization of single thermal conductivity

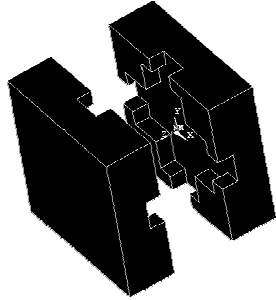
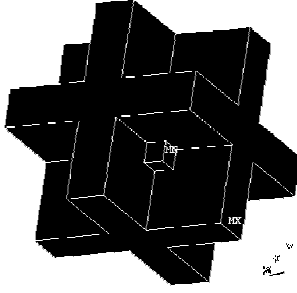
Max K_{11}^H		
Cases	Optimal configuration	Effective thermal conductivity ($\text{W}/(\text{m}\cdot\text{K})$)
The first model		$K_{11}^H = 690.6766$ $K_{22}^H = 511.0676$ $K_{33}^H = 511.0676$
The second model		$K_{11}^H = 689.7031$ $K_{22}^H = 528.4172$ $K_{33}^H = 528.4172$

3.3.5.2 Multi-objective design for the maximization of microstructure conductivity

In this section, uniaxial thermal conductivities terms defined in multi-directions are

maximized simultaneously with equal weighting coefficients. The volume fraction is 50%. Optimal microstructures are given in the Table 3.6. Because the thermal conductivity has no coupled terms, the material layout is mainly aligned to symmetrical axes (as shown in the Table 3.6), which corresponds to the heat transfer rule.

Table 3.6 Maximization of multiple thermal conductivities

Max	$K_{11}^H + K_{22}^H$	$K_{11}^H + K_{22}^H + K_{33}^H$
Optimal configuration		
Effective thermal Conductivity (W/(m·K))	$K_{11}^H = 465.0967$ $K_{22}^H = 465.0967$ $K_{33}^H = 2.292E-05$	$K_{11}^H = 389.898$ $K_{22}^H = 389.898$ $K_{33}^H = 389.898$

3.4 Summary

In this chapter, combining the finite element and the homogenization method for the numerical prediction of the effective material properties, we have applied the topology optimization techniques to maximize the stiffness and thermal conductivity of 3D unit cells. Maximization of uniaxial and multi-axial material properties is considered as single and multi-objective optimization problems. Optimal material layouts are successfully obtained with the given material volume fraction. In addition, a conclusion is drawn that the initial layout of the unit cell has a great effect on the optimal topology, which illustrates that the solution of topology optimization is not unique when the microstructure is designed with the homogenization method. That is also the local optimization which we often meet. In this part, the local optimization appears because the different initial models are given. In future works, other methods can be pursued for the global optimization, including the exact methods and heuristic strategies.

4. Topology optimization of periodic cellular solids

In this chapter, an integrated topology optimization procedure is developed for the global stiffness maximization of square, cyclic-symmetry and cylindrical cellular solids. To retain the structural periodicity and reduce the computational time, superelement (SE) and design variable linking techniques are introduced to characterize the RVE layout. The topology optimization problem is solved using the dual optimization algorithm. In addition, the polar moments of inertia of the optimal cyclic-symmetry structures are calculated and compared with the triangular subcells and foam cores.

4.1 Introduction

As reviewed in section 1.1.1 of chapter 1, many researches have been focused on cellular solids (Gibson and Ashby [1997]; Gibson [2005]; Evans et al. [2001]) in recent years. This is a kind of lightweight structures that can be classified into two types according to the cell characteristics. One is regular such as the hexagonal honeycomb cell; the other is irregular such as the foam-like cell. Actually, honeycomb and sandwich are available for the marketing (e.g., see <http://www.hexcel.com/markets>) and cellular solids have been used in panel structures of the aircraft, satellite, boat and aero-engine components. This is a research front across the material and structure disciplines. From the design point of view, the key issue is to optimize the cell shape, size and topology in order to maximally exploit remarkable performances, e.g., impacting resistance, capacity of energy absorption, sound and heat insulation under specific loading conditions.

At present, the RVE topology design of cellular solids is mainly developed for the optimization of material effective properties and macro-structural performances. Sigmund (Sigmund [1994; 1997; 2000]) obtained material microstructure configurations with the extreme thermal expansion coefficients and the negative Poisson's ratio by optimizing the distribution of two or three isotropic material phases. Neves (Neves [2000]) carried out the topological optimization of the periodic linear microstructure for the maximization of shear and bulk moduli. Yi (Yi [2000]) implemented the optimal design of microstructures of viscoelastic composites following the inverse homogenization approach. The objective function was defined as a combination of storage modulus, loss modulus, and loss tangent at operating frequencies with linear and exponential weighting factors on each component in order to improve stiffness and damping characteristics. Another development of designing the RVE configuration concerns the optimization of macrostructural performances, e.g., stiffness, frequency, buckling load and so on. Assuming that the macrostructure is made of microstructures of a single material phase with a known volume fraction, Fujii (Fujii [2001]) and Rodrigues (Rodrigues [2002]) studied the maximization of macrostructural stiffness. Based on the scale-related method and the proposed design element (DE) concept, Zhang and Sun (Zhang and Sun [2006]) carried out the RVE topological optimization for the stiffness maximum and revealed the scale effect of 2D cellular structures in a systematical way as opposed to the homogenization method. Takano and Zako (Takano and Zako [2000]) proposed a design methodology of graded

microstructures of heterogeneous materials for the emergence of macroscopic function. The microstructure design of a plate was performed and the macroscopic deflection was controlled under the condition of the temperature distribution. Nelli Silva (Nelli Silva [1998]) developed the optimal design of piezocomposite microstructures using the topology optimization techniques and the homogenization theory. The problem consisted in finding the distribution of the material and void phases in a periodic unit cell that optimizes the performance characteristics of the piezocomposite subjected to constraints such as property symmetry and stiffness. Guest and Prevost (Guest and Prevost [2006]) optimized multifunctional porous material microstructures for stiffness and fluid permeability.

However, when the RVE configuration is optimized, the number of RVEs that form the cellular solid and the number of finite elements in each RVE affect directly the computing scale and computational efficiency in the iterative design of the whole structure. In the earlier work of Yang and Lu (Yang and Lu [1996]), the superelement method was employed when a structure was locally designed by topology optimization. The fixed non-designable domain and the designable part were modeled as two superelements. The benefit is that only the stiffness matrix associated with the designable part of the structure needs to be reformulated each iteration.

In this chapter, the introduction of the superelement (SE) technique relies on the fact that RVE is periodically distributed. As illustrated in the following examples of square, cyclic-symmetry and cylindrical structures, this approach can decrease the finite element computation cost for the integrated design of materials and structures. Meanwhile, by means of the SIMP model, the dual solution strategy and quadratic perimeter control that are presented in chapter 3, one can achieve the topology design of RVE without the checkerboard patterns in the material layout. The results demonstrate that the scale effect of the RVE upon the optimal configuration is important and the obtained equivalent torsional resistances of the optimal cyclic-symmetry cellular solids are more significant when compared with the results given in the literature (Wang and McDowell [2003]). Here, it is necessary to notice that although considered examples are relatively simple, they are illustrative to validate the superelement technique and the design procedure which can be used later in practical applications of cellular structures.

4.2 Representative volume element (RVE) and superelement (SE)

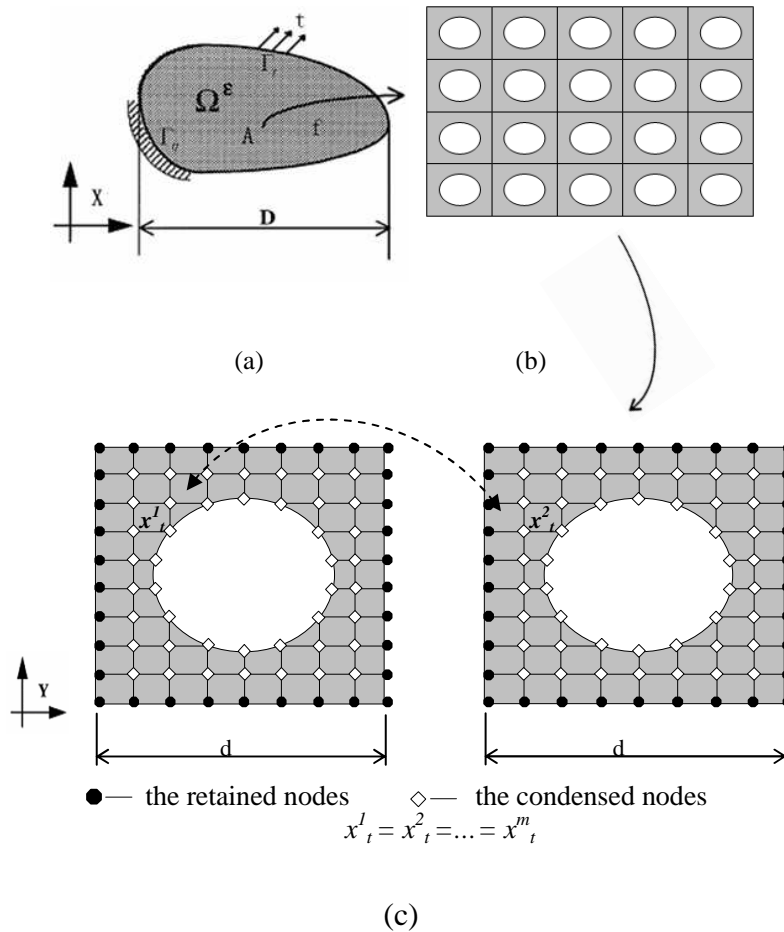


Fig.4.1 (a) Macrostructure (b) Cellular Structure

(c) Super-element (RVE-SE) with design variable linking

As shown in Fig.4.1, in a local region of a macrostructural body, cellular solids are spatially formed by a periodic repetition of a basic cell made of different or inhomogeneous materials. Suppose that the representative dimension of the microstructure, d , in the micro level y is much smaller than the representative dimension of the macrostructure, D , in the level x . Before the RVE configuration is optimized to attain the requirements of macrostructural responses, each RVE is modeled by the SE that is further discretized into finite elements. According to its periodicity, all the degrees of freedom (d.o.f.) associated with the interface connective nodes between adjacent RVE-SEs are retained including the d.o.f. of the boundary nodes on which the force and displacement loads are applied. All the others d.o.f. inside the RVE-SEs are condensed.

For a static problem of a structure, the general static finite element equation is

$$KU = F \quad (4.1)$$

The SE method consists in condensing the stiffness matrix K and the load vector F . Denote U_C and U_R to be condensed and retained d.o.f., respectively, the above equation system can be rewritten as follows:

$$\begin{bmatrix} K_{CC} & K_{CR} \\ K_{RC} & K_{RR} \end{bmatrix} \begin{bmatrix} U_C \\ U_R \end{bmatrix} = \begin{bmatrix} F_C \\ F_R \end{bmatrix} \quad (4.2)$$

where F_C and F_R are the equivalent force vectors applied on the condensed nodes and retained nodes, respectively. K_{RR} and K_{CC} are partial stiffness matrices of condensed and retained nodes, respectively.

From the first line of Eq. (4.2), the following expression is obtained:

$$U_C = K_{CC}^{-1}(F_C - K_{CR}U_R) \quad (4.3)$$

Its substitution into Eq. (4.2) results in

$$(K_{RR} - K_{RC}K_{CC}^{-1}K_{CR}) \cdot U_R = F_R - K_{RC}K_{CC}^{-1}F_C \quad (4.4)$$

The compact form is:

$$K_{RR}^* U_R = F_R^* \quad (4.5)$$

This is a reduced equation system compared to Eq. (4.1). Once the displacement vector U_R is known, the condensed displacement vector U_C will be derived from Eq. (4.3).

The advantage of integrating the SE method in topology optimization procedure is that the computational cost related to Eq. (4.5) is much less important than the cost of direct finite element analysis. Three steps are defined in the RVE-SE formulation:

- 1) Creation of the superelement for the RVE finite element model by generating the stiffness matrices of the retained and condensed nodes.
- 2) Development of the superelements by translating and rotating the RVE-SE periodically. This includes the generation of the stiffness matrix K_{RR}^* and force vector F_R^* for Eq. (4.5) and the solution of the latter for the displacement vector U_R of all retained nodes.
- 3) Recovery of the results including displacements and stresses within the RVE-SE by solving Eq. (4.3).

Before Eq. (4.4) is assembled and solved, the inverted stiffness matrices of condensed nodes are obtained. That means that a large scale problem is decomposed and simplified.

As a numerical method, the superelement technique is well adapted to the analysis of large scale structures. Especially in the topology optimization of periodic structures, much computing iterations are needed that are time-consuming. In fact, if the number of SE is small, then the number of condensed d.o.f will be bigger for each SE so that K_{CC} becomes larger and K_{RR}^* will be smaller. As a result, the creation time of SE associated with the construction of K_{CC} will increase, the time of using of SEs associated with K_{RR}^* for the solution of Eq. (4.5) will decrease and the time of recovery of SEs associated with K_{CC} will increase for each SE. However, it is observed that with the increase of the number of SE, the total computational time decreases as illustrated in Table 4.5 and Fig.4.9.

4.3 Optimal model and sensitivity analysis

Consider the topology optimization problem of the rigidity maximization of cellular solids subjected to the volume constraint. To ensure that the optimal configuration is periodic over the whole structure after optimization, the design variable linking technique is used to equalize the density variables for the finite elements having the same positions in different RVE-SEs. This connection is geometrically shown in Fig.4.1.

$$\begin{aligned}
 & \text{find } x = \{x_1, x_2, \dots, x_n\}^T \in R^n \\
 & \text{Min } C = F^T U = U^T K(x) U = \sum_{i=1}^m (U^i)^T K^i(x) U^i \\
 & \text{s.t. } K(x) U = F \\
 & \sum_{j=1}^n x_j v_j^i \leq f_v \cdot V_0^i \\
 & P(x) = \sum_{e=1}^r l_e \cdot (x_j - x_{j+1})^2 \leq \bar{P} \\
 & 0 < x_{\min} \leq x_j \leq 1 \\
 & (i = 1, 2, \dots, m \quad j = 1, 2, \dots, n)
 \end{aligned} \tag{4.6}$$

where C is the total compliance of the cellular solid, i.e., strain energy, m is the number of RVE-SEs; U^i is the displacement vector of the i -th RVE-SE; n is the finite element number in an RVE-SE, that defines also the number of design variables; x_j is the design variable of the j -th element; v_j^i is the volume of the j -th element in the i -th RVE-SE; f_v

is the prescribed volume fraction; V_0^i is the volume of the i -th RVE-SE; $P(x)$ is the quadratic perimeter constraint introduced to avoid the checkerboard effect in the RVE-SE; l_e is the interface length between adjacent elements j and $j+1$; \bar{P} is the upper limit of the perimeter constraint. Detailed explanations of $P(x)$ can be found in Ref. (Zhang and Duysinx [2003]).

In this chapter, the SIMP law is used for topology optimization. The following exponential relation holds between design variable, x_j , and the stiffness matrix, K_j^i , of the j -th finite element located in the i -th RVE-SE.

$$K_j^i(x_j) = (x_j)^p K_j^0 \quad (4.7)$$

where K_j^0 is the real stiffness matrix of element j before penalty, p is the penalty factor ($p=4$ in this chapter).

By differentiating Eq. (4.1), it follows that

$$\frac{\partial U}{\partial x_t} = -K^{-1} \frac{\partial K}{\partial x_t} U \quad (4.8)$$

With the above expression, the sensitivity of the objective function with respect to each variable x_j can be thus calculated as follows:

$$\frac{\partial C}{\partial x_t} = \frac{\partial}{\partial x_t} (F^T U) = F^T \frac{\partial U}{\partial x_t} = -(F^T K^{-1}) \frac{\partial K}{\partial x_t} U = -U^T \frac{\partial K}{\partial x_t} U \quad (4.9)$$

As only the element t is concerned with x_t , the following expression can be derived from Eq. (4.7)

$$\frac{\partial K_t^i(x_t)}{\partial x_t} = \frac{p}{x_t} K_t^i(x_t) \quad (4.10)$$

Thus, Eq. (4.9) can be rewritten for contributions of the elements t involved in m number of RVE-SEs.

$$\begin{aligned} \frac{\partial C}{\partial x_t} &= -U^T \frac{\partial K}{\partial x_t} U = -\sum_{i=1}^m \sum_{j=1}^n (U_j^i)^T \frac{\partial K_j^i(x_j)}{\partial x_t} U_j^i \\ &= -\sum_{i=1}^m (U_t^i)^T \frac{\partial K_t^i(x_t)}{\partial x_t} U_t^i = -\frac{p}{x_t} \sum_{i=1}^m (U_t^i)^T K_t^i(x_t) U_t^i \\ &= -\frac{p}{x_t} \sum_{i=1}^m C_t^i \end{aligned} \quad (4.11)$$

where U_j^i and C_j^i denote the displacement vector and compliance of the j -th finite

element in the i -th RVE-SE, respectively. Therefore, the compliance sensitivity of a periodic cellular solid is equal to the summation of strain energies of concerned finite elements multiplied by a negative scaling factor.

To have a global view, the whole design procedure consisting of five phases (creation of the SE, utilization of the SE, recovery of each SE, sensitivity analysis and optimization) is shown in Fig.4.2.

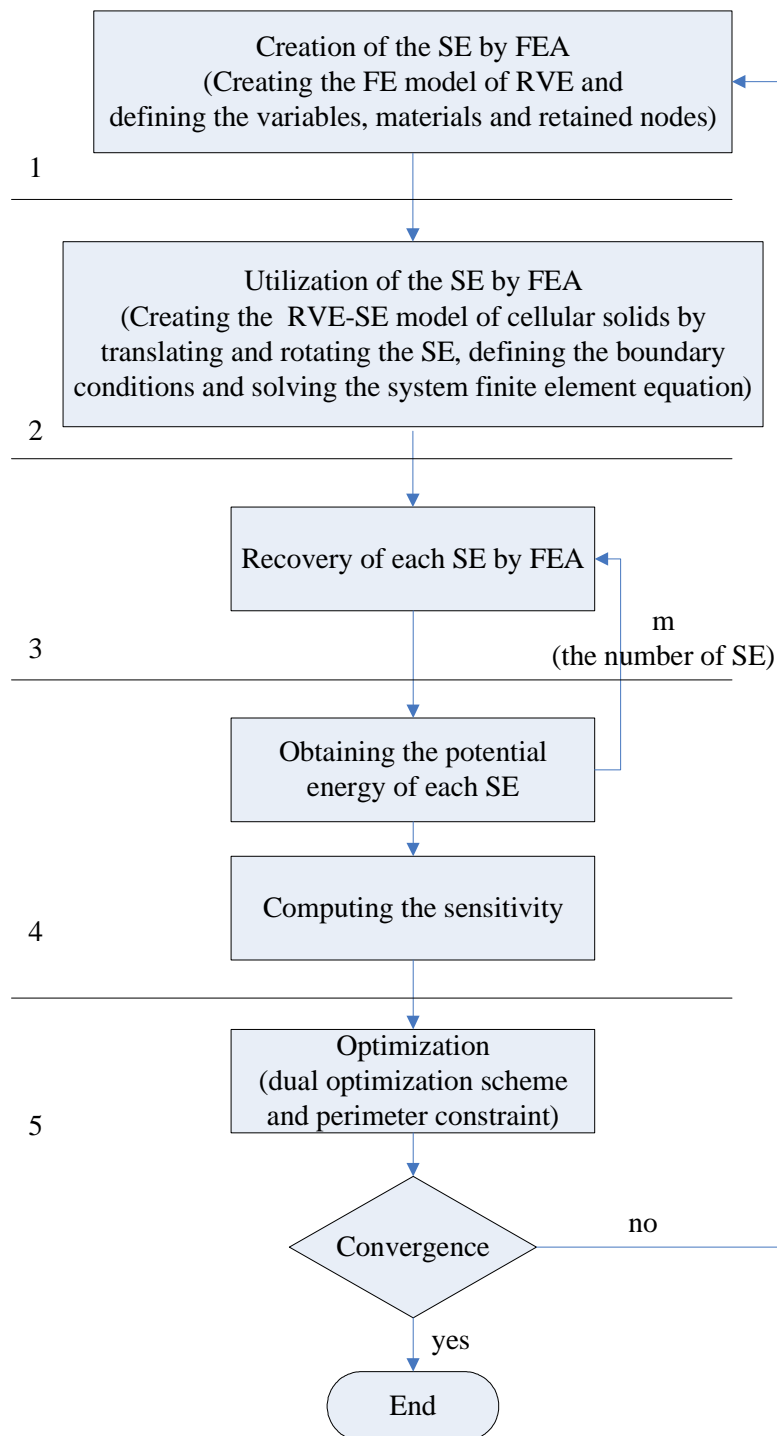


Fig.4.2 Flowchart of RVE-SE topology optimization procedure

4.4 Topology optimization of periodic cellular solids

According to the proposed design procedure, several numerical examples are studied below, including square, cyclic-symmetry, and three-dimensional cylinder cellular structures.

These cellular structures are periodically partitioned into RVEs, and each of them is modeled into an SE. With the given load conditions, the objective function is defined by the rigidity maximization of global cellular solids. The perimeter control is introduced at the level of topology optimization of the RVE-SE configuration.

4.4.1 Square structure

For this example, the solid volume fractions of 50% and 30% are considered, respectively. As shown in Fig.4.3, the design domain of the square cellular solid has a dimension $L \times L = 24 \times 24$ and the thickness is 0.1. The left side of the cellular solid is fixed and a downward force $F=100$ is applied on the right-bottom point. Young's modulus and Poisson's ratio of the material are $E=1000$ and $\nu=0.3$, respectively. Note that the units are omitted here with assumption of their consistence in this chapter. The total finite element number of the cellular solid is kept to be 57600 even when the size of each periodic RVE-SE $l \times l$ changes. It makes sure that the size of each finite element in the different size RVE-SE is same. According to the given size of RVE-SE, the square cellular structure is divided into 2×2 , 4×4 , 6×6 , 8×8 and 10×10 unit cells. The optimal configurations are shown in Table 4.1 and Table 4.2.

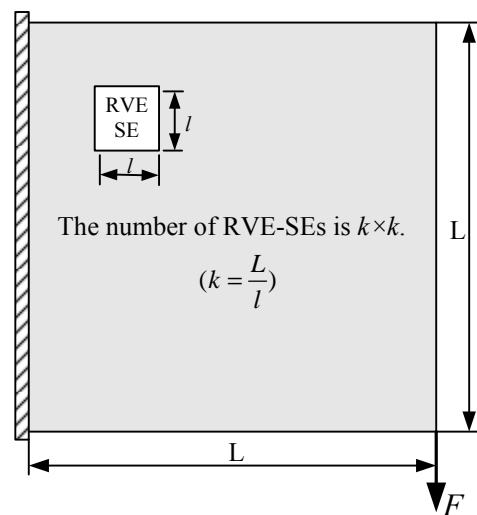
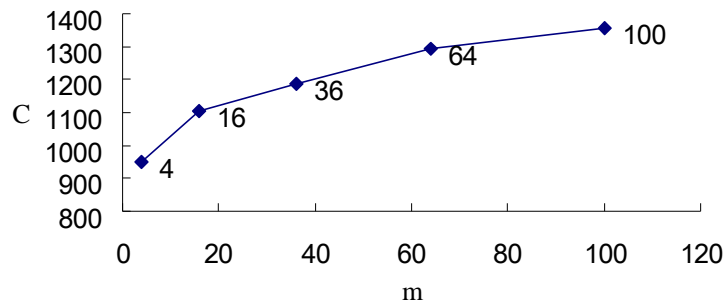


Fig.4.3 Design domain definition of square cellular solid and involved RVE-SE

a. Volume fraction 50%

Table 4.1 Optimal topology of RVE-SE with 50% volume fraction

Number of RVE-SEs (m)	10×10=100	8×8=64	6×6=36	4×4=16	2×2=4
Number of finite elements in one RVE-SE (n)	576	900	1600	3600	14400
RVE-SE configuration					
Cellular solids					
Minimum compliance	1357.28785	1292.30204	1185.08543	1106.27691	948.54478

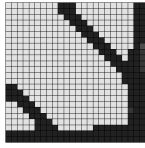
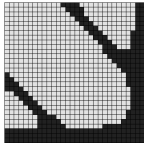
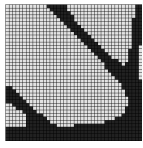
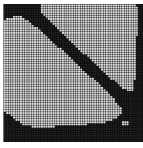
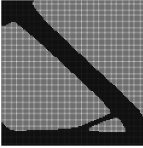
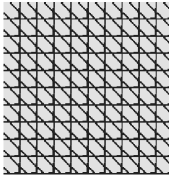
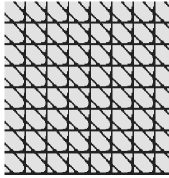
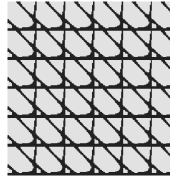
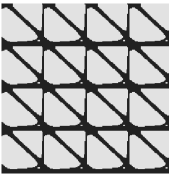



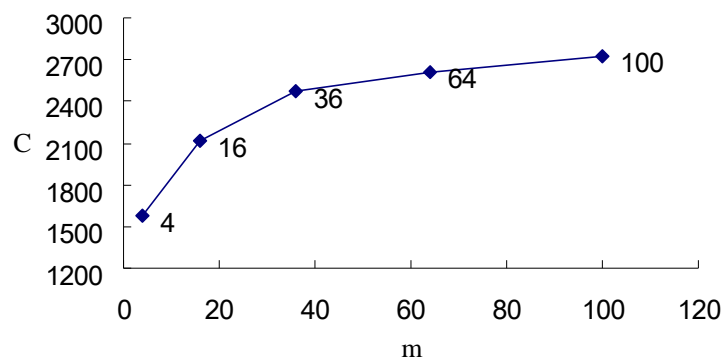
C-Compliance, m-Number of RVE-SEs

Fig.4.4 Influence of the number of RVE-SEs on structural rigidity

b. Volume fraction 30%

Table 4.2 Optimal topology of RVE-SE with 30% volume fraction

Number of RVE-SEs (m)	10×10=100	8×8=64	6×6=36	4×4=16	2×2=4
Number of finite elements in one RVE-SE (n)	576	900	1600	3600	14400
RVE-SE configuration n					
Cellular solids					
Minimum compliance	2728.63264	2605.22415	2472.74417	2115.91568	1576.5010



C-Compliance, m-Number of RVE-SEs

Fig.4.5 Influence of the number of RVE-SEs on structural rigidity

In Table 4.1 and Table 4.2, it is shown that for a fixed finite element mesh discretizing the cellular solid, the size variation of the RVE-SE will make the optimal configuration change and this scale effect is particularly important when a small number of RVE-SEs is used. As shown in Fig.4.4 and Fig.4.5, the global rigidity of cellular solids decreases with the reduction of RVE-SE dimension (increase of m) because the constraint defined by the periodic condition is more and more severe for the material layout over the design domain. In fact, the periodic arrangement of cellular cells is not always an efficient design strategy. From this example, it can be observed that since the periodicity condition enhanced by the decrease of RVE-SE dimension reduces the design space, the more reasonable distribution of materials is restricted so that the structure becomes thinner and thinner where the load is applied and hence the compliance increases with increasing cell number. Therefore, the periodicity condition has to be properly imposed on the local region of a structure where regular cells of desired configurations are needed. Meanwhile, the designed cells can change gradually from one region to another as graded materials. This point needs further investigations in the future work.

4.4.2 Cyclic-symmetry structure

4.4.2.1 Configuration design

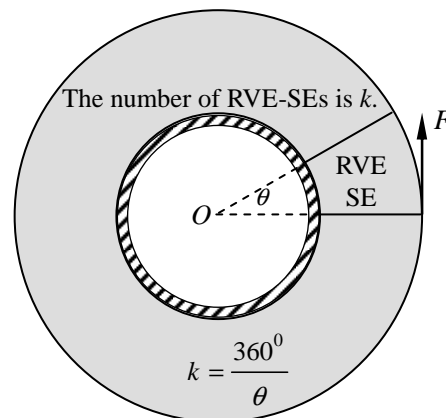


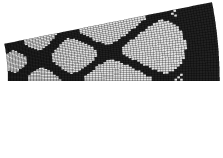
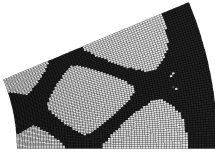
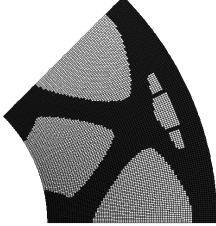
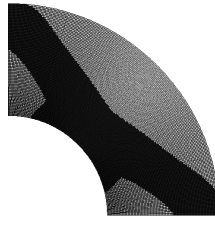
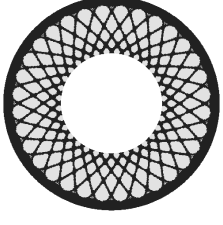
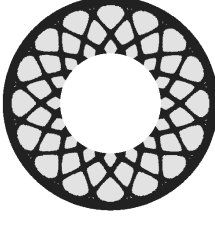
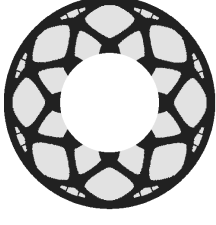
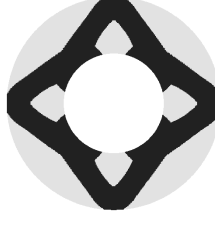
Fig.4.6 Design domain of cyclic-symmetry cellular solid and involved RVE-SE

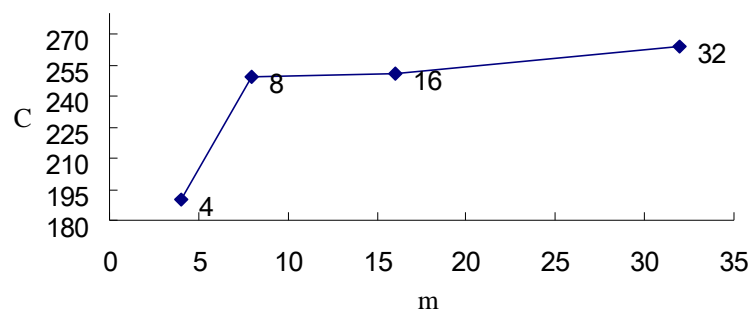
A cyclic-symmetry cellular solid is shown in Fig.4.6. The inner and outer radii are 10 and 21.25, respectively. The thickness is 0.1. Suppose the inner circle is fixed and an upward force $F=100$ is applied on the right-end point of the outer circle. Young's modulus and Poisson's ratio of the material are $E=4000$ and $\nu=0.3$, respectively. The total finite element number is 72000 for the cellular solid. The cyclic-symmetry cellular solid is divided into

different size RVE-SEs along the circumferential direction according to the different degree. The solid volume fractions of 50% and 30% are considered, respectively.

a. Volume fraction 50%

Table 4.3 Optimal topology of RVE-SE with 50% volume fraction

Number of RVE-SEs (m)	32 ($\theta = 11.25^\circ$)	16 ($\theta = 22.5^\circ$)	8 ($\theta = 45^\circ$)	4 ($\theta = 90^\circ$)
Number of finite elements in one RVE-SE (n)	2250	4500	9000	18000
RVE-SE configuration				
Cellular solids				
Minimum compliance	264.00308	251.07365	248.98018	190.33041

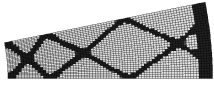
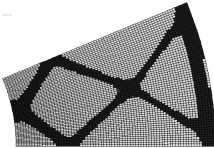
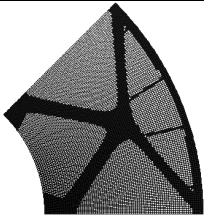
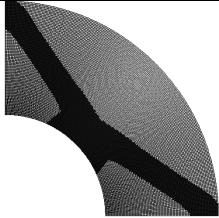
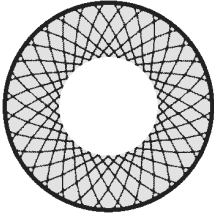
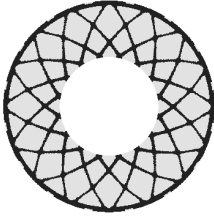
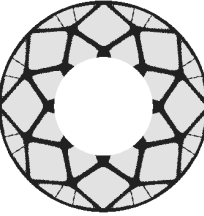
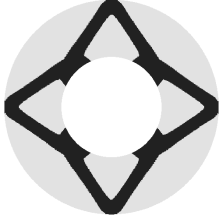


C-Compliance, m-Number of RVE-SEs

Fig.4.7 Influence of number of RVE-SEs on stiffness

b. Volume fraction 30%

Table 4.4 Optimal topology of RVE-SE with 30% volume fraction

Number of RVE-SEs (m)	32 ($\theta = 11.25^\circ$)	16 ($\theta = 22.5^\circ$)	8 ($\theta = 45^\circ$)	4 ($\theta = 90^\circ$)
Number of finite elements in one RVE-SE (n)	2250	4500	9000	18000
RVE-SE configuration				
Cellular solids				
Minimum compliance	452.28918	425.89111	406.36349	318.83632

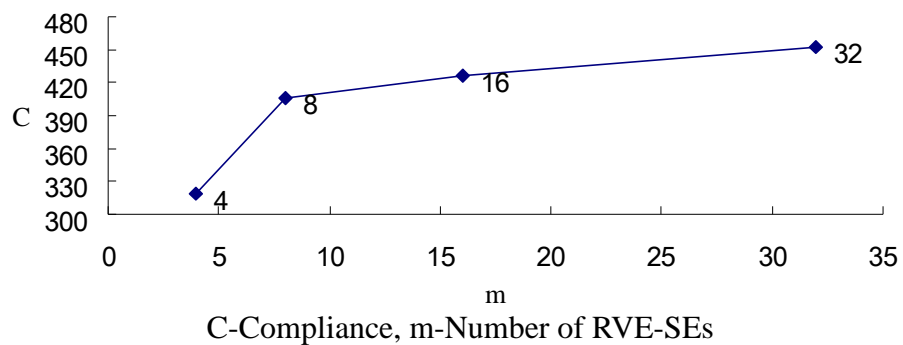


Fig.4.8 Influence of number of RVE-SEs on stiffness

Similarly, results given in Table 4.3 and Table 4.4 show a strong dependence of the optimal topology upon the size of RVE-SE. A clear distribution of materials becomes more and

more important along the outer contour when a refinement of the RVE-SE is made along the circumferential direction. In Fig.4.7 and Fig.4.8, we can see that the global rigidity of cellular solid reduces while the number of the RVE-SE increases.

Table 4.5 CPU Time during the finite element analysis (volume fraction 30%)

Number of RVE-SEs (m)	Time of creation of SE	Time of utilization of SEs	Time of recovery of SEs	Total time
32	2.20 Sec.	2.52 Sec.	$0.53 \times 32 = 16.96$ Sec.	21.68 Sec.
16	5.58 Sec.	1.52 Sec.	$0.97 \times 16 = 15.52$ Sec.	22.62 Sec.
8	12.94 Sec.	1.22 Sec.	$1.73 \times 8 = 13.84$ Sec.	28.00 Sec.
4	35.86 Sec.	1.02 Sec.	$3.55 \times 4 = 14.68$ Sec.	51.56 Sec.
Time of direct FE analysis without super-element				59.00 Sec.

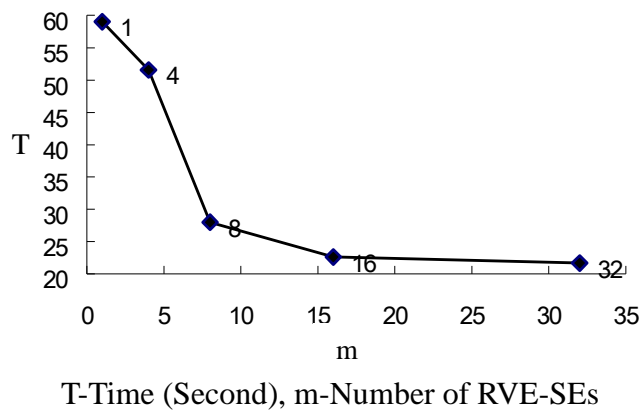


Fig.4.9 Comparison of total computing time with respect to the number of RVE-SEs

For this test, a comparison of the computational time is given in Table 4.5 and plotted in Fig.4.9. Clearly, the total time decreases when the number of RVE-SEs increases. In detail, as the decrease of the RVE-SE number leads to an increase of the finite element number in each RVE-SE, the number of both retained and condensed d.o.f. in each RVE-SE increases correspondingly. Therefore, the time used in the creation phase and the time used for the recovery of one RVE-SE become more and more important. Oppositely, the time of utilization of SEs, that depends upon the RVE-SE number is less. In contrast, if the whole

cyclic-symmetry structure is directly analyzed by the finite element method, it takes 59.00 Sec. Thus, the increase of RVE-SE number is beneficial to improve the computational efficiency.

4.4.2.2 Comparison of polar moments of inertia and torsional resistance

As it is known, the polar moment of inertia and the second moment of area are important measures of torsional and bending rigidities for a cross-sectional shape. Wang and McDowell (Wang and McDowell [2003]) considered the circular sandwich bar with triangular subcells as shown in Fig.10. The equivalent torsional and bending rigidities of the bar structure are estimated using standard analytical approaches. In our work, the topology of cyclic-symmetry structures is optimized for the maximum rigidity based on the RVE-SE method. It is therefore interesting to make a comparative study between both solutions.

(1) Comparison with the cross section of triangular subcells

In order to compute the polar moments of inertia of optimal topologies obtained with the different number of RVE-SEs, the corresponding finite element models are firstly converted into a discretized geometry models. That is to say, we keep the finite elements with solid materials and delete those with void materials. And then the retained finite elements are transformed into the discretized geometry areas. According to the definition of polar moments of inertia, the polar moments of inertia of combined areas with respect to an axis are equal to the sum of the moments of inertia of all areas with respect to the same axis. Here, the polar moments of inertia will be automatically evaluated by the ANSYS® software.

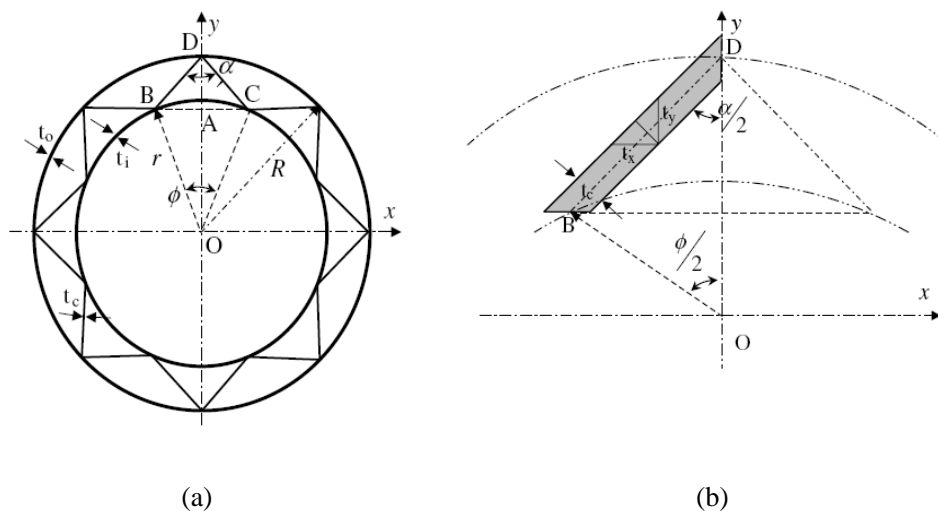


Fig.4.10 (a) A supercell with circle and triangle subcells (m=8)
 (b) A single representative cell wall for analysis

According to Wang and McDowell [2003], assume $R = 21.25$ and $r = 10$ for the outer and inner radii respectively, same as in the above cyclic-symmetry example. Here, the wall thickness is set to be $t_i = t_o = 0.1(R - r) = 1.125$. Consequently, areas of the core, outer and inner circular skins equal

$$A_c = \pi(R - t_o)^2 - \pi(r + t_i)^2 = 883.57 \quad (4.12a)$$

$$A_o = \pi R^2 - \pi(R - t_o)^2 = 146.23 \quad (4.12b)$$

$$A_i = \pi(r + t_i)^2 - \pi r^2 = 74.66 \quad (4.12c)$$

The lengths of the core, outer and inner circular skins are as follows:

$$S_c = 2m\overline{BD} = 2m\sqrt{R^2 + r^2 - 2Rr\cos\left(\frac{\phi}{2}\right)} \quad (4.13a)$$

$$S_o = 2\pi R \quad (4.13b)$$

$$S_i = 2\pi r \quad (4.13c)$$

Following Wang and McDowell [2003], the relative density of the core, ρ_c^* is given as:

$$\rho_c^* = \frac{t_c S_c}{A_c} = \frac{2mt_c\sqrt{R^2 + r^2 - 2Rr\cos\left(\frac{\phi}{2}\right)}}{\pi(R^2 - r^2)} \quad (4.14)$$

The solid volume fraction, f_v , can be then written as

$$f_v = \frac{A_o + A_i + \rho_c^* A_c}{A_c + A_o + A_i} \quad (4.15)$$

In our applications, $\rho_c^* = 0.375$ when $f_v = 50\%$, and $\rho_c^* = 0.175$ when $f_v = 30\%$. Following Wang and McDowell [2003], the polar moment of inertia of the core is calculated as

$$J_c \approx \frac{1}{S_c} 4A^2 t_c = \frac{1}{S_c} 4(mS_{OBDC})^2 t_c \quad (4.16a)$$

where $S_{OBDC} = Rr \sin \frac{\phi}{2}$. By combining Eq. (4.13a) and Eq. (4.14), Eq. (4.16a) is developed

as

$$J_c = \frac{\pi R^2 r^2 (R^2 - r^2) \rho_c^* \left(\sin \frac{\phi}{2} \right)^2}{R^2 + r^2 - 2Rr \cos \frac{\phi}{2}}, \quad \phi = \frac{2\pi}{m} \quad (4.16b)$$

Besides, the polar moments of inertia of the inside and outside face sheets are readily calculated by the membrane analogy method as

$$J_i \approx \frac{1}{S_i} 4A_i^2 t_i = 2\pi r^3 t_i = 7068.58 \quad (4.16c)$$

$$J_o \approx \frac{1}{S_o} 4A_o^2 t_o = 2\pi R^3 t_o = 67828.03 \quad (4.16d)$$

Finally, the total polar moment of inertia is $J = J_o + J_c + J_i$ and corresponding values are given in Table 4.6 for different numbers of subcells.

Table 4.6 Comparison of polar moments of inertia

Number of RVE-SEs (m)		32	16	8	4
Polar moments of inertia J ($f_v = 50\%$, $\rho_c^* = 0.375$)	Ref. (Wang and McDowell 2003)	7.6294E+04	8.0180E+04	9.2132E+04	1.1215E+05
	Optimal structures (Table 4.3)	1.6618E+05	1.6714E+05	1.6805E+05	1.3089E+05
Polar moments of inertia J ($f_v = 30\%$, $\rho_c^* = 0.175$)	Ref. (Wang and McDowell 2003)	7.5549E+04	7.7362E+04	8.2940E+04	9.2280E+04
	Optimal structures (Table 4.4)	9.3349E+04	9.8358E+04	9.5136E+04	7.8060E+04

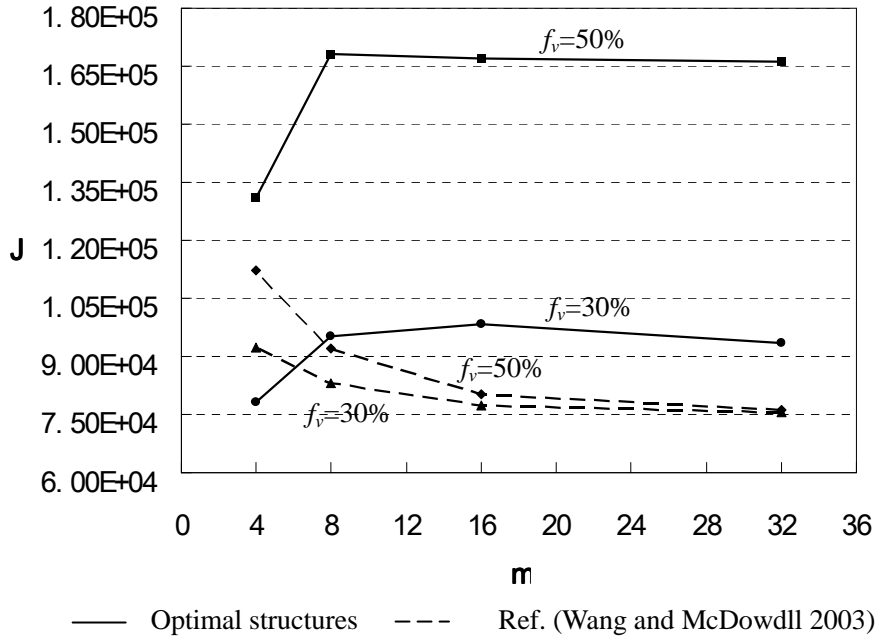


Fig.4.11 Comparison of polar moments of inertia

(2) Comparison with the foam core

Alternatively, when the core of the circular sandwich structure consists of the stochastic metallic foam, the equivalent normalized torsional resistance of metal foam can be estimated for open and closed cells (Gibson and Ashby [1997]).

- For the open cell foam core material,

$$\frac{J_c G_c^*}{R^2 r^2} = \frac{3}{16} \pi \left(\frac{R^2}{r^2} - \frac{r^2}{R^2} \right) E (\rho_c^*)^2 \quad (4.17)$$

- For the closed cell foam core material,

$$\frac{J_c G_c^*}{R^2 r^2} = \frac{3}{16} \pi \left(\frac{R^2}{r^2} - \frac{r^2}{R^2} \right) E \left(\omega^2 (\rho_c^*)^2 + (1 - \omega) \rho_c^* \right) \quad (4.18)$$

where G_c^* is the effective shear modulus of stochastic metal foam, ω is the fraction of solids (Gibson and Ashby [1997]) which is contained in the cell faces. For most stochastic foams, ω is in the range of 0.6~0.8. Here let $\omega=0.6$ for generic stochastic metal foams. ρ_c^* is the relative density of the stochastic metal foam.

- For the triangular subcells core (Wang and McDowell [2003]), the equivalent normalized torsional resistance is

$$\frac{J_c G_s}{R^2 r^2} = \pi G_s \frac{(R^2 - r^2) \rho_c^* \left(\sin \frac{\phi}{2} \right)^2}{R^2 + r^2 - 2Rr \cos \frac{\phi}{2}} \quad (4.19)$$

where G_s is the shear modulus of the solid cell wall.

Therefore, the equivalent normalized torsional resistance of circular sandwich is then

$$T_{eff} = \frac{(J_o + J_i)G}{R^2 r^2} + \frac{J_c G_c}{R^2 r^2} \quad (4.20)$$

where $G = E/(2(1+\nu))$ is the shear modulus of the inner and outer walls. Here, let $G_s = G$, $E=4000$ and $\nu=0.3$. The equivalent normalized torsional resistances are given in Table 4.7 for the three types of sandwich structures.

For the optimal configuration, the equivalent normalized torsional resistance can be calculated as

$$T_{eff} = \frac{JE}{2R^2 r^2 (1+\nu)} \quad (4.21)$$

Table 4.7 Comparison of equivalent normalized torsional stiffness

Number of RVE-SEs (m)		32	16	8	4
Equivalent torsional stiffness ($f_v=50\%$, $\rho_c^* = 0.375$)	Optimal Structures (Table 4.3)	5661.71	5694.42	5725.42	4459.39
	Ref. (Wang and McDowell 2003)	2599.316	2731.711	3138.913	3820.921
	With open cell foam core	3974.5			
	With closed cell foam core	4581.6			
Equivalent torsional stiffness ($f_v=30\%$, $\rho_c^* = 0.175$)	Optimal Structures (Table 4.4)	3180.38	4459.39	3241.26	2659.48
	Ref. (Wang and McDowell 2003)	2573.935	2635.703	2825.744	3143.955
	With open cell foam core	2861.6			
	With closed cell foam core	3371.5			

It is shown that the polar moments of inertia obtained by traditional approaches used in the literature (Wang and McDowell [2003]) decrease gradually with increasing the RVE-SE number. In comparison, the polar moments of inertia associated with the optimal topologies under the point-wise tangential load in this work are however larger and do not change monotonously. The reasons that cause different results consist in that in triangular subcells structures the mass distribution is close to the axis of rotation because configurations of unit cells are invariable when the dimensions of unit cells become small, and in the optimized structures the mass distribution of optimal topologies is the farthest to the axis of rotation when $m=8$ for $f_v=50\%$ and $m=16$ for $f_v=30\%$.

Similarly, the comparison given in Table 4.7 indicates that for $f_v=50\%$, the optimal structure has the largest torsional stiffness when the number RVE-SE is $m=8$. For $f_v=30\%$, the optimal structure attains the maximal torsional stiffness when $m=16$. In addition, it is

seen that for the current ratio of r/R , the normalized torsional stiffness of the circular sandwich obtained by the traditional approach of the literature (Wang and McDowell 2003) is smaller than that of the stochastic metal foams. Therefore, it is necessary to adopt different types of cores in terms of the ratio of r/R so as to obtain the better torsional stiffness.

4.4.3 Cyclic-symmetry with non-designable domain

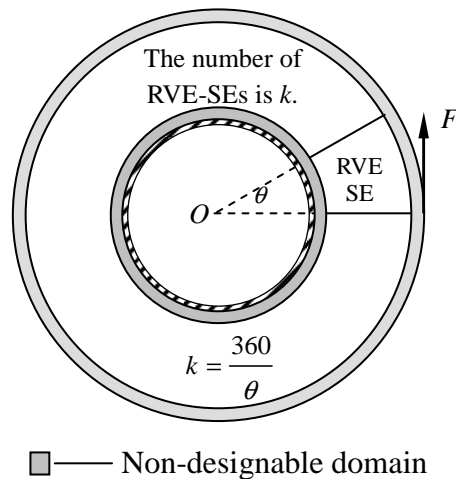


Fig.4.12 Cyclic-symmetry cellular solid and involved RVE-SE with non-designable domain

A cyclic-symmetry cellular solid with the non-designable domains in the inner and outer circle is shown in Fig.4.12. The inner and outer radii in the designable domain are 11.125 and 20.125, respectively. The width of two non-designable domains is 1.125. The thickness is 0.1. Similarly suppose the inner circle is fixed and an upward force $F=100$ is applied on the right-end point of the outer circle. Young's modulus and Poisson's ratio of the material are $E=4000$ and $\nu=0.3$, respectively. The solid volume fractions 10% and 30% in the designable domain are considered, corresponding to the solid volume fractions 28% and 44% for the whole cellular structure.

Table 4.8 Optimal topology of RVE-SE with 10% volume fraction

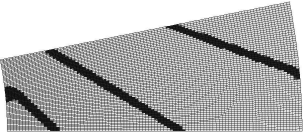
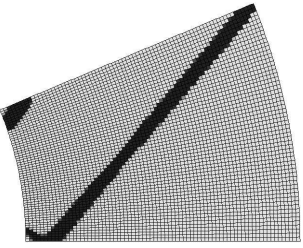
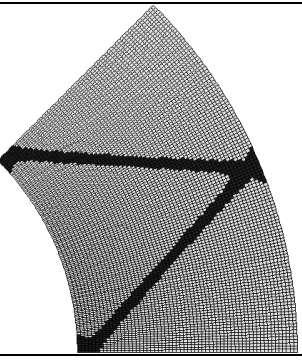
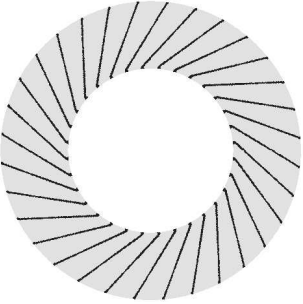
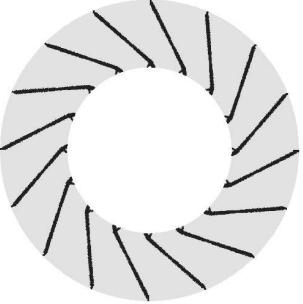
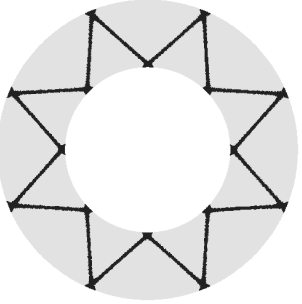
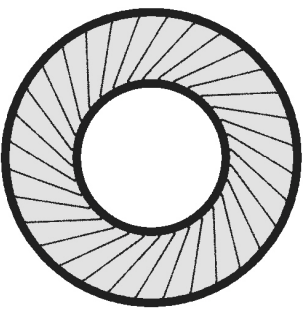
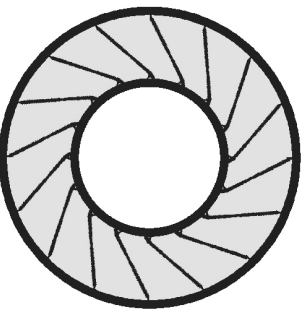
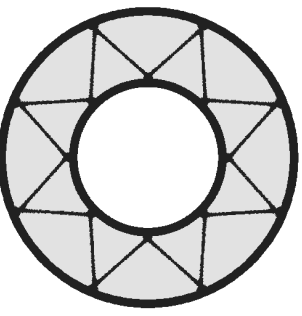
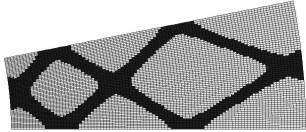
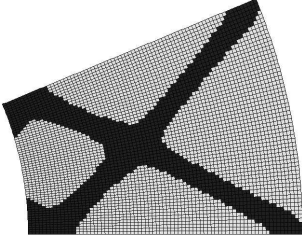
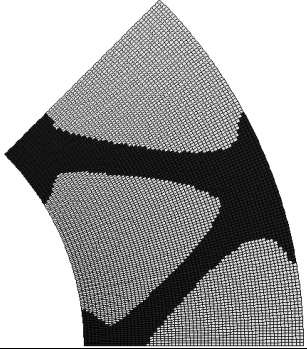
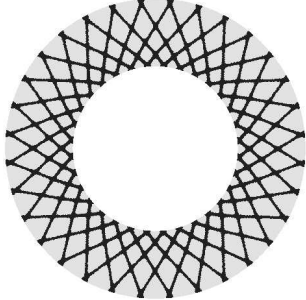
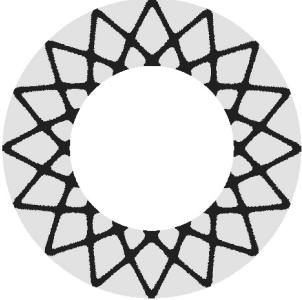

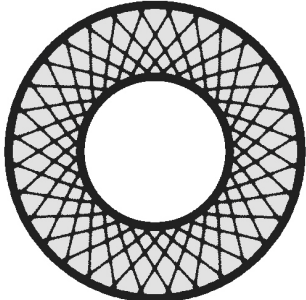
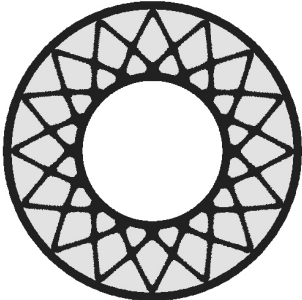
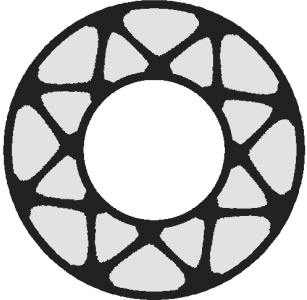
Number of RVE-SE	32 ($\theta = 11.25^\circ$)	16 ($\theta = 22.5^\circ$)	8 ($\theta = 45^\circ$)
RVE-SE configuration			
Cellular solids (designable domain)			
Whole structure			
Minimum compliance	370.38	368.65	391.43

Table 4.9 Optimal topology of RVE-SE with 30% volume fraction

Number of RVE-SE	32 ($\theta = 11.25^\circ$)	16 ($\theta = 22.5^\circ$)	8 ($\theta = 45^\circ$)
RVE-SE configuration			
Cellular solids (designable domain)			
Whole structure			
Minimum compliance	132.7	130.04	95.41

Similarly, the results given in Table 4.8 and Table 4.9 show a strong dependence of the optimal topology upon the size of RVE-SE. Compared with the examples in 4.4.2; the non-designable domains have the great influence on the optimal configurations of RVE-SE. Normally, with increasing the number of RVE-SEs or decreasing the size of RVE-SEs, the minimum compliance reduces. However, from Table 4.8 we know that the minimum compliance becomes oppositely big when the number of RVE-SEs is eight and the volume fraction is 10% in the designable domain. That illustrates that the optimal results are affected by the material amount and the non-designable domain.

4.4.4 Cylinder structure

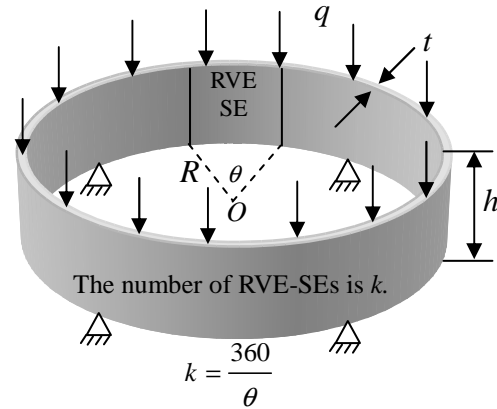


Fig.4.13 Designable domain of cylinder structure and involved RVE-SE

In this example, a cylindrical design space is shown in Fig.4.13. The inner radius R of cylinder structure is 58 and its wall thickness t is 0.5. The cylinder height h is 20. Suppose the four places distributed averagely in the bottom are fixed and every node on the top surface is acted by a downward force $q=10$ as seen in Fig.4.13. The Young's modulus and Poisson's ratio of the material are $E=1000$ and $\nu=0.3$, respectively. The total number of finite elements is 38400 for this cylindrical cellular solid. Here we use the 3D finite elements to discretize the cylinder structure. The cellular solid is averagely divided into 32, 16, 8 and 4 RVE-SEs along the circumferential direction which have the corresponding number of 3D finite elements 1200, 2400, 4800 and 9600. There are 20 finite elements along the height direction and one finite element along the wall thickness direction. The solid volume fractions of 50% and 30% are considered, respectively. The optimal configurations are seen from Fig.4.15 to Fig.4.21.

a. Volume fraction 50%

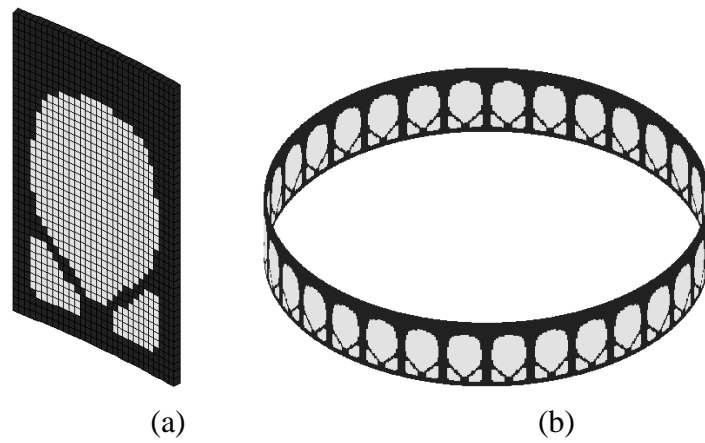


Fig.4.14 Optimal configurations with (a) Unit cell (b) Cellular cylinder with 32 unit cells

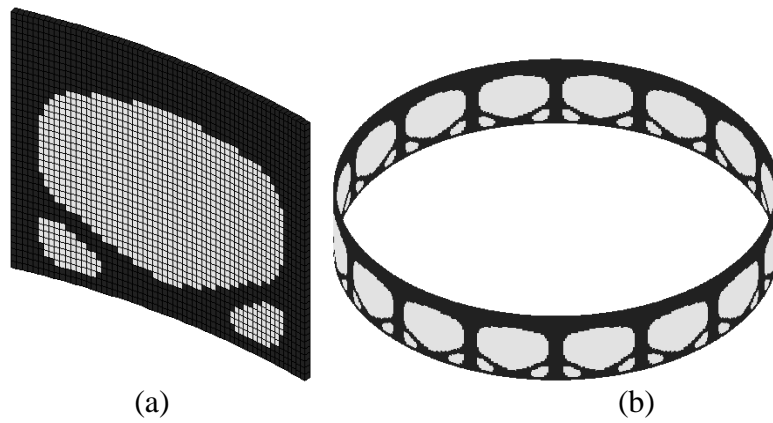


Fig.4.15 Optimal configurations with (a) Unit cell (b) Cellular cylinder with 16 unit cells

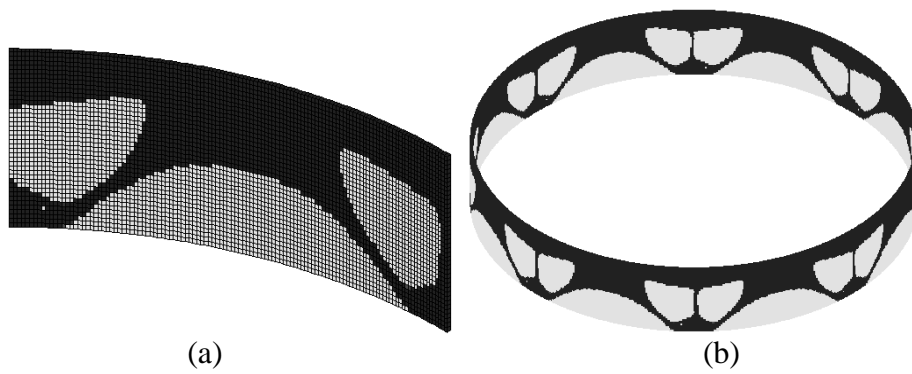


Fig.4.16 Optimal configurations with (a) Unit cell (b) Cellular cylinder with 8 unit cells

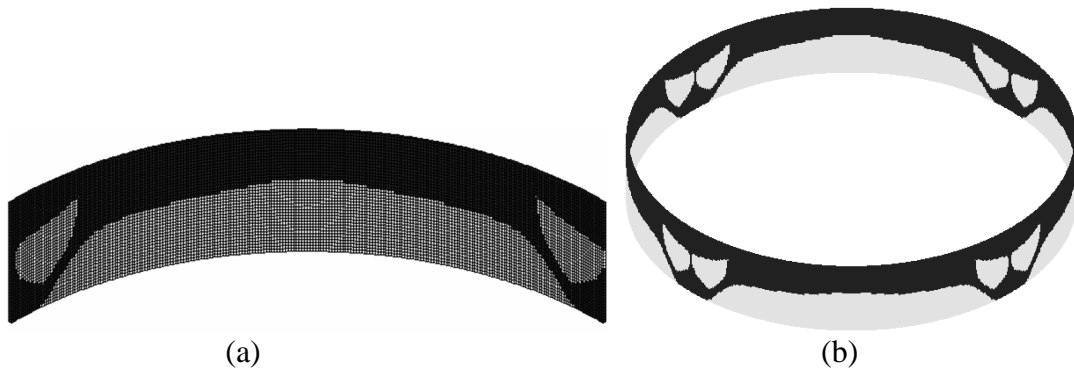


Fig.4.17 Optimal configurations with (a) Unit cell (b) Cellular cylinder with 4 unit cells

b. Volume fraction 30%

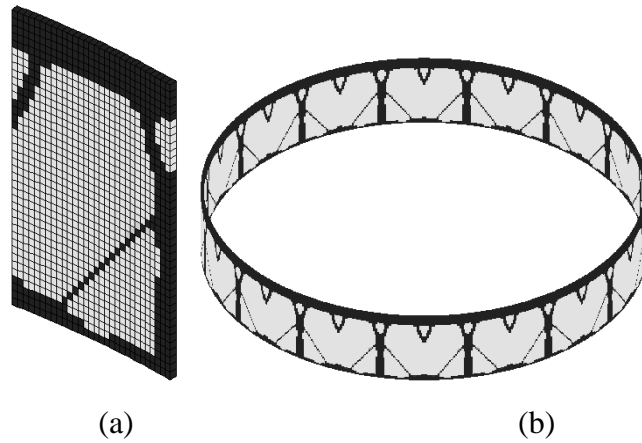


Fig.4.18 Optimal configurations with (a) Unit cell (b) Cellular cylinder with 32 unit cells

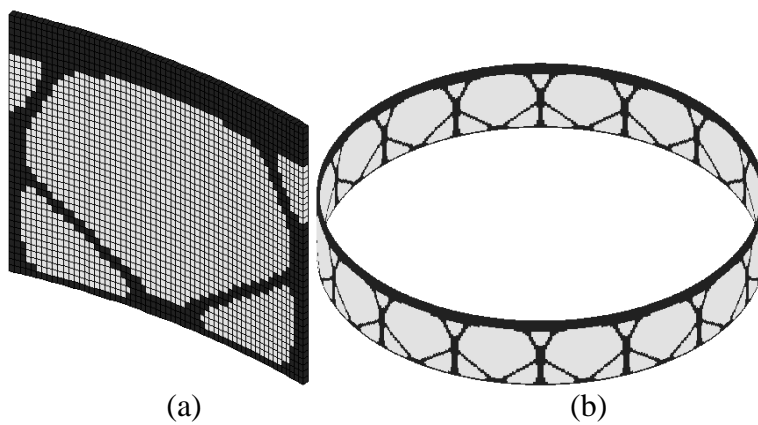


Fig.4.19 Optimal configurations with (a) Unit cell (b) Cellular cylinder with 16 unit cells

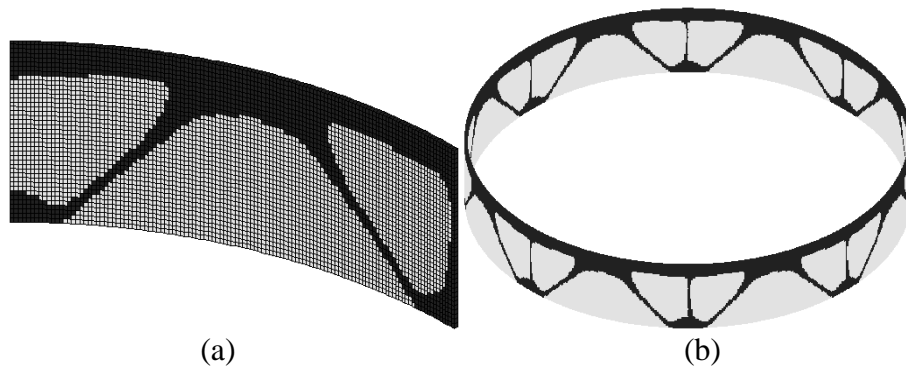


Fig.4.20 Optimal configurations with (a) Unit cell (b) Cellular cylinder with 8 unit cells

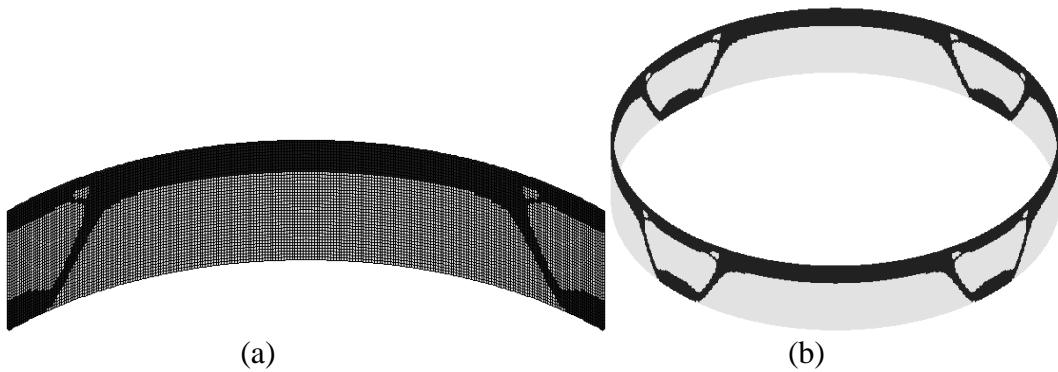


Fig.4.21 Optimal configurations with (a) Unit cell (b) Cellular cylinder with 4 unit cells

Table 4.10 Optimal topology of RVE-SE with 50% and 30% volume fraction

Number of RVE-SEs (m)	32 ($\theta = 11.25^\circ$)	16 ($\theta = 22.5^\circ$)	8 ($\theta = 45^\circ$)	4 ($\theta = 90^\circ$)
Number of finite elements in one RVE-SE (n)	1200	2400	4800	9600
Minimum compliance 50% volume fraction	3.3138E+07	3.2657E+07	2.7950E+07	2.6840E+07
Minimum compliance 30% volume fraction	6.2081E+07	5.9221E+07	5.05332E+07	4.67372E+07

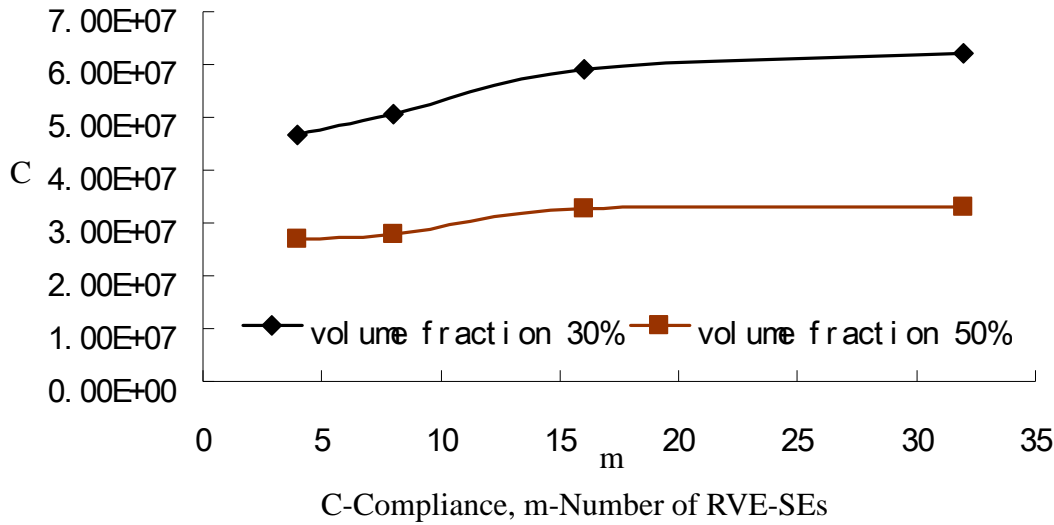


Fig.4.22 Influence of the number of RVE-SEs on structural rigidity

Similarly, the results given from Fig.4.15 to Fig.4.21 show a strong dependence of the optimal topology upon the size of RVE-SE and the material amount. From Table 4.10 and Fig.4.22, we can see that the global rigidity of cylindrical cellular solid reduces with respect to the number increase of the RVE-SE.

4.5 Summary

In conclusion, this chapter is mainly focused on the implementation of the RVE-SE topology optimization procedure. AN RVE-SE topology optimization procedure is developed for the structural rigidity maximization of cellular solids. A flowchart is given for the RVE-SE topology optimization procedure of periodic structure and the computation efficiency is analyzed for different numbers of RVE-SEs. Several examples including square, cyclic-symmetry and cylindrical cellular solids are considered to investigate the scale effects of RVE-SE upon the optimal topologies and the computation efficiency. The optimal results show that the size variation of the RVE-SE influences greatly the optimal configuration which is not unique. It is advantageous to adopt the SE technique so that the integrated design of the cellular material and structure can be made efficiently. Besides, the comparisons of the equivalent torsional resistances of the optimal cyclic-symmetry cellular solids reveal that the innovative configurations of the circular sandwich structure can be obtained for a better performance of torsional resistance by means of the proposed design procedure.

5. Bending analysis of sandwich panels and topological design of cores

In this chapter, the bending analysis and the layout design of the multilayered sandwich panels with the size variation of different cores are developed. The hexagonal and square honeycomb cores and the circle and X corrugated cores are analyzed. Bending responses of sandwich panels are also computed numerically and theoretically using the homogenized cores. According to the ratio of the span dimensions to thickness, Levy and Navier methods in the laminate plate theory are used for sandwich panels with the homogenized honeycomb cores. And then, considering the upper and bottom skin layers as non-designable parts, the 3D layout optimization of scale-related sandwich cores with different sizes are carried out for the global stiffness maximization.

5.1 Introduction

In the Chapter 1 and Chapter 2, we have pointed out that sandwich panel is a kind of typical structural form in sandwich structures. Usually, a sandwich panel is composed of the upper and lower skins and a lightweight core. Common patterns of the sandwich core such as foam, truss, honeycombs and corrugated cores (Gibson and Ashby [1997]; Wicks and Hutchinson [2004]; Petras and Sutcliffe [1999]; Valdevit et al. [2006]) are as shown in Fig.1.4. In these sandwich cores, the detailed different structural forms are involved, e.g., the foam core with the open or close cells, different truss configurations, honeycomb cores and the corrugated cores with different shapes, etc. Moreover, such attractive properties as high specific stiffness and strength, high impact energy absorption, sound damping, electromagnetic wave absorption, thermal insulation and non combustibility (Lukkassen and Meidell [2003]; Zhu and Sankar [2007]; Styles et al. [2007]) can be obtained by the optimal design. Therefore, sandwich panels are extensively used in the aerospace, building, automobile, package, and shipbuilding industries.

Most studies on the sandwich panel presently focus on the two following aspects. Firstly, different kinds of methods involved in the homogenization technique, the analytical and the experimental method are pursued to obtain the effective properties of sandwich panels with the various cores. Buannic (Buannic [2003]) computed the effective properties of the corrugated core sandwich panel with the homogenization method and derived the equivalent Kirchhoff-Love and Reissner-Mindlin homogeneous plate. Meraghni (Meraghni [1999]) developed three approaches of finite element analysis, analytical study and experimental tests to determine the mechanical properties of the honeycomb and tubular cores for sandwich panels. Xu and Qiao (Xu and Qiao [2002]) applied the multi-pass homogenization technique to solve the equivalent stiffness of the sandwich with the skin effect. Hohe and Becker (Hohe and Becker [2001b]) used a strain energy-based representative volume element procedure for the determination of the effective properties of two-dimensional cellular sandwich cores with arbitrary cell topology and geometry. Xue and Hutchinson (Xue and Hutchinson [2004]) proposed a valid constitutive model for quasi-static deformation of three kinds of metallic sandwich cores. Secondly, structural responses of sandwich panels including the bending, impact, vibration and bulking responses are also evaluated. Romanoff and Varsta (Romanoff and Varsta [2007]) evaluated the bending response of web-core sandwich plates by transforming an originally

discrete core into an equivalent homogenous continuum with the effect of thick-face-plates. The equivalent stiffness properties of the plate were determined by analytical formulations. Glenn and Hyer (Glenn and Hyer [2005]) developed a theory to predict the out-of-plane deflections of sandwich plates. Paik (Paik [1999]) investigated the strength characteristics of aluminum sandwich panels with aluminum honeycomb core. Koissin (Koissin [2004]) addressed the elastic response of sandwich panels to local static and dynamic loading. Meo (Meo [2005]) made an experimental investigation and a numerical simulation on the impact damage over a range of sandwich panels. They revealed the load distribution in damaged sandwich structures and studied the failure mechanisms of such a structure in the presence of impact damage. Pokharel and Mahendran (Pokharel and Mahendran [2004]) investigated local buckling behavior of sandwich panels using experimental and finite element analysis. Frostig and Thomsen (Frostig and Thomsen [2004]) presented free vibration analysis of sandwich panels with a flexible core based on the high-order sandwich panel theory. Chang (Chang [2005]) presented a closed-form solution based on the Mindlin-Reissner plate theory to describe the behavior of corrugated-core sandwich plate in bending with various boundary conditions.

The above-presented researchers and many others have carried out plenty of outstanding and in-depth studies on the sandwich panel. However, fewer attentions are paid on the size effect of sandwich cores concerning the mechanical properties of sandwich panels. Tekoglu and Onck (Tekoglu and Onck [2005]) pointed out that mechanical properties of cellular materials depended strongly on the ratio of the specimen size to the cell size. The size effect was studied by Onck (Onck [2001]) for the in-plane elastic constants of hexagonal honeycombs based on the finite element modeling and experimental tests. Recently, Dai and Zhang (Dai and Zhang [2008]) theoretically and numerically studied size effects of the 2D basic cell of sandwich beams in a systematic way and demonstrated the importance of size effect. Therefore, it's necessary to further explore the size effect of 3D sandwich cores in analyzing the mechanical response of sandwich panel.

In this chapter, firstly, we introduce the classical laminate plate theory that is used for the analysis of sandwich panel. Secondly, the bending responses of sandwich panels with the honeycombs and corrugated cores of different sizes are computed numerically. And also, the laminate plate theory and the finite element method are adopted to analyze the bending responses of sandwich panels with the homogenized cores predicted by the 3D

homogenization method. And then, the representative volume elements (RVEs) configuration of sandwich cores is optimized by the scale-related method for the global stiffness maximization of sandwich panel. By means of the SIMP model, the dual solution strategy and quadratic perimeter control (Zhang and Duysinx [2003]), one can achieve the topology design of RVE of sandwich cores without the checkerboard patterns.

5.2 Laminate plate theory

The sandwich panel can be considered as a multi-layered plate when the sandwich core is homogenized by the homogenization method. Therefore, the laminate plate theory (Vinson and Sierakowski [1987]; Reddy [1984]) can be used to analyze its bending response. According to the assumption of the laminate plate theory that the lines perpendicular to the surface of the laminate remain straight and perpendicular to the deformed surface as well. The functional forms of the displacements for the laminate plate are:

$$\begin{aligned} u(x, y, z) &= u_0(x, y) + z\bar{\alpha}(x, y) \\ v(x, y, z) &= v_0(x, y) + z\bar{\beta}(x, y) \\ w(x, y, z) &= w_0(x, y) \end{aligned} \quad (5.1)$$

where u_0 , v_0 and w_0 are the displacements of the mid-plane (that is, the x-y plane in Fig.5.1 below) of the laminate plate on x , y and z direction respectively. The second terms in the first two equations are related to the rotations of the lineal element. In classical plate theory,

$$\bar{\alpha} = -\frac{\partial w}{\partial x}, \quad \bar{\beta} = -\frac{\partial w}{\partial y} \quad (5.2)$$

The equilibrium equations for the three dimensional elasticity can be written as follows:

$$\begin{aligned} \frac{\partial \sigma_x}{\partial x} + \frac{\partial \sigma_{yx}}{\partial y} + \frac{\partial \sigma_{zx}}{\partial z} + F_x &= 0 \\ \frac{\partial \sigma_{xy}}{\partial x} + \frac{\partial \sigma_y}{\partial y} + \frac{\partial \sigma_{zy}}{\partial z} + F_y &= 0 \\ \frac{\partial \sigma_{xz}}{\partial x} + \frac{\partial \sigma_{yz}}{\partial y} + \frac{\partial \sigma_z}{\partial z} + F_z &= 0 \end{aligned} \quad (5.3)$$

In the classical laminate plate theory, we define and use stress resultants (N), stress couples (M), and shear resultants (Q) for the overall plate.

$$\begin{Bmatrix} N_x \\ N_y \\ N_{xy} \\ Q_x \\ Q_y \end{Bmatrix} = \int_{-h/2}^{+h/2} \begin{Bmatrix} \sigma_x \\ \sigma_y \\ \sigma_{xy} \\ \sigma_{xz} \\ \sigma_{yz} \end{Bmatrix} dz, \quad \begin{Bmatrix} M_x \\ M_y \\ M_{xy} \end{Bmatrix} = \int_{-h/2}^{+h/2} \begin{Bmatrix} \sigma_x \\ \sigma_y \\ \sigma_{xy} \end{Bmatrix} z dz \quad (5.4)$$

Then the body force items (F_x, F_y, F_z) are neglected. It is further assumed that the plate is composed of a laminated composite material that is mid-plane symmetric. From Eq. (5.3) and Eq. (5.4) through integrating term by term across each layer, the plate equilibrium equations for the bending of the plate, due to lateral loads can be expressed as

$$\frac{\partial M_x}{\partial x} + \frac{\partial M_{xy}}{\partial y} - Q_x = 0 \quad (5.5)$$

$$\frac{\partial M_{xy}}{\partial x} + \frac{\partial M_y}{\partial y} - Q_y = 0 \quad (5.6)$$

$$\frac{\partial Q_x}{\partial x} + \frac{\partial Q_y}{\partial y} + P(x, y) = 0 \quad (5.7)$$

Eq. (5.5) and Eq. (5.6) can be substituted into Eq. (5.7), which generates

$$\frac{\partial^2 M_x}{\partial x^2} + 2 \frac{\partial^2 M_{xy}}{\partial x \partial y} + \frac{\partial^2 M_y}{\partial y^2} = -P(x, y) \quad (5.8)$$

From the following equation:

$$\begin{Bmatrix} N \\ M \end{Bmatrix} = \begin{bmatrix} A & B \\ B & D \end{bmatrix} \begin{Bmatrix} \varepsilon \\ k \end{Bmatrix} \quad (5.9)$$

and according to Eq. (5.1) and Eq. (5.2) and the relations among displacements, strains and stresses of the laminate plate, we obtain:

$$\begin{aligned} M_x &= D_{11}k_x + D_{12}k_y \\ M_y &= D_{12}k_x + D_{22}k_y \\ M_{xy} &= 2D_{66}k_{xy} \end{aligned} \quad (5.10)$$

where

$$k_x = \frac{\partial \bar{\alpha}}{\partial x} = -\frac{\partial^2 w}{\partial x^2}, k_y = \frac{\partial \bar{\beta}}{\partial y} = -\frac{\partial^2 w}{\partial y^2}, k_{xy} = \frac{1}{2} \left(\frac{\partial \bar{\alpha}}{\partial x} + \frac{\partial \bar{\beta}}{\partial y} \right) = -\frac{\partial^2 w}{\partial x \partial y} \quad (5.11)$$

$$D_{ij} = \frac{1}{3} \sum_{k=1}^N (Q_{ij})_k [h_k^3 - h_{k-1}^3] \quad (5.12)$$

Here the principal material directions (1, 2, 3) coincide with the x-y-z coordinate system.

The Q_{ij} quantities are the stiffness matrix quantities that have the following simple forms by ignoring the fine accuracy.

$$\begin{aligned} Q_{11} &= E_{11} / (1 - \nu_{12}\nu_{21}) \\ Q_{22} &= E_{22} / (1 - \nu_{12}\nu_{21}) \\ Q_{12} &= Q_{21} = \nu_{21}E_{11} / (1 - \nu_{12}\nu_{21}) = \nu_{12}E_{22} / (1 - \nu_{12}\nu_{21}) \\ Q_{66} &= G_{12} \end{aligned} \quad (5.13)$$

Substitute Eq. (5.10) and Eq. (5.11) into Eq. (5.8), which results in:

$$D_{11} \frac{\partial^4 w}{\partial x^4} + 2(D_{12} + 2D_{66}) \frac{\partial^4 w}{\partial x^2 \partial y^2} + D_{22} \frac{\partial^4 w}{\partial y^4} = P(x, y) \quad (5.14)$$

According to Eq.(5.14), the bending response of a sandwich panel, except transverse shear deformation and coupling terms subjected to a lateral distributed load $P(x, y)$, can be obtained by the Levy solution and the Navier solution.

5.3 Analysis of bending responses of sandwich panels

5.3.1 Sandwich panels with the honeycomb cores

5.3.1.1 Hexagonal core

A sandwich panel with the hexagonal honeycomb core, as shown in Fig.5.1, is simply supported on the left and right side. The line load P 100N/m is applied on the center of the plate. The sandwich panel has the dimensions assigned as: width $a=0.8865\text{m}$, length $b=1.5354\text{m}$, thickness $h_u=h_l=0.0125\text{m}$, $h_c=0.0375\text{m}$ (u-upper skin, l-lower skin, c-core), and the material properties: elastic moduli $E_u=E_l=2.0\text{GPa}$ and $E_c=0.91\text{GPa}$.

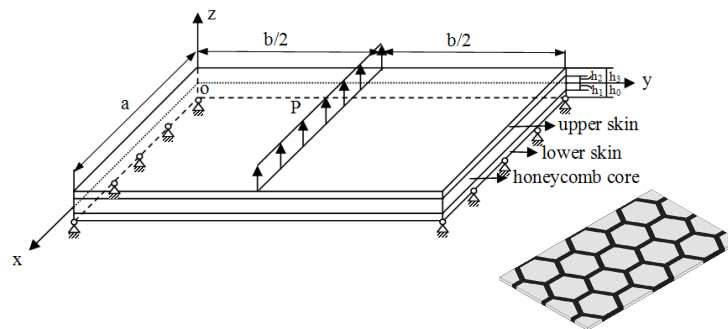


Fig.5.1 Sandwich panel with hexagonal cores

The effective material properties of hexagonal honeycomb core are obtained by the 3D

homogenization method.

$$\begin{aligned} E_x^H &= 3.118352\text{E}+07\text{Pa}, E_y^H = 3.116449\text{E}+07\text{Pa}, E_z^H = 2.414286\text{E}+08\text{Pa} \\ G_{xy}^H &= 8.770264\text{E}+06\text{Pa}, G_{yz}^H = 5.272060\text{E}+07\text{Pa}, G_{xz}^H = 5.273506\text{E}+07\text{Pa} \\ v_{xy}^H &= 7.818590\text{E}-01, v_{xz}^H = 3.874876\text{E}-02, v_{yz}^H = 3.872511\text{E}-02 \end{aligned}$$

According to the boundary conditions on those edges: $w(x, 0)=0$, $w(x, b)=0$, and $M_y(x, 0)=0$, $M_y(x, b)=0$, Levy assumed the following solution form of Eq.(5.14): a single infinite half range sine series:

$$w(x, y) = \sum_{n=1}^{\infty} \phi_n(x) \sin \frac{n\pi y}{b} \quad (5.15)$$

The load $P(x, y)$ is also expanded in terms of a half range sine series. Then, by substituting Eq. (5.15) into Eq. (5.14), the equation concerning $\phi_n(x)$ is obtained. Its solution is composed of the particular solution $\phi_{n_p}(x)$ and the homogenous solution $\phi_{n_H}(x)$ that has three different forms depending on the relative plate stiffness in various directions.

The total potential energy is:

$$U = \int_0^a w(x, b/2)P(x, b/2)dx \quad (5.16)$$

Via the calculation, the Levy solution converges when the expansion number n equals to 5. The maximum displacement module is $2.94 \times 10^{-4}\text{m}$, and the total potential energy is $2.44 \times 10^{-2}\text{N}\cdot\text{m}$. The deformation of the sandwich panel is shown in Fig.5.2.

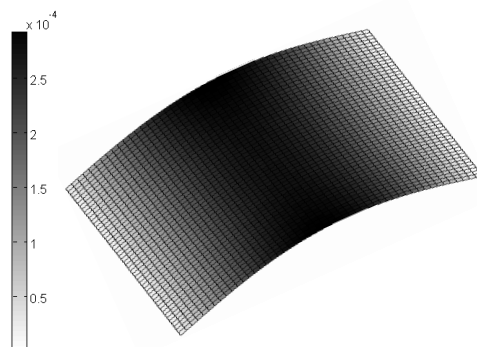


Fig.5.2 Levy solution of sandwich panel with hexagonal cores

The bending response of the sandwich panel made of three-layered homogeneous media is obtained via the finite element software SAMCEF[®]. The maximum displacement module

is 2.57×10^{-4} m, and the total potential energy is 2.139×10^{-2} N·m. The detailed deformation is shown in Fig.5.3.

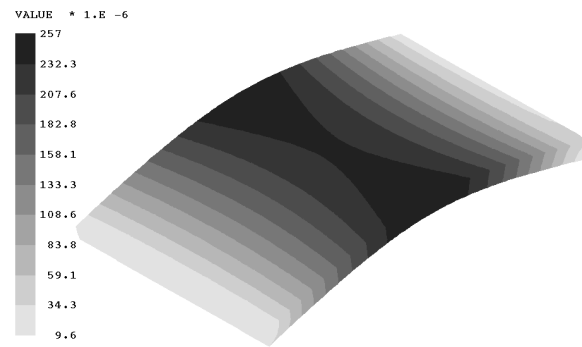
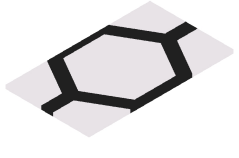
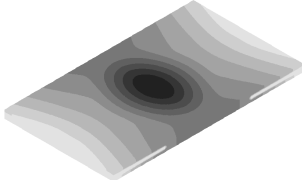

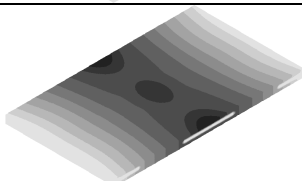
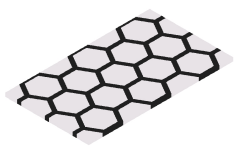
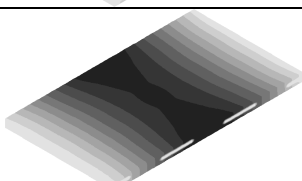

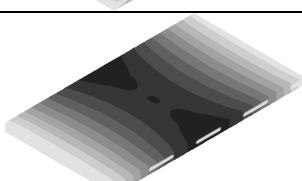

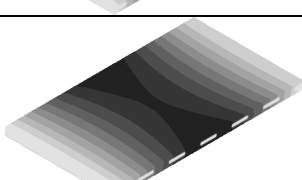
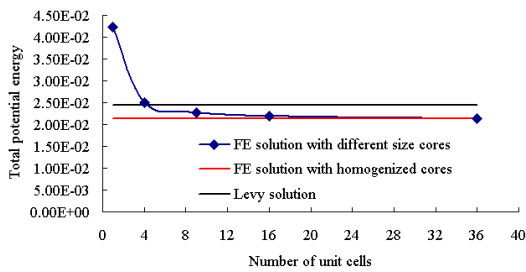


Fig.5.3 Finite element solution of sandwich panel with the homogenized core

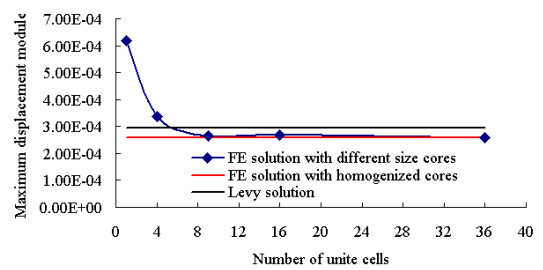
The finite element models of sandwich panels with the different size hexagonal cores are built and their bending responses are calculated in Table 5.1. The total potential energy and the maximum displacement module tend towards the solution obtained by using the homogenization method, as shown in Fig 5.4.

Table 5.1 Bending deflections of sandwich panels with different size hexagonal cores

Number of unit cells	Different size cores	Bending responses of sandwich panels	Bending values of sandwich panels	
			Total potential energy (N·m)	Maximum displacement module (m)
1×1=1			4.239329E-02	6.193E-04
2×2=4			2.507296E-02	3.374E-04
3×3=9			2.261694E-02	2.657E-04
4×4=16			2.183737E-02	2.668E-04
6×6=36			2.134839E-02	2.578E-04



(a)



(b)

Fig.5.4 (a) Total potential energy and (b) Maximum displacement module of sandwich panel with the hexagonal core

5.3.1.2 Square core

Consider a sandwich panel with the square honeycomb core as shown in Fig.5.5. All the four edges are simply supported. The uniform surface loading $q=100\text{N/m}^2$ is applied on the upper surface. The sandwich panel has the dimensions assigned as: $a=1.1\text{m}$, $h_u=h_l=0.0125\text{m}$, $h_c=0.0375\text{m}$ (u-upper skin, l-lower skin, c-core), and the material properties: elastic moduli $E_u=E_l=2.0\text{GPa}$ and $E_c=0.91\text{GPa}$.

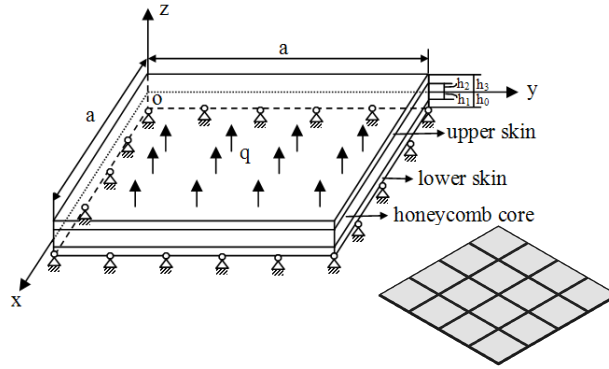


Fig.5.5 Sandwich panel with square cores

The effective properties of the square honeycomb core are obtained by the homogenization method.

$$E_x^H = 8.769525\text{E}+07\text{Pa}, E_y^H = 8.769525\text{E}+07\text{Pa}, E_z^H = 1.579339\text{E}+08\text{Pa}$$

$$G_{xy}^H = 4.154834\text{E}+05\text{Pa}, G_{yz}^H = 3.270143\text{E}+07\text{Pa}, G_{xz}^H = 3.270143\text{E}+07\text{Pa}$$

$$\nu_{xy}^H = -6.337963\text{E}-03, \nu_{xz}^H = 1.665797\text{E}-01, \nu_{yz}^H = 1.665797\text{E}-01$$

According to the boundary conditions on the four edges, in the Navier approach we can simply expand the deflection $w(x, y)$ and the applied uniform loading $q(x, y)$ into a doubly infinite half range sine series.

$$w(x, y) = \sum_{m=1}^{\infty} \sum_{n=1}^{\infty} \frac{a^4 q_{mn}}{D\pi^4} \sin \frac{m\pi x}{a} \sin \frac{n\pi y}{a} \quad (5.17)$$

$$q(x, y) = \sum_{m=1}^{\infty} \sum_{n=1}^{\infty} q_{mn} \sin \frac{m\pi x}{a} \sin \frac{n\pi y}{a} \quad (5.18)$$

where

$$q_{mn} = \frac{16q}{mn\pi^2}, \quad m, n = 1, 3, 5, \dots \quad (5.19)$$

$$D = D_{11} \left(\frac{m}{a} \right)^4 + 2(D_{12} + 2D_{66}) \left(\frac{mn}{a^2} \right)^2 + D_{22} \left(\frac{n}{a} \right)^4 \quad (5.20)$$

The total potential energy is:

$$U = \iint_A w(x, y)q(x, y)dxdy \quad (5.21)$$

Via the calculation, the Navier solution converges when the expansion number n is 7. The maximum displacement is 1.687×10^{-5} m, and the total potential energy is 1.4×10^{-3} N·m. The deformation of the sandwich panel for the detail is shown in Fig.5.6.

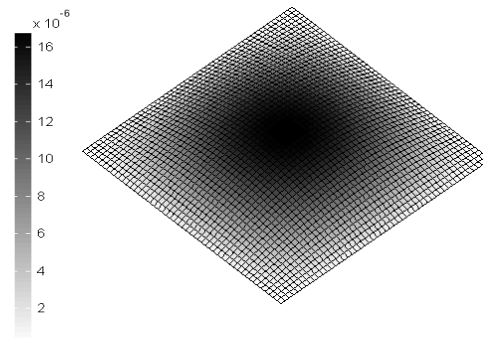


Fig.5.6 Navier solution of sandwich panel with the square core

Similar to the previous analysis, for this kind of sandwich panel made of three-layered homogeneous media, the maximum displacement module is 1.975×10^{-5} m, and the total potential energy is 9.868×10^{-4} N·m. The deformation is shown in Fig.5.7.

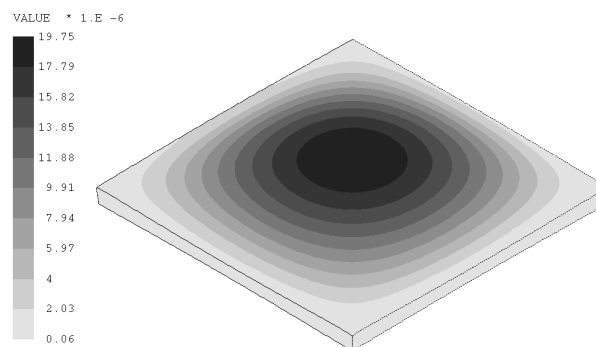
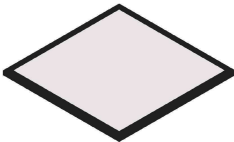
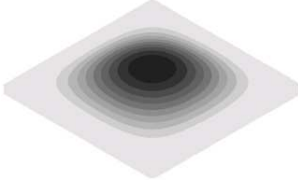
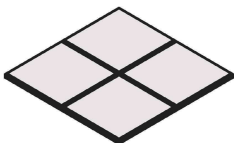
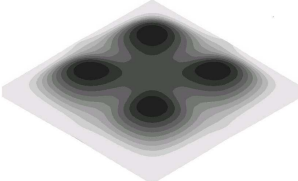
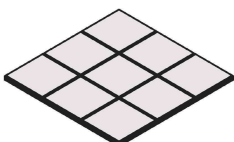
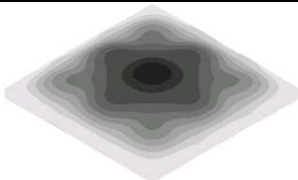
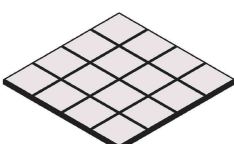
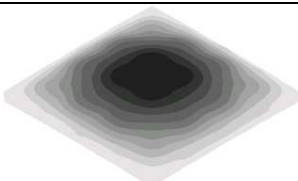
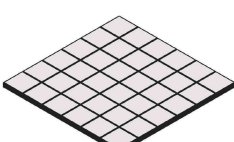
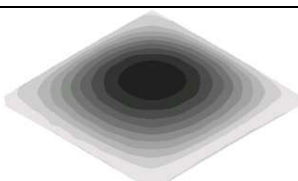


Fig.5.7 Finite element solution of sandwich panel with the homogenized core

Likewise, the finite element models of sandwich panels with the different size square cores are built and their bending responses are calculated in Table 5.2.

Table 5.2 Bending deflections of sandwich panel with different size square cores

Number of unit cells	Different size cores	Bending responses of sandwich panels	Bending values of sandwich panels	
			Total potential energy (N·m)	Maximum displacement module (m)
1×1=1			1.283338E-2	3.927E-4
2×2=4			2.40426E-3	0.4306E-4
3×3=9			1.580408E-3	0.3158E-4
4×4=16			1.37336E-3	0.2495E-4
6×6=36			1.277849E-3	0.2383E-4

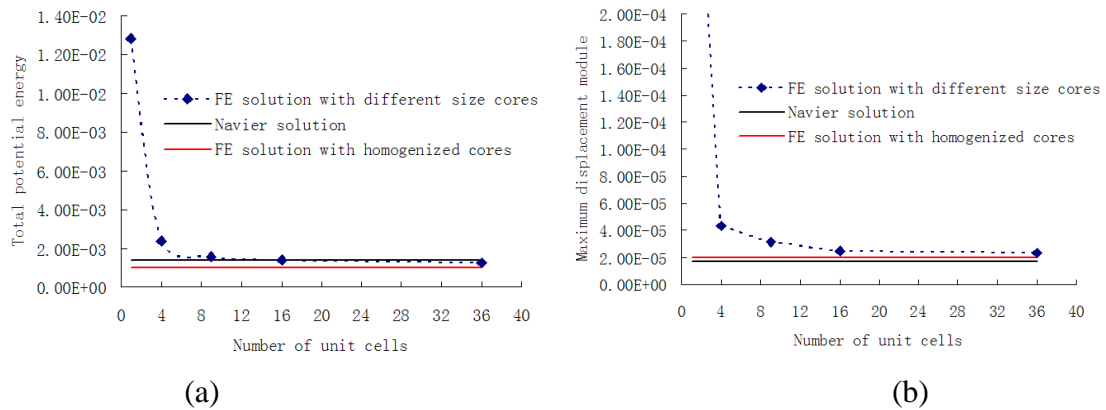


Fig.5.8 (a) Total potential energy and (b) Maximum displacement module of sandwich panel with the square core

5.3.1.3 Discussion

According to the figures and tables of the above two examples, it is found that bending response of sandwich panel tend to a limit case with the decreasing size of honeycomb core. This limit case is approximately the bending response of sandwich panel with homogenized cores with the same boundary conditions. At the same time, we also find that the coincidence between Levy solution and FE solution with homogenized hexagonal cores is worse than that between Navier solution and FE solution with homogenized square cores. The reason lies in the fact that the ratio of the span dimensions to thickness ($\alpha = a/(h_u + h_c + h_l)$) is 14.184 for the hexagonal core and 17.6 for the square core. According to the basic assumption of the laminate plate theory, the classical lamination theory is only valid for thin laminates with small displacement in the transverse direction (Vinson and Sierakowski [1987]). Therefore, when the ratio α increases, the theoretical solution is closer to the finite element solution with the homogenized core.

5.3.2 Sandwich panels with the corrugated cores


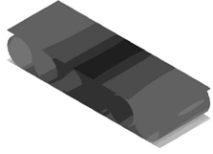
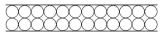
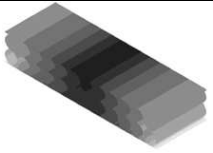
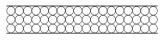
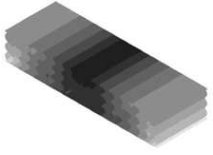

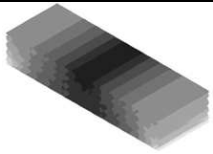

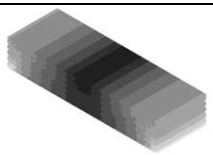

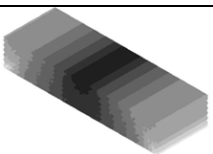
In this section, the bending responses of sandwich panel with corrugated cores are analyzed with different sizes. Two forms of the cores i.e. the circle-core and the X-core are involved here. The boundary condition of three points bending is the same as in Fig.5.1. The material properties of two sandwich panels are assigned as: $E_u = E_l = 2.0 \text{ GPa}$ for upper and lower skins, $E_c = 0.91 \text{ GPa}$ for cores. The difference between the two sandwich panels lies in that the simply supported sides are parallel to the extended direction of the unit cell

for the circle-core, and vertical to the extended direction of the unit cell for the X-core. Here, only finite element solutions with the different size cores and homogenized cores are obtained. The Levy method is not adopted because the ratio of the span dimensions to thickness of sandwich panels ($\alpha = W / (h_u + h_c + h_l)$) is 1.9 for circle core and 2.857 for x-core. The laminate plate theory is no more applicable by the validation of examples in section 5.3.1.

5.3.2.1 Circle-core

For the sandwich structure with the circle-core, the dimensions are set as: length $L=2.4\text{m}$, width $W=0.8\text{m}$, thickness $h_u=h_l=0.01\text{m}$, $h_c=0.40\text{m}$ (u-upper skin, l-lower skin, c-core).

Table 5.3 Bending deflections of sandwich structures with different size circle cores

Number of unit cells	Different size cores	Bending response of sandwich structures	Bending value of sandwich structures	
			Total potential energy (N·m)	Maximum displacement module (m)
1×6=6			1.254997E2	8.635E-2
2×12=24			7.11977E1	4.823E-2
3×18=54			6.45108E1	4.359E-2
4×24=96			5.938279E1	4.013E-2
5×30=150			5.345289E1	3.6E-2
6×36=216			5.17339E1	3.072E-2

The effective properties of the circle core are obtained by the homogenization method as follows.

$$E_x^H = 4.388174E+05 \text{ Pa}, E_y^H = 4.461644E+05 \text{ Pa}, E_z^H = 6.961283E+07 \text{ Pa}$$

$$G_{xy}^H = 5.557200E+05 \text{ Pa}, G_{yz}^H = 1.132639E+07 \text{ Pa}, G_{xz}^H = 1.132639E+07 \text{ Pa}$$

$$\nu_{xy}^H = 8.938214E-01, \nu_{xz}^H = 1.891106E-03, \nu_{yz}^H = 1.922768E-03$$

Bending deflections of sandwich structure with the homogenized core is shown in Fig.5.9.

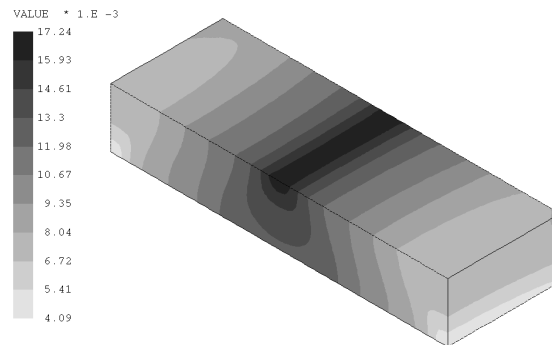


Fig.5.9 Finite element solution of sandwich structure with the homogenized core

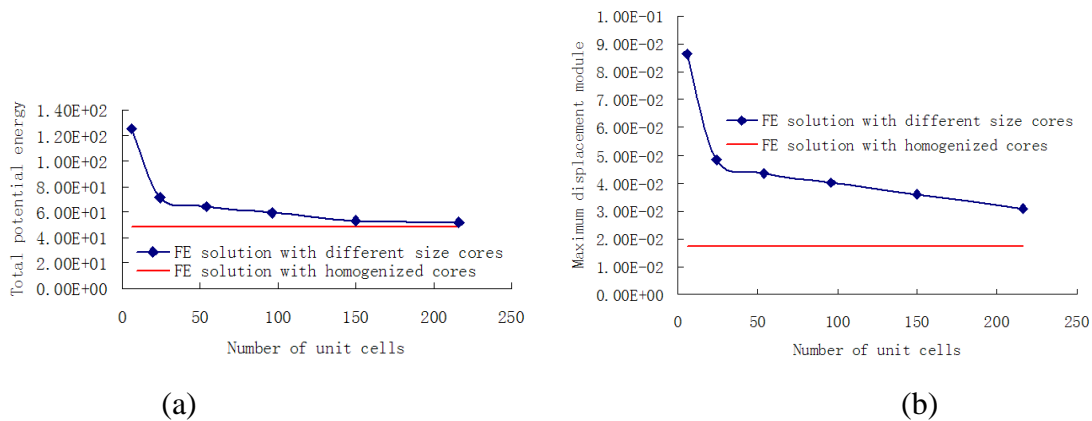


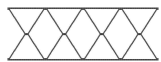
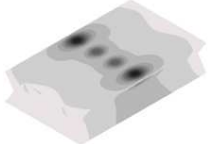
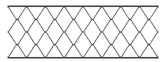
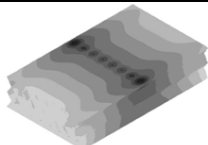
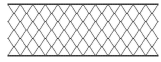
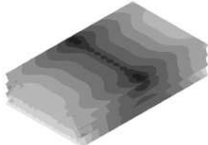
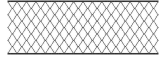
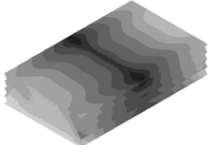

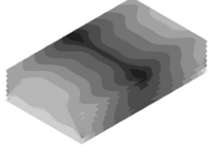
Fig.5.10 (a) Total potential energy and (b) Maximum displacement module of sandwich structure with the circle core

Fig.5.10 shows the values of the potential energy and the maximum displacement versus the number of the unit cells that have been used in the sandwich core.

5.3.2.2 X-core

For the sandwich structure with the X-core, the dimensions are: length $L=2.0\text{m}$, width $W=1.2\text{m}$, thickness $h_u=h_l=0.01\text{m}$, $h_c=0.4\text{m}$ (u-upper skin, l-lower skin, c-core).

Table 5.4 Bending deflections of sandwich structures with different size X-cores

Number of unit cells	Different size cores	Bending response of sandwich structures	Bending value of sandwich structures	
			Total potential energy (N·m)	Maximum displacement module (m)
1×4=4			6.230433E-03	8.917E-5
2×8=16			3.401562E-03	3.589E-5
3×12=36			3.165816E-03	3.015E-5
4×16=64			3.124686E-03	2.938E-5
6×24=144			3.117234E-03	2.913E-5

The effective properties of the X-core are obtained by the homogenization method.

$$E_x^H = 3.927310E+04\text{Pa}, E_y^H = 1.666816E+05\text{Pa}, E_z^H = 5.940933E+07\text{Pa}$$

$$G_{xy}^H = 2.988478E+06\text{Pa}, G_{yz}^H = 1.542861E+07\text{Pa}, G_{xz}^H = 8.097270E+06\text{Pa}$$

$$\nu_{xy}^H = 4.839506E-01, \nu_{xz}^H = 1.983178E-04, \nu_{yz}^H = 8.416942E-04$$

The bending deformation of sandwich structure with the homogenized core is shown in Fig.5.11. And the values of the potential energy and the maximum displacement versus the number of the unit cells that have been used in the sandwich core are plotted as shown in Fig.5.12.

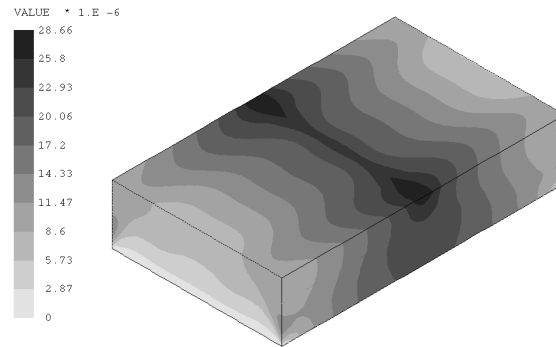


Fig.5.11 Finite element solution of sandwich structure with the homogenized core

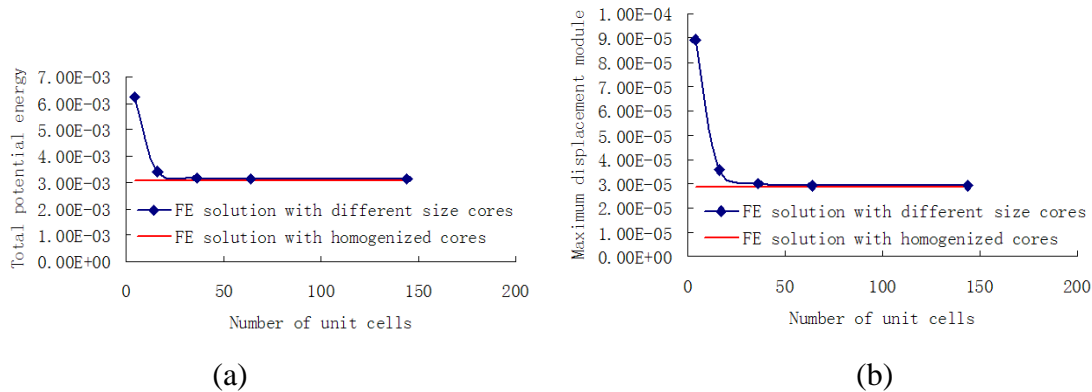


Fig.5.12 (a) Total potential energy and (b) Maximum displacement module of sandwich panel with the X-core

As known from Table 5.3, Table 5.4 and Fig.5.9, Fig.5.10, Fig.5.11, Fig.5.12, the bending responses of sandwich structures with both circle cores and X-cores similarly converge to those obtained with homogenized cores when the sizes of honeycomb cores decrease. But the latter is faster and closer. There are two reasons. On the one hand, the latter ratio α of span dimensions to thickness is bigger. On the other hand, the simply supported sides are vertical to the extended direction of the unit cell for the X-core so that they are more homogeneous than circle cores under the action of the transverse line load.

Therefore, for both the honeycomb core and the corrugated core, the bending response of sandwich panel has the common regularity with the size effect that the overall bending stiffness gradually increases along with the ratio of the specimen size to the cell size. The conclusion is also verified by Tekoglu and Onck (Tekoglu and Onck [2005]).

5.4 Topology design of sandwich cores

5.4.1 Optimization model

The topology optimization problem of minimizing the global compliance of the sandwich panel subjected to the volume constraint is considered. The upper and lower skins are assigned as non-designable domains. To ensure the periodicity of the optimal configuration of the sandwich core base cell in the designable domain, the periodic condition is imposed by the variable-linking method. The detailed optimal model can be expressed as follows:

$$\begin{aligned}
 & \underset{\mathbf{x}=\{x_1, x_2, \dots, x_n\}^T \in R^n}{\text{Min}} \quad C = \mathbf{U}^T \mathbf{K}(\mathbf{x}) \mathbf{U} \\
 & \quad = C_D + C_{ND} \\
 & \quad = \sum_{i=1}^m (\mathbf{U}_D^i)^T \mathbf{K}_D^i(\mathbf{x}) \mathbf{U}_D^i + \mathbf{U}_{ND}^T \mathbf{K}_{ND} \mathbf{U}_{ND} \\
 \text{s.t.} \quad & \mathbf{K}(\mathbf{x}) \mathbf{U} = \mathbf{F} \\
 & \sum_{j=1}^n x_j v_j^i \leq f_v \cdot V_0^i \\
 & P(x) = \sum_{e=1}^r l_e \cdot (x_j - x_{j+1})^2 \leq \bar{P} \\
 & 0 < x_{\min} \leq x_j \leq 1 \\
 & (i = 1, 2, \dots, m \quad j = 1, 2, \dots, n)
 \end{aligned} \tag{5.22}$$

where C is the total compliance of the sandwich panel, m is the number of the core unit cells; C_D and C_{ND} are respectively compliances of the sandwich core in the designable domain and the non-designable domains. \mathbf{U}_D^i is the displacement vector of the i -th core unit cell; n is the finite element number in a single core unit cell and also the number of design variables; x_j is the design variable of the j -th element; v_j^i is the volume of the j -th element in the i -th core unit cell; f_v is the prescribed volume fraction; V_0^i is the volume of the i -th core unit cell; $x_{\min}=10^{-3}$ is used to avoid the singularity of the elementary stiffness matrix during optimization; $P(x)$ is the quadratic perimeter constraint introduced to avoid the checkerboard effect in the core unit cell; l_e is the interface length between adjacent elements j and $j+1$; \bar{P} is the upper limit of the perimeter constraint. Detailed explanations of $P(x)$ can be found in the literature (Zhang and Duysinx [2003]).

5.4.2 Sensitivity analysis

Here the SIMP interpolation model is used for the topological design of sandwich cores. The following power relation holds between design variable x_j and the stiffness matrix \mathbf{K}_{Dj}^i of the j -th finite element located in the i -th unit cell.

$$\mathbf{K}_{Dj}^i(x_j) = (x_j)^p \mathbf{K}_{Dj}^0 \quad (5.23)$$

where \mathbf{K}_{Dj}^0 is the stiffness matrix of element j when it is solid, p is the penalty factor ($p=4$ in this chapter).

For a structure, the general static finite element equation is

$$\mathbf{K}\mathbf{U} = \mathbf{F} \quad (5.24)$$

By differentiating Eq. (5.24), it follows that

$$\frac{\partial \mathbf{U}}{\partial x_j} = -\mathbf{K}^{-1} \frac{\partial \mathbf{K}}{\partial x_j} \mathbf{U} \quad (5.25)$$

With the above expression, the sensitivity of the objective function with respect to each variable x_j can be derived as follows:

$$\frac{\partial C}{\partial x_j} = \frac{\partial}{\partial x_j} (\mathbf{F}^T \mathbf{U}) = \mathbf{F}^T \frac{\partial \mathbf{U}}{\partial x_j} = -(\mathbf{F}^T \mathbf{K}^{-1}) \frac{\partial \mathbf{K}}{\partial x_j} \mathbf{U} = -\mathbf{U}^T \frac{\partial \mathbf{K}}{\partial x_j} \mathbf{U} \quad (5.26)$$

As only the element j is concerned with x_j , the following expression can be derived from Eq. (5.23)

$$\frac{\partial \mathbf{K}_{Dj}^i(x_j)}{\partial x_j} = \frac{p}{x_j} \mathbf{K}_{Dj}^i(x_j) \quad (5.27)$$

Thus, Eq. (5.26) can be rewritten as

$$\begin{aligned} \frac{\partial C_D}{\partial x_j} &= -\mathbf{U}_D^T \frac{\partial \mathbf{K}_D}{\partial x_j} \mathbf{U}_D \\ &= -\sum_{i=1}^m (\mathbf{U}_{Dj}^i)^T \frac{\partial \mathbf{K}_{Dj}^i(x_j)}{\partial x_j} \mathbf{U}_{Dj}^i = -\frac{p}{x_j} \sum_{i=1}^m (\mathbf{U}_{Dj}^i)^T \mathbf{K}_{Dj}^i(x_j) \mathbf{U}_{Dj}^i \\ &= -\frac{p}{x_j} \sum_{i=1}^m C_{Dj}^i \end{aligned} \quad (5.28)$$

where \mathbf{U}_{Dj}^i and C_{Dj}^i are the displacement vector and compliance of the j -th finite element in the i -th core unit cell, respectively. And from Eq. (5.22), we obtain:

$$\frac{\partial C}{\partial x_j} = \frac{\partial C_D}{\partial x_j} + \frac{\partial C_{ND}}{\partial x_j} = \frac{\partial C_D}{\partial x_j} = -\frac{p}{x_j} \sum_{i=1}^m C_{Dj}^i \quad (5.29)$$

Therefore, the compliance sensitivity of a sandwich panel is equal to the summation of strain energies of the variable-linking finite elements in the designable domain multiplied by a negative scaling factor.

5.4.3 Numerical examples

5.4.3.1 Optimal configurations

Here, the configurations of unit cells in sandwich cores with different sizes and different boundary conditions are designed. The solid volume fractions of 10% and 30% are considered respectively. The perimeter control is introduced to generate checkerboard-free and mesh independent structural layouts. In the designable domain, the sandwich cores are respectively divided into 1, 4, 9, 16 and 36 unit cells whose sizes are changed proportionally in the x and y directions.

(1) Sandwich panel with three points bending

In this example, the boundary conditions are the same as those defined as shown in Fig.5.1. The optimization configurations of sandwich cores are given in Table 5.5 for 10% volume fraction and in Table 5.6 for 30% volume fraction. Fig.5.13 gives the comparison of objective values with the different size cores.

Table 5.5 Optimal configuration of sandwich cores with different size unit cells and volume fraction 10% for sandwich panel with the three points bending

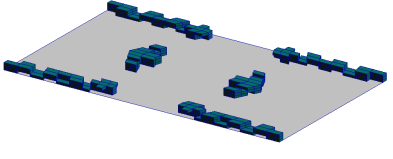
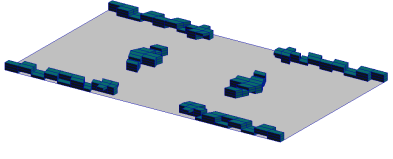
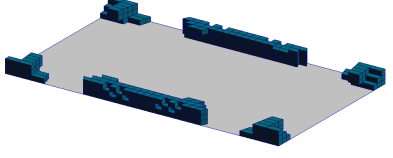
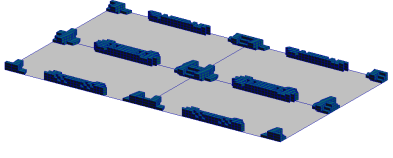
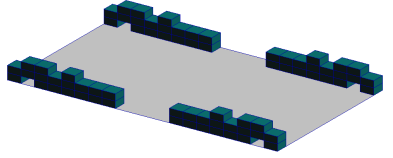
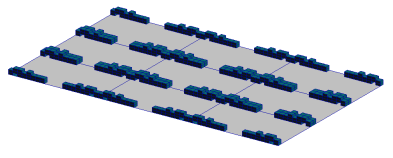
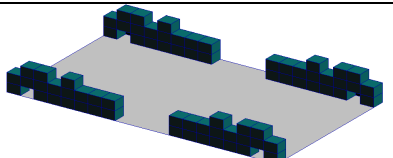
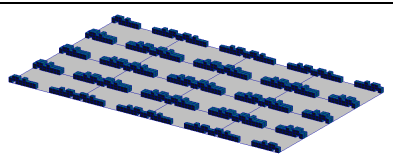
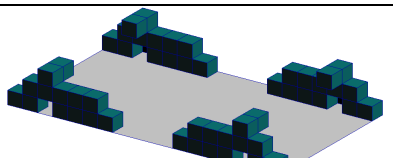
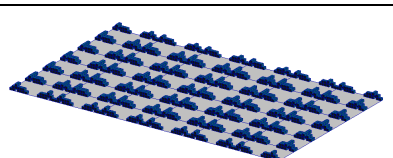
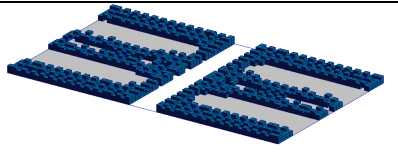
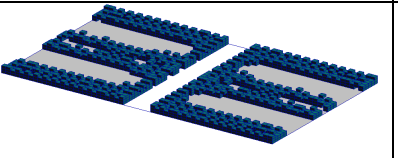
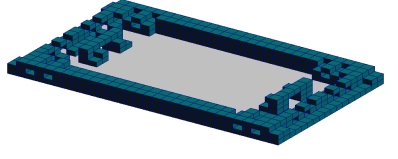
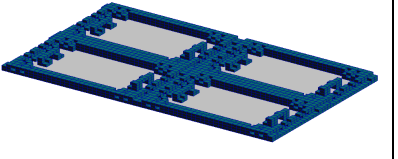
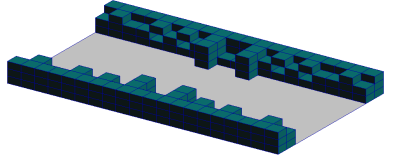
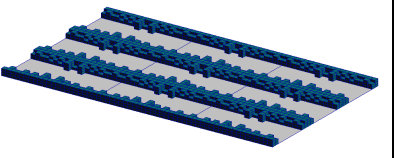
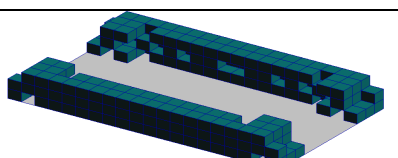
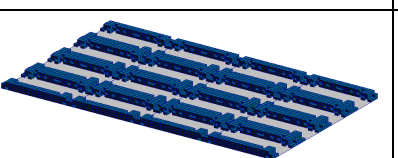
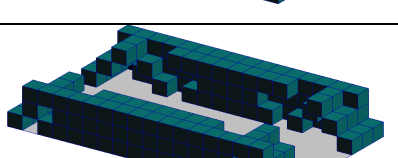
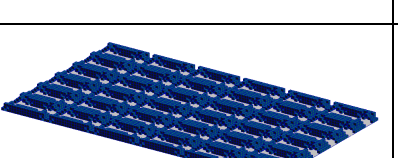
Number of unit cells	Unit cell	Sandwich cores	Potential energy (N·m)
1x1=1			4.266181E-2
2x2=4			3.379944E-2
3x3=9			3.32211E-2
4x4=16			2.87177E-2
6x6=36			2.79763E-2

Table 5.6 Optimal configuration of sandwich cores with different size unit cells and volume fraction 30% for sandwich panel with the three points bending

Number of unit cells	Unit cell	Sandwich cores	Potential energy (N·m)
1x1=1			2.14914E-2
2x2=4			2.17498E-2
3x3=9			2.11298E-2
4x4=16			2.07999E-2
6x6=36			2.07306E-2

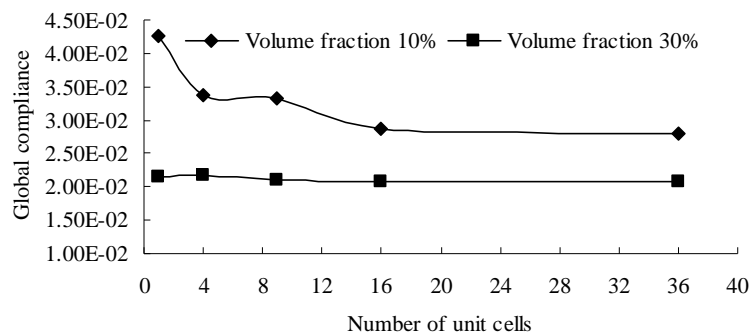


Fig.5.13 Objective function values with the different size cores for three points bending

In Table 5.5 and Table 5.6, the optimal configurations of unit cells are dependent on the size. However the material in one unit cell is basically distributed in its two edges along the longitudinal (y) direction. In Fig.5.13, the objective function value is gradually decreased with the increasing number of unit cells, especially for the 10% volume fraction because the material distribution is more and more homogeneous in the x-y plane. When the volume fraction is set to be 30%, the objective function values are close to each other. That illustrates that the size of unit cell has little influence on the objective function values when the amount of material is bigger.

(2) Sandwich plate with four edges clamped

In this example, the four edges of sandwich plate are clamped as shown in Fig.5.5. The optimal configurations of sandwich cores are illustrated in Table 5.7 for 10% volume fraction and in Table 5.8 for 30% volume fraction. Fig.5.14 gives the comparison of objective function values with the different size cores.

Table 5.7 Optimal configuration of sandwich cores with different size unit cells and volume fraction 10% for sandwich panel with the four edges clamped

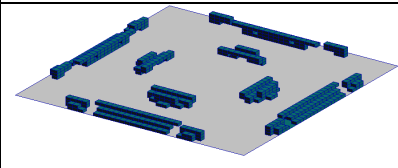
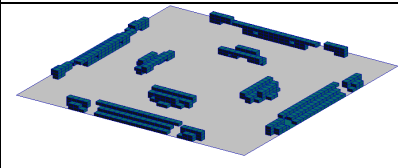
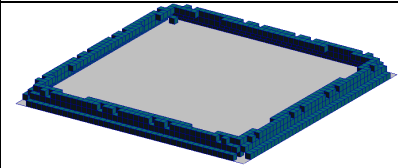
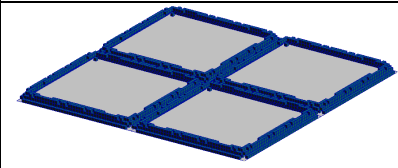
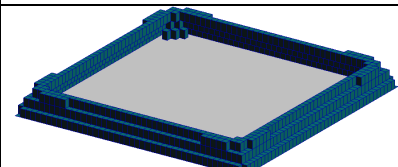
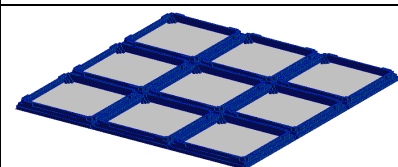
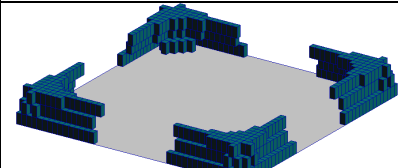
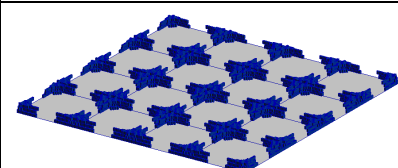
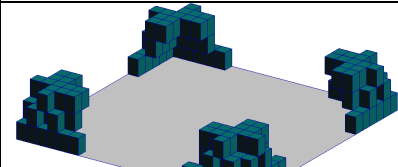
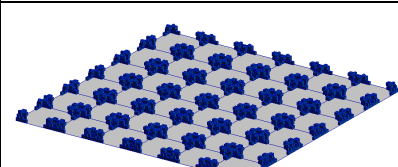
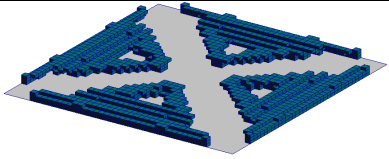
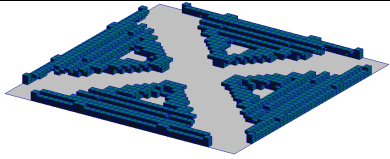
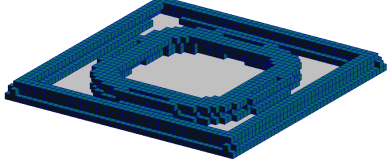
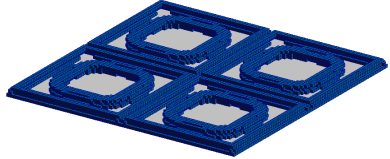
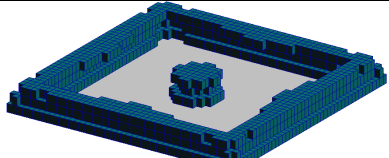
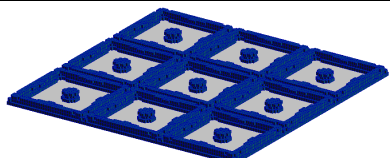
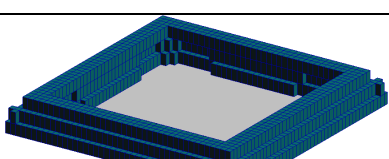
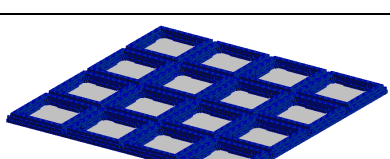
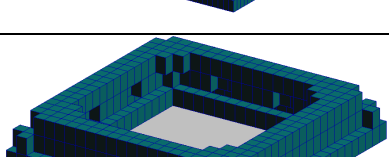
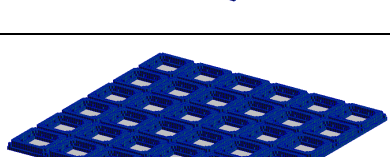
Number of unit cells	Unit cell	Sandwich cores	Potential energy (N·m)
1x1=1			3.159064E-3
2x2=4			2.562556E-3
3x3=9			1.874002E-3
4x4=16			2.400981E-3
6x6=36			2.158045E-3

Table 5.8 Optimal configuration of sandwich cores with different size unit cells and volume fraction 30% for sandwich panel with the four edges clamped

Number of unit cells	Unit cell	Sandwich cores	Potential energy (N·m)
1x1=1			1.130067E-3
2x2=4			1.188605E-3
3x3=9			1.215906E-3
4x4=16			1.170257E-3
6x6=36			1.106158E-3

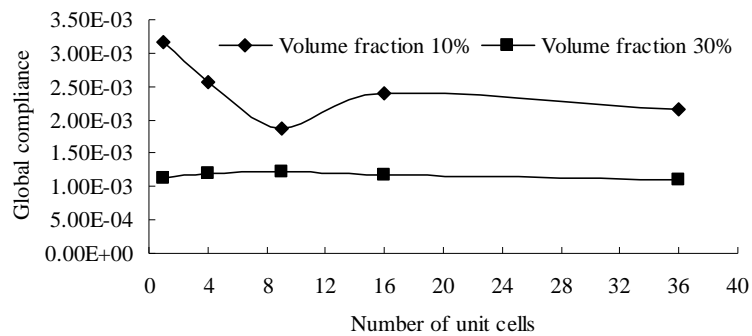


Fig.5.14 Objective function values with the different size cores for four clamped edges

For the plate with four edges clamped and a surface loading, the material of optimal configurations is distributed averagely on the horizontal and longitudinal directions. Observing the optimal configurations of unit cells in Table 5.7 and Table 5.8, we find that the material moves towards the edge of each unit cells along with the decreasing size of unit cells. Actually, when a designable space is divided into many parts, the material is factitiously separated and homogeneously distributed. In Fig.5.14, when the volume fraction is 10%, the objective function values have great difference. However the objective function values are very close when the volume fraction is 30%. This once again demonstrates that the size of unit cell has a little influence on the objective values when the amount of material is bigger.

5.4.3.2 Discussion

Intuitively, the reduction of design space restricts the reasonable distribution of material with the decreasing size of unit cells. However in our examples, conversely the optimal results are better with increasing the number of unit cells, especially for the 10% volume fraction. On the one hand, only the in-plane size of unit cells is different and the size of unit cells along the loading direction does not vary; on the other hand, the material distribution in the optimal configurations is more and more homogeneous for overall sandwich panels with increasing the number of unit cells. So the decreasing size of unit cells prompts the more beneficial distribution of in-plane materials. And the analysis results in section 5.3 also show that the bending response of sandwich panel tends to the one with homogenized sandwich cores and the same boundary conditions when decreasing the size of unit cells. From another point of view, only in the case of sufficient amount of material, the material distribution is more flexible when the design space becomes bigger. That is the reason why the objective function values are very close when the volume fraction is 30% in two numerical examples. Consequently in practical applications, the topology optimization considering the size effect of the sandwich core is a concept design that shows some suitable configurations with the certain number and size of unit cells and the given amount of material under the specific boundary condition.

5.5 Summary

In this chapter, we analyzed the bending responses of sandwich panels with the cores of different layout. The configurations of sandwich cores were designed by topology optimization method considering the in-plane size effect. Conclusions can be drawn as follows: (1) with the decreasing of the size of unit cells, the deformation of the sandwich panel with different size cores tends to the one with homogenized cores. So the homogenization method is valid in analyzing the sandwich panel when the number of core unit cells is large enough. (2) It is verified that the classical laminate plate theory is adapted to the analysis for sandwich panel with the homogenized sandwich core when the ratio α of span dimensions to thickness of sandwich panel satisfies the requirement of the lamination theory. (3) The size of the unit cells influences the optimal configuration of sandwich cores. Some new forms of sandwich cores can be obtained using topology optimization. And the optimal results converge to a limit value when increasing the number of unit cells. On the basis of this research, the higher order laminate plate theory can be adopted in order to improve the analytical accuracy for sandwich panel with the homogenized cores. In the next chapter, we will continue to study the influence of size effect of sandwich cores on the free vibrations in the dynamic analysis of sandwich panels and the configuration design of sandwich cores.

6. Dynamic analysis of sandwich panels and optimal design of cores

In this chapter, free vibrations of sandwich panels with the different size hexagonal and square honeycomb cores and homogenized cores are numerically analyzed. The boundary conditions are represented by the four simply supported edges. The first five orders of eigen-frequencies of sandwich panels for the different cores are compared. In addition, the laminate plate theory including transverse shear deformation is utilized to calculate the natural frequencies of sandwich panel with the homogenized cores. And then, considering the upper and bottom skins as non-designable parts, unit cells with different sizes in sandwich cores are designed for the first order eigen-frequency maximization with the limitations concerning 10% and 30% volume fractions.

6.1 Introduction

Dynamic response prediction of sandwich panels is also of considerable interest for engineers and researchers. Because of their superior performance under dynamic loading, sandwich structures are more extensively used in a wide range of industrial applications such as aeronautical, naval and vehicle construction. An important facet is a correct understanding of the dynamic behavior of such structural systems. Many research works have been developed concerning their dynamic behavior. The major research approaches include the analytical methods based on various plate and shell theories and the numerical methods using the finite element analysis. Qatu (Qatu [2002]) reviewed recent research advances in the dynamic behavior of shells from the following points of view: theoretical aspects, analysis methodology, and different effects concerning various shell geometries. Yuan and Dawe (Yuan and Dawe [2002; 2004]) developed a spline finite strip method for predicting the natural frequencies and modes of vibration and the buckling stresses of rectangular sandwich panels. Nayak (Nayak [2002]) used two new C^0 strain finite element formulations of Reddy's higher-order theory to determine the natural frequencies of various composite and sandwich plates. Rao and Desai (Rao and Desai [2004]) presented a semi-analytical method to evaluate the natural frequencies for simply supported, cross-ply laminated and sandwich plates by using higher order mixed theory. Prusty and Satsangi (Prusty and Satsangi [2001]) carried out the transient dynamic response analysis of composite stiffened plates and shells using finite element method and Newmark's method. They derived the formulation of the general curved-shell-element using the eight-node isoparametric quadratic element on the basis of Mindlin-Reissner's theory and satisfying C^0 continuity for the interpolation functions. Meunier and Sheno (Meunier and Sheno [1999]) studied the free vibration behavior of FRP (fiber reinforced plastic) sandwich plates using analytical methods based on either FSDT (first-order shear deformation theory) or HSDT (high-order shear deformation theory), and also investigated the influence of material property parameters and plate geometry variables on natural frequencies. Kim (Kim [2007]) developed two enhanced plate theories for laminated and sandwich plates via the mixed variational formulation to study free vibration of laminated and sandwich plates. Ghosh and Biswal (Ghosh and Biswal [1996]) studied the free-vibration response of stiffened laminated plates using higher-order shear deformation theory that assumed a realistic cross-sectional deformation pattern and eliminated the use of shear correction coefficients.

Most of these researches focus on the vibration analysis of sandwich panels with flexible foam and honeycomb cores and stiffener plates through developing the different plate theories. They enriched and extended the plate theories and their applications.

In this chapter, we mainly study the size effect of sandwich cores on the free vibration response of the simply supported honeycomb sandwich panels, and investigate the optimal configurations of sandwich cores with the respective different core size for the free vibration response. Our works include the following two aspects. Firstly, the natural frequencies for simply-supported sandwich panels with the periodic honeycomb cores are calculated numerically with the different sizes and same configuration of unit cells. At the same time, we obtain the equivalent properties of sandwich cores with the homogenization method. And then we make the vibration analysis of sandwich panels with the homogenized core using the finite element method and laminate plate theory including transverse shear deformation and compared with the previous analysis results. Thus the relationship of vibration responses between the different size cores and the homogenized core is revealed. Secondly, with the upper and lower skins as non-designable domains, three dimensional configurations of scale-related sandwich cores with the different size are designed for the natural frequency maximization of the sandwich panel. The topology optimization problem is solved by the GCM (global convergence method) using the software BOSS-QUATTRO V5.0 on the basis of the external gradient sensitivity. And the sensitivity filtering is employed to eliminate checkerboards occurring in the design process (Sigmund [1998]). Similarly numerical results reveal the influence of the size variation of involved unit cells on the optimal topology.

6.2 Dynamic analysis of sandwich panel

6.2.1 Dynamic analysis of laminate plate including transverse shear deformation

As given in the (Vinson and Sierakowski [1987]), for the laminate plate simply supported on all four edges, the solutions for the flexural vibration may be written as

$$w(x, y, t) = \sum_{m=1}^{\infty} \sum_{n=1}^{\infty} C_{mn} \sin \frac{m\pi x}{a} \sin \frac{n\pi y}{b} e^{i\omega t} \quad (6.1)$$

$$\bar{\alpha}(x, y, t) = \sum_{m=1}^{\infty} \sum_{n=1}^{\infty} A_{mn} \cos \frac{m\pi x}{a} \sin \frac{n\pi y}{b} e^{i\omega t} \quad (6.2)$$

$$\bar{\beta}(x, y, t) = \sum_{m=1}^{\infty} \sum_{n=1}^{\infty} B_{mn} \sin \frac{m\pi x}{a} \cos \frac{n\pi y}{b} e^{i\alpha t} \quad (6.3)$$

The governing differential equations including the transverse shear deformation and neglecting the rotatory inertia terms are following

$$D_{11} \frac{\partial^2 \bar{\alpha}}{\partial x^2} + D_{66} \frac{\partial^2 \bar{\alpha}}{\partial y^2} + (D_{12} + D_{66}) \frac{\partial^2 \bar{\beta}}{\partial x \partial y} - 2A_{55} \left(\bar{\alpha} + \frac{\partial w}{\partial x} \right) = 0 \quad (6.4)$$

$$(D_{12} + D_{66}) \frac{\partial^2 \bar{\alpha}}{\partial x \partial y} + D_{66} \frac{\partial^2 \bar{\beta}}{\partial x^2} + D_{22} \frac{\partial^2 \bar{\beta}}{\partial y^2} - 2A_{44} \left(\bar{\beta} + \frac{\partial w}{\partial y} \right) = 0 \quad (6.5)$$

$$2A_{55} \left(\frac{\partial \bar{\alpha}}{\partial x} + \frac{\partial^2 w}{\partial x^2} \right) + 2A_{44} \left(\frac{\partial \bar{\beta}}{\partial y} + \frac{\partial^2 w}{\partial y^2} \right) = \rho h \frac{\partial^2 w}{\partial t^2} \quad (6.6)$$

where h is the thickness of laminate plate and

$$\rho = \frac{1}{h} \sum_{k=1}^N \rho_k (h_k - h_{k-1}) \quad (6.7)$$

$$A_{ij} = \frac{5}{4} \sum_{k=1}^N (\bar{Q}_{ij})_k \left[h_k - h_{k-1} - \frac{4}{3} (h_k^3 - h_{k-1}^3) \frac{1}{h^2} \right], \quad i, j = 4, 5 \quad (6.8)$$

Substituting the solutions (Eq.(6.1)-Eq.(6.3)) into the governing equations (Eq.(6.4)-Eq.(6.6)) results in a set of homogeneous equations as follows

$$\begin{bmatrix} L_{11} & L_{12} & L_{13} \\ L_{12} & L_{22} & L_{23} \\ L_{13} & L_{23} & L'_{33} \end{bmatrix} \begin{Bmatrix} A_{mn} \\ B_{mn} \\ C_{mn} \end{Bmatrix} = \begin{Bmatrix} 0 \\ 0 \\ 0 \end{Bmatrix} \quad (6.9)$$

where $L'_{33} = L_{33} - \rho h \omega_{mn}^2$.

The square of the remaining natural frequency can be obtained by solving the above homogeneous equations.

$$\omega_{mn}^2 = \left[(L_{11}L_{22} - L_{12}^2)L_{33} + 2L_{12}L_{23}L_{13} - L_{22}L_{13}^2 - L_{11}L_{23}^2 \right] / \rho h (L_{11}L_{22} - L_{12}^2) \quad (6.10)$$

where, m and n are the number of x and y axial half-waves respectively. If $\lambda_m = m\pi/a$ and $\lambda_n = n\pi/b$,

$$L_{11} = D_{11}\lambda_m^2 + D_{66}\lambda_n^2 + 2A_{55} \quad (6.11)$$

$$L_{12} = (D_{12} + D_{66})\lambda_m\lambda_n \quad (6.12)$$

$$L_{13} = 2A_{55}\lambda_m \quad (6.13)$$

$$L_{22} = D_{66}\lambda_m^2 + D_{22}\lambda_n^2 + 2A_{44} \quad (6.14)$$

$$L_{23} = 2A_{44}\lambda_n \quad (6.15)$$

$$L_{33} = 2A_{55}\lambda_m^2 + 2A_{44}\lambda_n^2 \quad (6.16)$$

6.2.2 With hexagonal honeycomb cores

A sandwich panel with the hexagonal honeycomb core, as shown in Fig.6.1, is simply supported on the four bottom edges. The dimensions of the sandwich panel are following: width $a=0.8865\text{m}$, length $b=1.5354\text{m}$, thickness $h_u=h_l=0.01\text{m}$, $h_c=0.03\text{m}$ (u-upper skin, l-lower skin, and c-core). The elastic moduli of the upper and lower skins are 210GPa . The density is 7800kg/m^3 . For the core, the elastic modulus is 75GPa and the density is 2700kg/m^3 (solid or black part). In order to calculate the effective elastic constants of sandwich core, we assume that the void or white part is a very weak material: the elastic modulus is 0.00001GPa and density is 0.00001kg/m^3 .

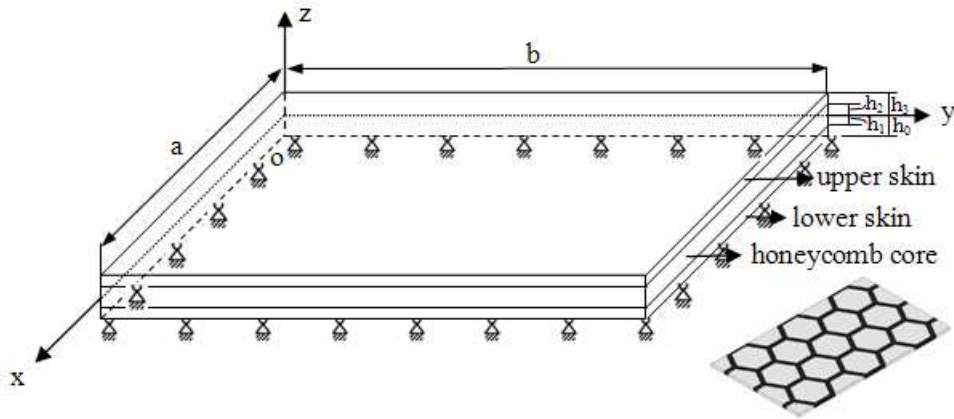


Fig.6.1 Sandwich panel with four simply-supported edges and hexagonal honeycomb cores

The effective material properties of hexagonal honeycomb core are obtained by the 3D homogenization method.

$$\begin{aligned} E_x^H &= 2.570071\text{E}+09\text{Pa}, E_y^H = 2.568502\text{E}+09\text{Pa}, E_z^H = 1.989796\text{E}+10\text{Pa} \\ G_{xy}^H &= 7.228240\text{E}+08\text{Pa}, G_{yz}^H = 4.345104\text{E}+09\text{Pa}, G_{xz}^H = 4.346297\text{E}+09\text{Pa} \\ v_{xy}^H &= 7.818590\text{E}-01, v_{xz}^H = 3.874876\text{E}-02, v_{yz}^H = 3.872511\text{E}-02 \end{aligned} \quad (6.17)$$

And the effective density of hexagonal honeycomb core is

$$\rho_c = ((S_T - S_{\text{void}}) \times 2700 + S_{\text{void}} \times 0.00001) / S_T = 716.32653388\text{kg/m}^3 \quad (6.18)$$

where S_T is the area of whole core in the x - y plane and S_{void} is the area of void part.

$$S_T=4 \times 0.767709841 \times 0.443237483=1.36111111 \tag{6.19}$$

$$S_{\text{void}}=8 \times 0.5 \times (0.219345669+0.438691338) \times 0.379917843=1.00000000124 \tag{6.20}$$

The average of the mass density across the thickness for sandwich panel is

$$\rho = \frac{1}{h} \sum_{k=1}^N \rho_k (h_k - h_{k-1}) = \frac{1}{0.05} (7800 \times 0.02 + 716.3265 \times 0.03) = 3549.796 \text{ kg/m}^3 \tag{6.21}$$

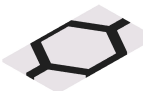

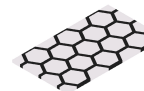

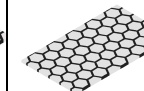

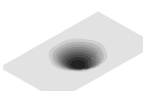
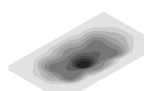
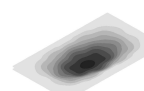
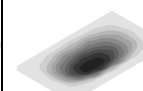
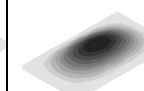
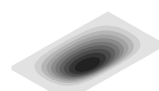
According to Eq.(6.10), the natural frequencies of sandwich panel with the homogenized core are obtained in Table 6.1.

Table 6.1 Natural frequencies with different values of m and n

<i>m, n</i>	<i>m=1</i> <i>n=1</i>	<i>m=1</i> <i>n=2</i>	<i>m=1</i> <i>n=3</i>	<i>m=2</i> <i>n=1</i>	<i>m=2</i> <i>n=2</i>	<i>m=2</i> <i>n=3</i>	<i>m=3</i> <i>n=1</i>	<i>m=3</i> <i>n=2</i>	<i>m=3</i> <i>n=3</i>
Natural frequency	272.75	474.17	803.55	868.13	1061.99	1379.2	1810.4	1992.7	2291.4

The finite element models of sandwich panels with the different sizes of hexagonal cores and the homogenized cores are built and their eigen-frequencies and the first five orders of vibration modes are calculated as shown in Table 6.2 to Table 6.6. The variation tendency of the first five orders of vibration frequencies with different size hexagonal cores is shown in Fig 6.2 to Fig.6.6.

Table 6.2 The first order vibration response with the different size hexagonal cores

Number of unit cell	1×1	2×2	3×3	4×4	5×5	Homogenized core
Different size cores						
Frequency	158.651	262.166	290.595	302.899	309.461	317.962
Mode of sandwich panel						

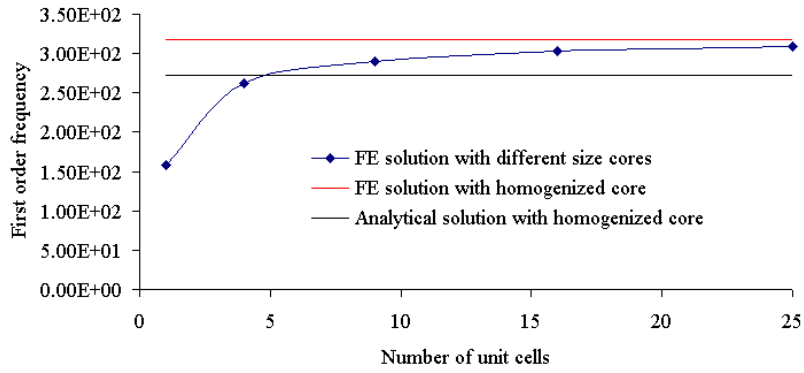


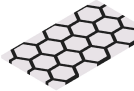

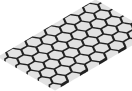

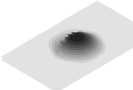
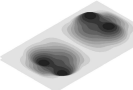
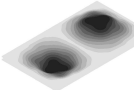
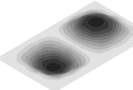
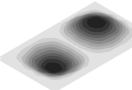
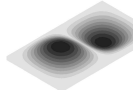


Fig.6.2 Frequency variation of first order vibration with different size hexagonal cores

Table 6.3 The second order vibration response with the different size hexagonal cores

Number of unit cell	1×1	2×2	3×3	4×4	5×5	Homogenized core
different sizes cores						
Frequency	164.100	354.534	414.361	437.267	449.470	467.109
Mode of sandwich panel						

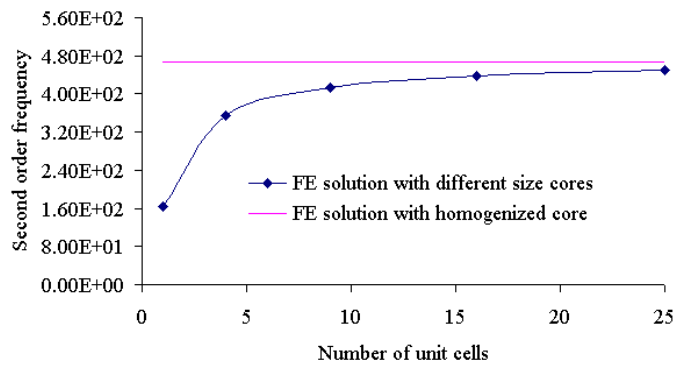

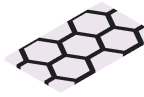
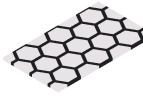



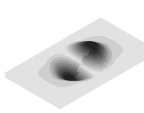
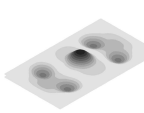
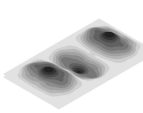
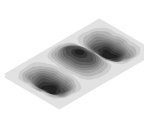
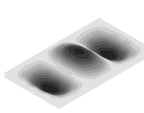
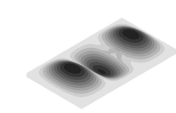


Fig.6.4 Frequency variation of second order vibration with different size hexagonal cores

Table 6.3 The third order vibration response with the different size hexagonal cores

Number of unit cell	1×1	2×2	3×3	4×4	5×5	Homogenized core
different sizes cores						
Frequency	311.883	452.913	606.443	657.847	683.032	720.121
Mode of sandwich panel						

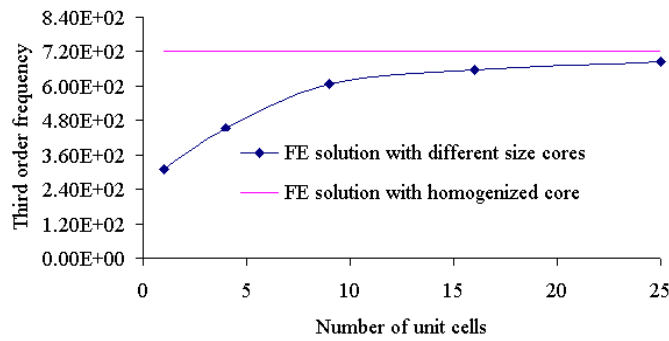

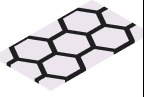
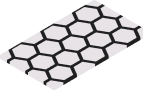
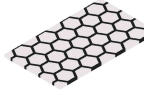


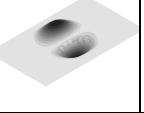
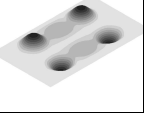
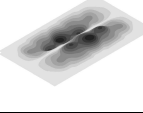
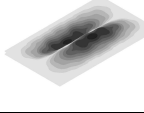
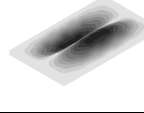
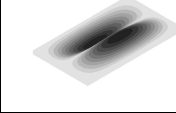


Fig.6.4 Frequency variation of third order vibration with different size hexagonal cores

Table 6.5 The fourth order vibration response with the different size hexagonal cores

Number of unit cell	1×1	2×2	3×3	4×4	5×5	Homogenized core
different sizes cores						
Frequency	330.122	453.406	624.765	674.202	698.656	732.926
Mode of sandwich panel						

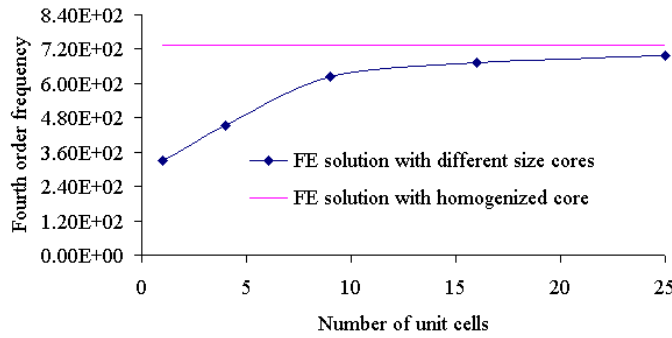

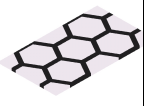
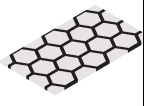


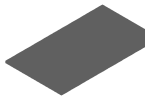
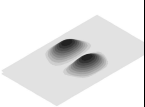
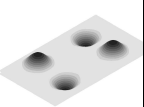
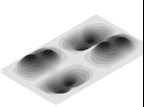
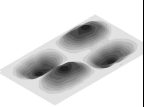
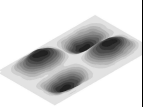
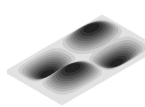


Fig.6.5 Frequency variation of fourth order vibration with different size hexagonal cores

Table 6.6 The fifth order vibration response with the different size hexagonal cores

Number of unit cell	1×1	2×2	3×3	4×4	5×5	Homogenized core
different sizes cores						
Frequency	338.457	453.438	733.716	806.044	8418.07	893.415
Mode of sandwich panel						

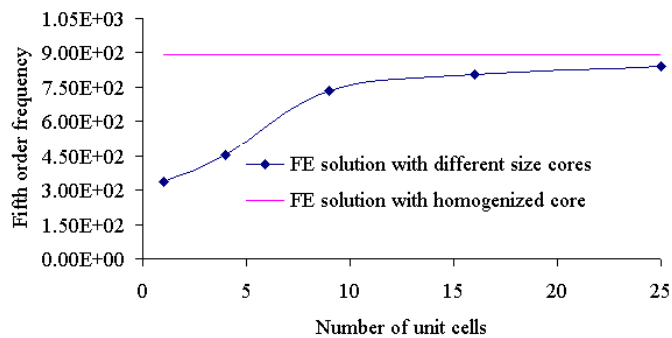


Fig.6.6 Frequency variation of fifth order vibration with different size hexagonal cores

6.2.3 With square honeycomb cores

Consider a sandwich panel with the square honeycomb core as shown in Fig.6.7. All the four edges are simply supported. The dimensions of the sandwich panel are assigned as: $a=1.1\text{m}$, $h_u=h_l=0.01\text{m}$, $h_c=0.03\text{m}$ (u-upper skin, l-lower skin, and c-core). Similar to the

hexagonal core in the section 6.2.1, the elastic moduli of the upper and lower skins are 210GPa. The density is 7800kg/m³. For the core, the elastic modulus is 75GPa and the density is 2700 kg/m³ (solid or black part). In the same way, we assume that the void or white part is a very weak material: the elastic modulus is 0.00001GPa and density is 0.00001kg/m³.

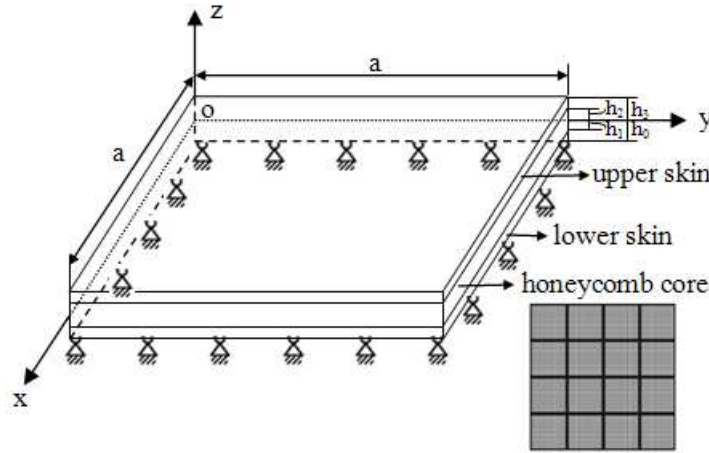


Fig.6.7 Sandwich panel with four simply-supported edges and square honeycomb cores

With the 3D homogenization method, the effective material properties of square honeycomb core are

$$\begin{aligned} E_x^H &= 7.227631E+09\text{Pa}, E_y^H = 7.227631E+09\text{Pa}, E_z^H = 1.301653E+10\text{Pa} \\ G_{xy}^H &= 3.424314E+07\text{Pa}, G_{yz}^H = 2.695173E+09\text{Pa}, G_{xz}^H = 2.695173E+09\text{Pa} \\ \nu_{xy}^H &= -6.337963E-03, \nu_{xz}^H = 1.665797E-01, \nu_{yz}^H = 1.665797E-01 \end{aligned} \quad (6.22)$$

And the effective density of square honeycomb core is similarly computed as,

$$\rho_c = ((1.1^2 - 1^2) * 2700 + 1^2 * 0.00001) / 1.1^2 = 468.595 \text{ kg/m}^3 \quad (6.23)$$

The average of the mass density across the thickness for sandwich panel:

$$\rho = \frac{1}{h} \sum_{k=1}^N \rho_k (h_k - h_{k-1}) = \frac{1}{0.05} (7800 \times 0.02 + 468.595 \times 0.03) = 3401.157 \text{ kg/m}^3 \quad (6.24)$$

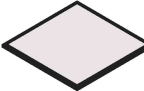
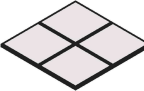
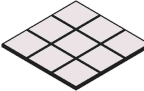
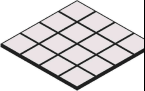
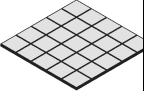

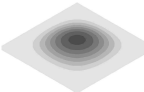
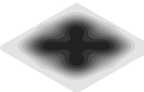
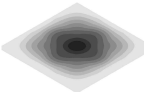
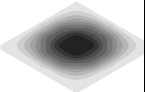
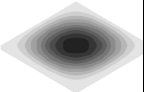
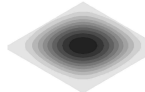
According to Eq.(6.10), the natural frequencies of sandwich panel with the homogenized core are obtained in Table 6.7.

Table 6.7 Natural frequencies with different values of m and n

m, n	$m=1$ $n=1$	$m=1$ $n=2$	$m=1$ $n=3$	$m=2$ $n=1$	$m=2$ $n=2$	$m=2$ $n=3$	$m=3$ $n=1$	$m=3$ $n=2$	$m=3$ $n=3$
Natural frequency	271.29	669.17	1308.9	669.17	1055.2	1677.6	1308.9	1677.6	2273.3

The finite element models of sandwich panels with the different sizes of square cores and the homogenized core are built and their first five orders of eigen-frequencies and vibration modes are calculated as seen in Table 6.8 to Table 6.12. The variation tendency of the first five orders of vibration frequencies with different size square cores is shown in Fig 6.8 to Fig.6.12.

Table 6.8 The first order vibration response with the different size square cores

Number of unit cell	1×1	2×2	3×3	4×4	5×5	Homogenized core
Different size cores						
Frequency	86.2326	217.753	255.191	272.099	280.880	294.799
Mode of sandwich panel						

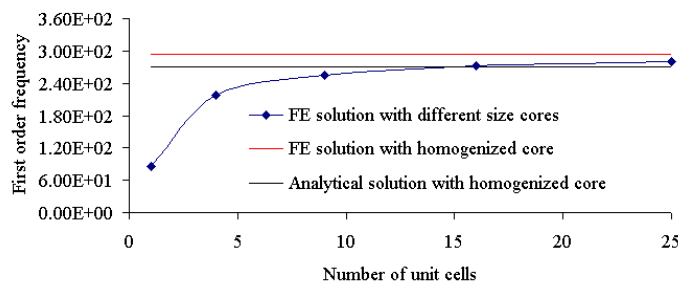
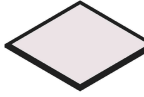
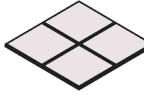
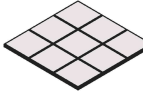
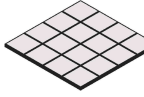
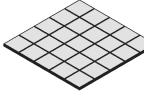

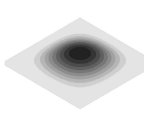
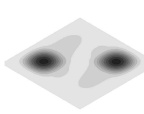
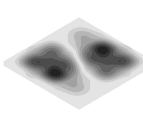
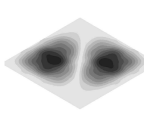
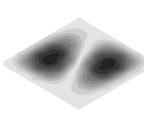
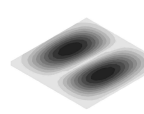


Fig.6.8 Frequency variation of first order vibration with different size square cores

Table 6.9 The second order vibration response with the different size square cores

Number of unit cell	1×1	2×2	3×3	4×4	5×5	Homogenized core
Different size cores						
Frequency	87.7724	309.870	447.477	497.928	523.819	563.427
Mode of sandwich panel						

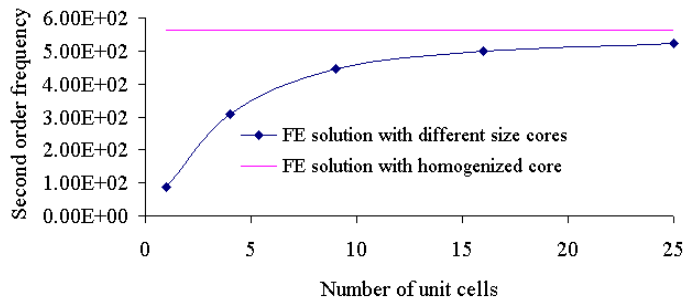
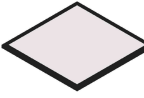
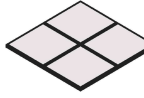
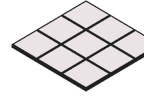
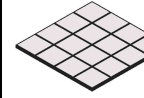
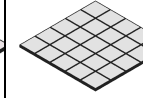

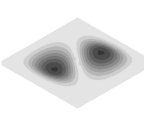
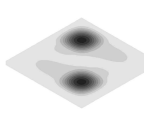
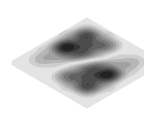
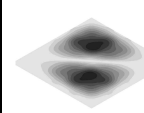
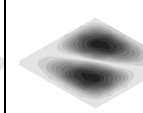
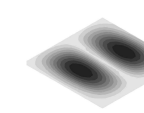


Fig.6.9 Frequency variation of second order vibration with different size square cores

Table 6.10 The third order vibration response with the different size square cores

Number of unit cell	1×1	2×2	3×3	4×4	5×5	Homogenized core
Different size cores						
Frequency	171.702	309.870	447.477	497.928	523.819	563.427
Mode of sandwich panel						

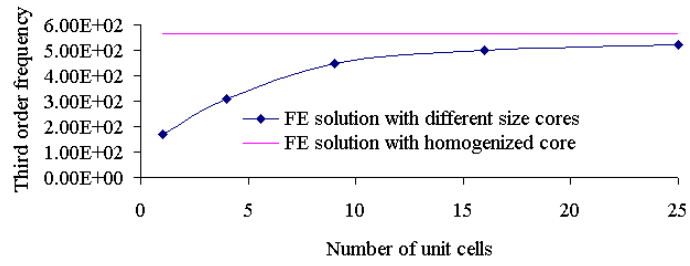
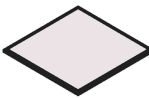
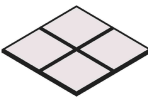
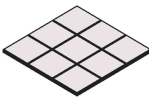

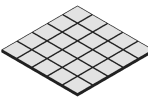

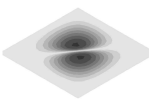
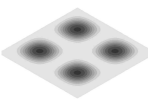
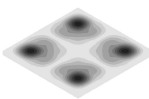
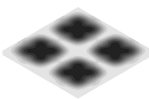
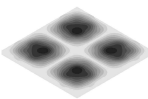
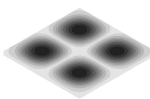


Fig.6.10 Frequency variation of third order vibration with different size square cores

Table 6.11 The fourth order vibration response with the different size square cores

Number of unit cell	1×1	2×2	3×3	4×4	5×5	Homogenized core
Different size cores						
Frequency	171.702	330.987	597.467	698.005	747.543	824.285
Mode of sandwich panel						

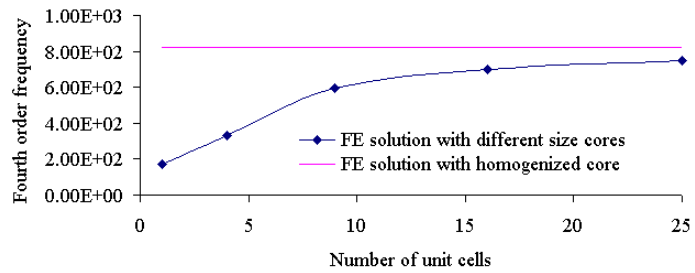
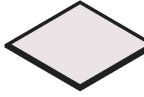
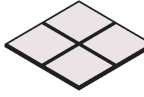
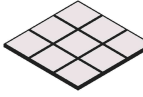
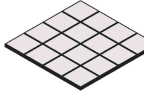
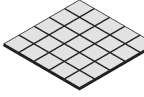

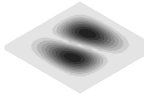
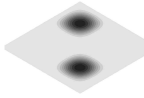
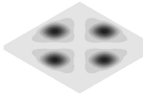
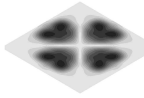
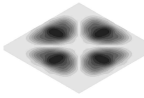
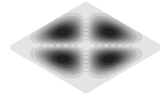


Fig.6.11 Frequency variation of fourth order vibration with different size square cores

Table 6.12 The fifth order vibration response with the different size square cores

Number of unit cell	1×1	2×2	3×3	4×4	5×5	Homogenized core
Different size cores						
Frequency	179.032	337.729	646.546	781.996	850.521	968.868
Mode of sandwich panel						

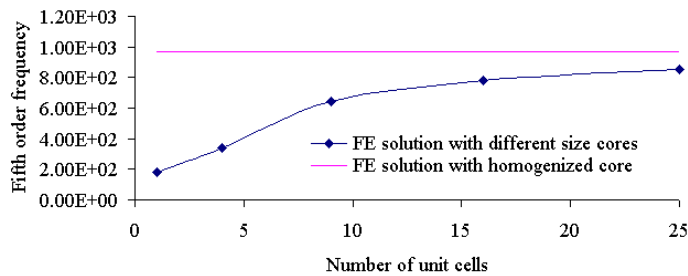


Fig.6.12 Frequency variation of fifth order vibration with different size square cores

6.2.4 Discussion

From Tables 6.2-6.6, Tables 6.8-6.12 and Fig.6.2-6.6, Fig.6.8-6.12 for two types of sandwich panels with hexagonal and square honeycomb cores, it is also demonstrated that the vibration frequencies and modes of sandwich panel tend to the limit values with the homogenized cores when increasing the number of unit cells or decreasing the size of unit cells. This fact can be easily explained. We can imagine that the material distributions are more and more homogeneous with the increasing number of unit cells under the same material amount and configurations of unit cells. Therefore the performance of sandwich panels for the free vibration is improved. In addition, the natural frequencies of sandwich panels are obtained with the laminated plate theory including the transverse shear deformation on the basis of the homogenized cores. The fundamental frequency occurs with $m=n=1$, which is for one half sine wave in each direction. Natural frequencies for the two sandwich panels are listed in Table 6.1 and Table 6.7 with the different m and n . Variation of m has greater influence on natural frequencies than n for sandwich panel with

the hexagonal core because m is the number of x axial half-waves corresponding to the short side. By observing the Fig.6.2 and Fig.6.8, the deviation between the analytical solution and the FE solution with homogenized square cores is less than with homogenized hexagonal cores. Similar to section 5.3.1, the ratio of the span dimensions to thickness ($\alpha = a/h$) is 17.73 for the hexagonal core which is less than for the square core ($\alpha = 22$). Therefore, the laminated plate theory for dynamic analysis is also more applicable to the thin plate.

6.3 Topology design of sandwich cores

6.3.1 Optimization model

The configurations of sandwich cores are designed by maximizing the first order eigen-frequency of the whole sandwich panel subjected to the volume constraint of sandwich cores. The upper and lower skins are considered as the non-designable domains. Similarly the variable linking method is adopted in order to ensure the periodicity of the optimal configuration of sandwich core in the designable domain. The detailed optimal model can be expressed as follows:

$$\begin{aligned}
 & \underset{x=\{x_1, x_2, \dots, x_n\}^T \in R^n}{Max} \quad \underset{k=1, \dots, 5}{Min} \quad \omega_k^2 \\
 & s.t. \quad (K - \omega_k^2 M)\phi_k = 0 \\
 & \quad \sum_{i=1}^n x_i v_i \leq f_v \cdot V_0 \\
 & \quad 0 < x_{\min} \leq x_i \leq 1 \\
 & \quad (i = 1, 2, \dots, n)
 \end{aligned} \tag{6.25}$$

where ω_k and ϕ_k are respectively the eigen-frequencies and eigen-modes of the sandwich panel. K and M are respectively the stiffness matrix and mass matrix of sandwich panel; $x_i (i = 1, 2, \dots, n)$ are the design variables which are the pseudo densities of each element in one unit cell of sandwich core; n is the number of finite elements in a single core unit cell and also the number of design variables; $x_{\min} = 10^{-3}$ is used to avoid the singularity during the optimal process; v_i is the volume of the i -th element in the core unit cell; f_v is the prescribed volume fraction; V_0 is the volume of the core unit cell.

6.3.2 Sensitivity analysis

Pedersen (Pedersen [2000]) pointed out that one of the main problems in the optimization

of eigen-frequencies using topology optimization is the occurrence of localized modes in low density areas and the author discussed several methods of avoiding localized modes. Here we choose an elastic modulus value for the void material $E_{\text{void}}=10^{-3}E_{\text{solid}}$. RAMP and SIMP interpolation models are used for the stiffness matrix and the mass matrix respectively.

$$K = \sum_{i=1}^n \left(10^{-3} + \frac{x_i}{1+p(1-x_i)} (1-10^{-3}) \right) K_{i0} \quad (6.26)$$

$$M = \sum_{i=1}^n x_i^q M_{i0} \quad (6.27)$$

where p and q are the penalization factors. In later examples $p=35$ and $q=1$ are used (Luo [2004]). According to the mass-to-stiffness ratio (Hansen [2005]), the problem of the localized modes in the low-density areas can be avoided.

The generalized eigenvalue problem can be cast in the form,

$$(K - \omega_j^2 M) \phi_j = 0 \quad (6.28)$$

By substituting Eq. (6.26) and Eq. (6.27) into Eq. (6.28) and differentiating Eq. (6.28), it follows that,

$$\frac{\partial}{\partial x_i} \left(\phi_j^T \left(\sum_{i=1}^n \left(10^{-3} + \frac{x_i}{1+p(1-x_i)} (1-10^{-3}) \right) K_{i0} - \omega_j^2 \sum_{i=1}^n \left(10^{-3} + \frac{x_i}{1+q(1-x_i)} (1-10^{-3}) \right) M_{i0} \right) \phi_j \right) = 0 \quad (6.29)$$

After the derivation, the sensitivity of the eigen-frequency squared is obtained,

$$\frac{\partial \omega_j^2}{\partial x_i} = \omega_j^2 (C_p * SER - C_q * KER) \quad (6.30)$$

In the sensitivity expression,

$$C_p = \frac{\left(\frac{(1+p)(1-10^{-3})}{(1+p(1-x_i))^2} \right)}{\left(10^{-3} + \frac{x_i}{1+p(1-x_i)} (1-10^{-3}) \right)} \quad (6.31)$$

$$C_q = \frac{q}{x_i} \quad (6.32)$$

$$SER = \frac{(\phi_j^t)^T K_i \phi_j^t}{\phi_j^T K \phi_j} \quad (6.33)$$

$$KER = \frac{(\phi_j^t)^T M_t \phi_j^t}{\phi_j^T M \phi_j} \quad (6.34)$$

where SEr represents the strain energy ratio of element t , and KER represents the kinetic energy ratio of element t . Filtering is used on the sensitivities of the optimization to prevent checkerboard patterns in the design. For the details on this filter, see Section 3.2 in Chapter 3 and the reference (Sigmund and Petersson [1998]).

6.3.3 Numerical examples

The structural configurations of the sandwich cores with different size are designed within a sandwich panel with four simply supported edges. The design model is shown as Fig. 6.13. The solid volume fractions of 10% and 30% for rectangular and square unit cells respectively are considered. In the designable domain, the sandwich cores are respectively divided into 1, 4, 9, 16 and 25 unit cells whose sizes are changed proportionally in the x and y directions.

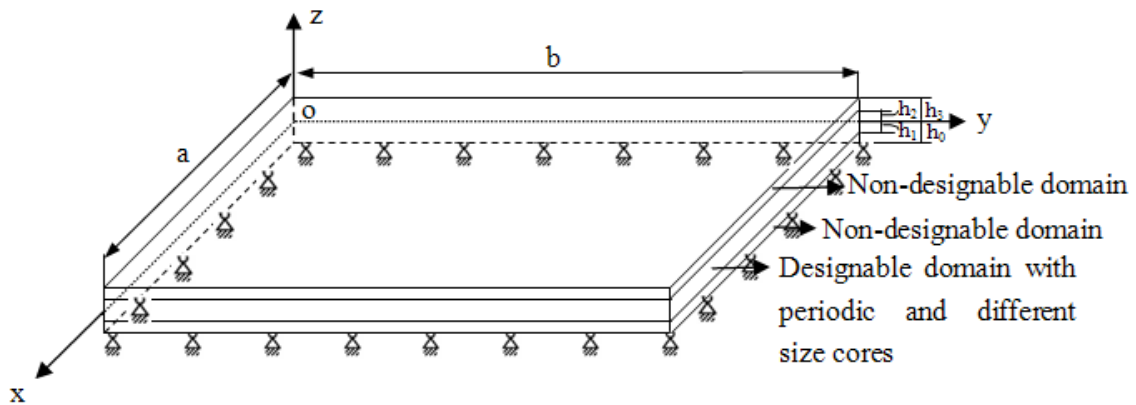


Fig.6.13 Design model of sandwich panel with four simply-supported edges

(1) For rectangular unit cells

The optimization configurations of sandwich cores are seen in Table 6.13 for 10% volume fraction and Table 6.14 for 30% volume fraction. Fig.6.14 gives the comparison of objective values with the different size cores.

Table 6.13 Optimal results of sandwich cores with different size unit cells and volume fraction 10% for rectangular unit cells

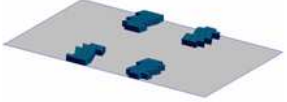
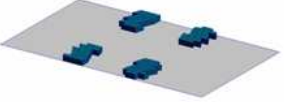
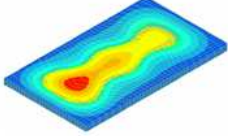
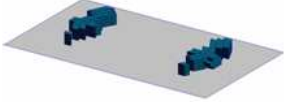
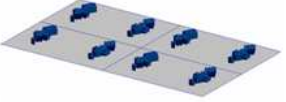
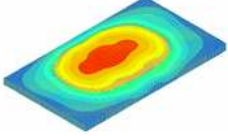
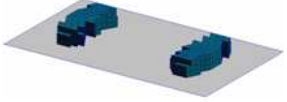
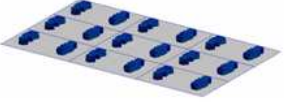
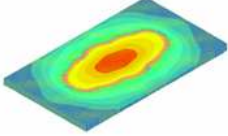
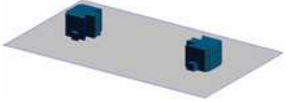
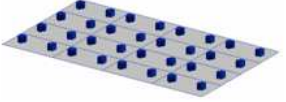
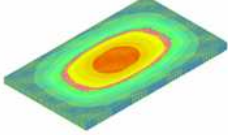
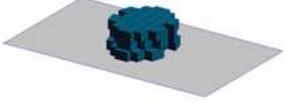
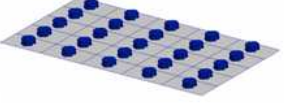
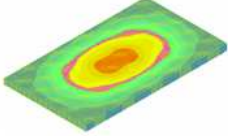
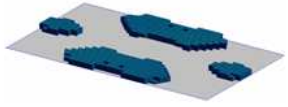

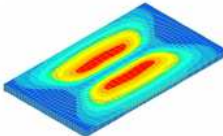
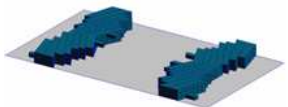

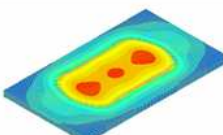
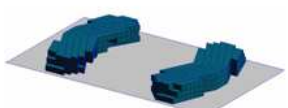
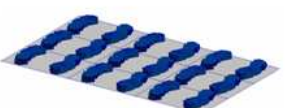
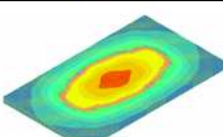
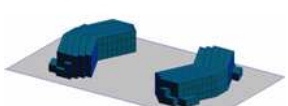

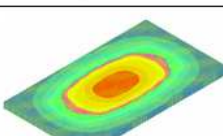


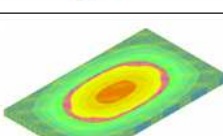
Number of unit cells	Unit cell	Sandwich cores	Natural frequency	Vibration mode of sandwich panel
1x1=1			21.95247	
2x2=4			18.69374	
3x3=9			21.9582	
4x4=16			21.1315	
5x5=25			23.48789	

Table 6.14 Optimal results of sandwich cores with different size unit cells and volume fraction 30% for rectangular unit cells

Number of unit cells	Unit cell	Sandwich cores	Natural frequency	Vibration mode of sandwich panel
1x1=1			32.5751	
2x2=4			31.1322	
3x3=9			32.5093	
4x4=16			33.8549	
5x5=25			33.6996	

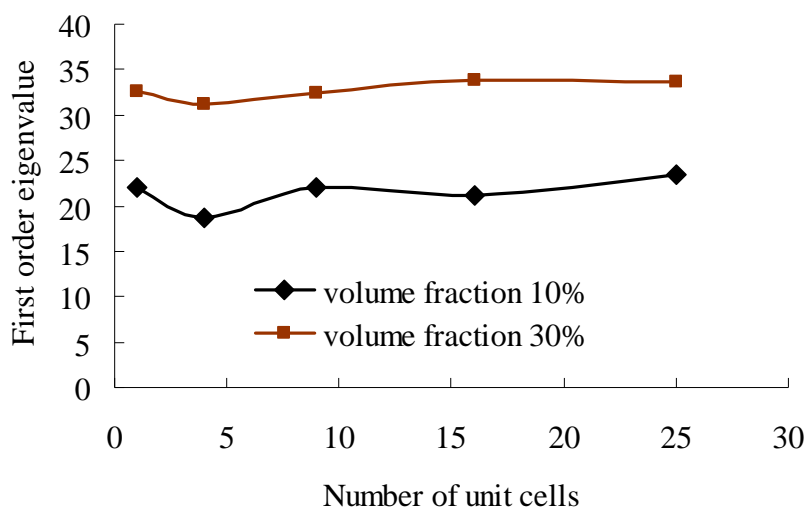


Fig.6.14 Objective values with the different size cores for rectangular unit cells

Table 6.13 and Table 6.14 show that the optimal configurations of unit cells are greatly influenced by the size variation. For the first case of 10% volume fraction, the material is mainly distributed along the x direction when the number of unit cells is 1, 4 and 9. Because of the decrease of the material amount and the size of unit cells, the material is concentrated together when the number of unit cells is 16 and 25. However for the second case of 30% volume fraction, the materials is mainly distributed along the y direction when the number of unit cells is 1. With the increasing number of unit cells, the material gradually goes along the x direction. This shows that the distribution trend of material is completely different because of the different amount of materials although they have the same size of unit cells.

(2) For square unit cells

The optimization configurations of sandwich cores are shown in Table 6.15 for 10% volume fraction and Table 6.16 for 30% volume fraction. Fig.6.15 gives the comparison of objective values with the different size cores.

Table 6.15 Optimal results of sandwich cores with different size unit cells and volume fraction 10% for square unit cells

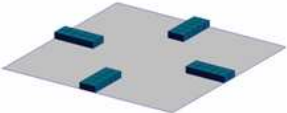
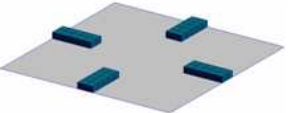
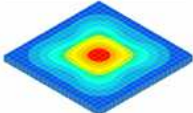
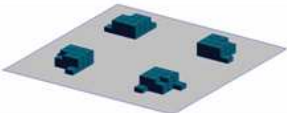
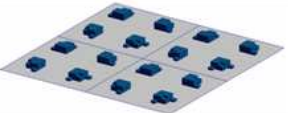
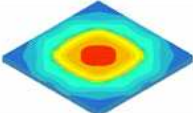
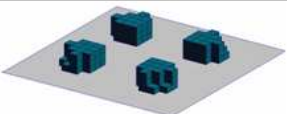
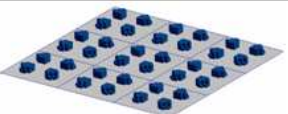
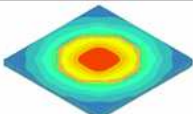
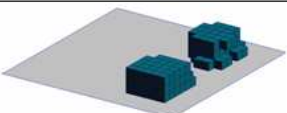
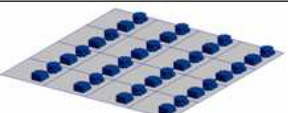
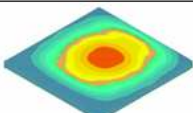
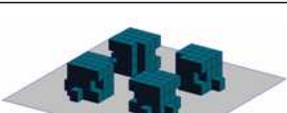

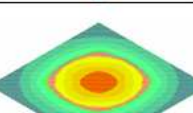
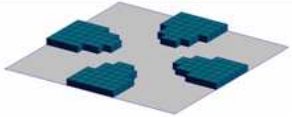
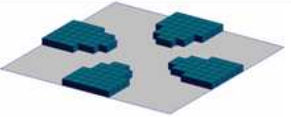
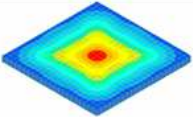
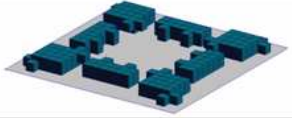
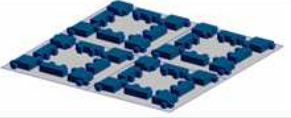
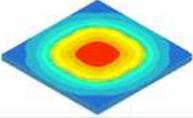
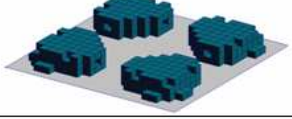

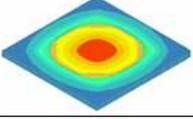
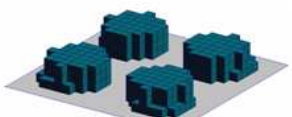

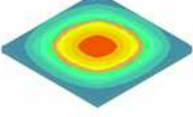
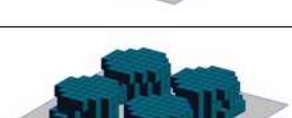

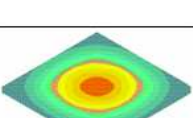
Number of unit cells	Unit cell	Sandwich cores	Natural frequency	Vibration mode of sandwich panel
1x1=1			21.631	
2x2=4			19.353	
3x3=9			21.615	
4x4=16			21.563	
5x5=25			29.569	

Table 6.16 Optimal results of sandwich cores with different size unit cells and volume fraction 30% for square unit cells

Number of unit cells	Unit cell	Sandwich cores	Natural frequency	Vibration mode of sandwich panel
1x1=1			33.0935	
2x2=4			29.9925	
3x3=9			29.8739	
4x4=16			31.52846	
5x5=25			31.59089	

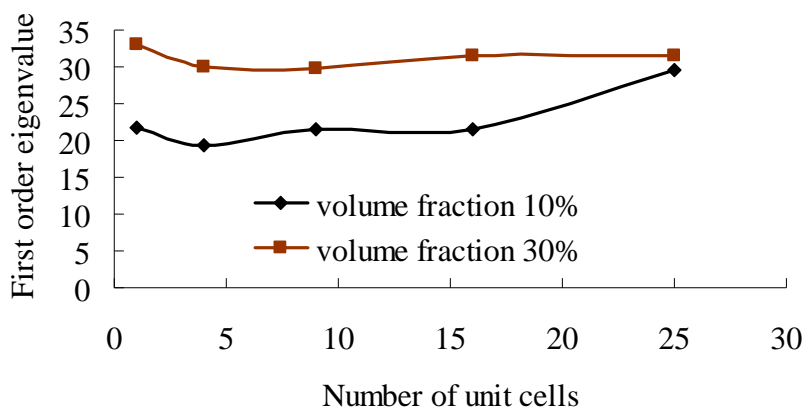


Fig.6.15 Objective values with the different size cores for square unit cells

Table 6.15 and Table 6.16 show that the optimal configurations of unit cells are obviously different with the size variation. However the material is mostly distributed at the four symmetrical places.

In Fig.6.14 and Fig.6.15, one can see that these two examples have a common point: the objective values are not monotonously changing with the increasing number of unit cells. Moreover both of them have the same trends for the same volume fraction with the increasing number of unit cells. We think that this coincidence is reasonable. In the following, we will analyze this phenomenon from two aspects. Firstly we have known from Fig.6.6 and Fig.6.8 and the analysis results in section 6.2 that the vibration frequencies of sandwich panel increase and tend to limit values of the homogenized cores with increasing the number of unit cells or decreasing the size of unit cells. Secondly when we reduce the number of unit cells or increase the size of unit cells, the design space becomes larger, so it is beneficial to the more efficient distribution of material in order to improve the vibration performance of sandwich panel. Therefore the first order eigen-value is greater when the number of unit cells equals one than when the number of unit cells equals 4, 9, 16 or 25. After the decreasing, some eigen-values start to rise and even exceed it with the creasing number of unit cells. So this coincidence is also the result of trade-off between the two aspects.

6.4 Summary

In this chapter, we firstly realized the free vibration analysis of simply supported sandwich panels with the different form and size cores. And then the configurations of sandwich cores were designed by topology optimization considering the in-plane size effect of sandwich cores. Conclusions can be drawn as follows from the dynamic point of view: (1) when decreasing the size of unit cells and increasing the number of unit cells, the dynamic response of the sandwich panel with different size cores tends to the one with homogenized cores. So the homogenization method is also valid in analyzing the dynamic response of sandwich panel when the number of core unit cells is large enough. (2) The size variation of unit cells greatly influences the optimal configuration of sandwich cores. In order to fully exert the function of sandwich panel with the given size cores, the innovative configuration of sandwich cores can be obtained by the topology optimization.

7. Conclusions and future works

In this chapter, we conclude our works and refer them to the goal of this thesis concerning the analysis and optimal design of lightweight sandwich structures and materials. The future works to be developed in this domain are also proposed and discussed.

7.1 Conclusions

In the introduction of this thesis, we stated our goal as follows:

- 1) To use the three-dimensional homogenization method to calculate effective properties of unit cells in multilayer structures and materials.
- 2) To use the superelement method in order to improve the computational efficiency in designs of periodic structures and materials.
- 3) To explore the size effect in static and dynamic response analysis and integrated designs of sandwich structures and materials.

To establish these goals, we first described, in Chapter 2, the homogenization method and its numerical application to calculate the effective elastic constants for 3D honeycomb cores. We compared the obtained results with other methods including the Gibson's formula and its modification as well as the energy method. Thus we confirmed the validity and accuracy of 3D homogenization method. The honeycomb sandwich is a kind of typical multiplayer structure. Based on the effective calculation of honeycomb core, we adopted the multi-step layered homogenization method to compute the effective properties of honeycomb sandwich structure. Fairly good agreement with the engineering empirical method shows that the multi-step layered homogenization is valid and adaptable for calculating the effective properties of multilayer structures and materials. Inspired by the calculation of effective properties of 3D honeycomb cores by the homogenization method, the prescribed properties for cellular materials and structures can be obtained by the inverse homogenization design.

In chapter 3, we applied the topology optimization technique and the homogenization method to design the 3D microstructures with the maximization of the stiffness and thermal conductivity. Optimal structural layouts of unit cells are obtained by the maximization of uniaxial and multiaxial stiffness and thermal conductivity that is considered as single and multiobjective optimization problems.

In chapter 4, we proposed an RVE-SE topology optimization procedure for the structural rigidity maximization of cellular solids. According to the periodic characteristics of RVEs in cellular solids, we used the superelement to model each RVE. The benefits of using the superelement method are: (1) the improvement of computation efficiency in the iteration process for the optimal design of periodic structures and materials; (2) the automatic implementation of mutual scale relation among the RVEs. Through several examples

including square, cyclic-symmetry, cyclic-symmetry with non-designable domain and cylindrical cellular solids, we developed the topology design method of various periodic cellular solids using the superelement technique. Besides, the comparisons of the equivalent torsional stiffness of the optimal cyclic-symmetry cellular solids reveal that the innovative configurations of the circular sandwich structure can be obtained for a better performance of torsional stiffness by means of the proposed design procedure.

In chapter 5 and chapter 6, we respectively analyzed bending response and dynamic response of sandwich panels and designed the core configurations considering the in-plane size variation of sandwich cores. From the analysis results, with decreasing the size of unit cells, the bending deformation and the dynamic response of the sandwich panel with different size cores tend to the ones with homogenized cores. For the static response, the total potential energy and maximum displacement of sandwich panels are reducing with increasing the number of unit cells or decreasing the size of unit cells as shown in Fig.5.4 and Fig.5.8. For the dynamic response, the first five orders of eigen-frequencies of sandwich panels are rising with increasing the number of unit cells or decreasing the size of unit cells as shown in Fig.6.2 to Fig.6.6 and from Fig.6.8 to Fig.6.12. This illustrates that the decrease of the size of unit cells or the increase of the number of unit cells can help to improve the structure behavior of sandwich panels. From the optimal results, the size variation of the unit cells influences the optimal configuration of sandwich cores. The objective function values are not monotonous with the increasing number of unit cells. From Fig.5.13 and Fig.5.14 for the stiffness maximization and Fig.6.14 and Fig.6.15 for the maximization of the first order vibration frequency, the size variation has a greater influence on the objective function values with 10% volume fraction than with 30% volume fraction. It is shown that the optimal results are influenced not only by the size of unit cells but also by the material amount. Moreover, in the topology optimization of sandwich cores under the bending response, the size of unit cells only varies in the x - y plane. However the load is along the z direction. So sometimes the size effect of unit cells on optimal results is not predominant. For the optimal design of sandwich cores considering the dynamic response, the size variation of unit cells brings two totally opposite effects on the optimal results. When decreasing the size of unit cells or increasing the number of unit cells, on the one hand the design space becomes smaller so that it is not beneficial to the more efficient distribution of material; on the other hand the material

distribution factitiously becomes more and more homogeneous. Therefore the optimal result is the trade-off between the two aspects.

To summarize, the major contributions of this thesis are the following:

- ✧ Proposing multi-step homogenization method for computing the equivalent properties of the three dimensional multi-layered sandwich structures.
- ✧ First application of the superelement method to design the configurations of representative volume elements for periodic cellular solids.
- ✧ Systematic study of the size effect on structural responses of honeycomb sandwich panels and the topology design of sandwich cores.

7.2 Future works

Based on the research works in this thesis, the scope of future developments is identified and recommended as follows:

(1) Microstructure design subject to local stress constraints

In our work, we implemented the microstructure design subject to the volume constraint on the base of the inverse homogenization. However, for structures built from materials with periodic microstructure it is necessary to consider strength, instability and vibration at the microscale level. That is to say, the local stress, critical load and vibration frequency constraints are added in the microstructure design besides the volume constraints. Some well-known scholars have attempted this aspect of research. Neves (Neves [2002]) carried out the topology optimization of periodic microstructures by maximizing a given linear combination of the homogenized elastic properties and introducing a lower bound on the local critical load value. In this research, it also may be concerned with the microstructure design to satisfy the macrostructure response subject to the local constraints at the microscale level.

(2) Improvement of computational efficiency in the multi-scale design of structures and materials

As we know, during the multi-scale design of structures and materials, the computational cost is very tremendous. In chapter 4, we made a simple attempt in this research by introducing the superelement method. In the future work, we can further study the application of superelement method in the multi-scale design of structures and materials with the periodicity to improve the computational efficiency.

(3) Size effect on buckling response of sandwich structures concerning the topology design of sandwich cores

The sandwich panels with periodic honeycomb cores are sensitive to local buckling effects under loading conditions such as direct compression, bending, or their combinations. Therefore, it is necessary to analyze the stability of sandwich panels with the different size cores concerning the static and dynamic analysis presented in chapter 5 and in chapter 6. The configurations of unit cells in sandwich cores considering the size effect can be designed by maximizing the buckling load under the given boundary conditions. Therefore we can reveal the importance of the influence of size variation of unit cells in sandwich cores on the topology design of unit cells and the structure responses of sandwich panels.

References

- [1] Allaire G., Jouve F., [2005]. A level-set method for vibration and multiple loads structural optimization. *Computer Methods in Applied Mechanics and Engineering*, 194:3269–3290.
- [2] Andrews E.W., Gioux G., Onck P., Gibson L.J., [2001]. Size effects in ductile cellular solids. Part II: experimental results. *International Journal of Mechanical Sciences*, 43:701–703.
- [3] Ashby M.F., Evans A.G., Fleck N.A., Hutchinson J.W., Gibson L.J., Wadley H. [2000]. *Metal foams-a design guide*, Vol 1, Butterworth-Heinemann (June), 0750672196.
- [4] Banerjee J.R., Cheung C.W., Morishima R., Perera M., Njuguna J., [2007]. Free vibration of a three-layered sandwich beam using the dynamic stiffness method and experiment. *International Journal of Solids and Structures*, 44:7543–7563.
- [5] Beckers M., [1999]. Topology optimization using a dual method with discrete variables. *Structural Optimization*, 17:14–24.
- [6] Beckers M., [2000]. Dual methods for discrete structural optimization problems. *International Journal for Numerical Methods in Engineering*, 48:1761–1784.
- [7] Bendsøe M.P., Kikuchi N., [1988]. Generating optimal topologies in structural design using a homogenization method. *Computer Methods in Applied Mechanics and Engineering*, 71:197–224.
- [8] Bendsøe M.P., [1989]. Optimal shape design as a material distribution problem. *Structural Optimization*, 1: 193–202.
- [9] Bendsøe M.P., Sigmund O., [1999]. Material interpolations in topology optimization. *Archives of Applied Mechanics*, 69:635-654.
- [10] Bendsøe M.P., Sigmund O., [2003]. *Topology Optimization: Theory, Methods and Applications*. Springer, Berlin.
- [11] Berger H., Kari S., Gabbert U., Rodriguez-Ramos R., Guinovart R., Otero J.A., Bravo-Castillero J., [2005]. An analytical and numerical approach for calculating effective material coefficients of piezoelectric fiber composites. *International Journal of Solids and Structures*, 42:5692–5714.

- [12] Besant T., Davies G.A.O., Hitchings D., [2001]. Finite element modeling of low velocity impact of composite sandwich panels. *Composites: Part A*, 32:1189–1196.
- [13] Birman V., [2004]. Dynamic wrinkling in sandwich beams. *Composites: Part B*, 35:665–672.
- [14] Borsellino C., Calabrese L., Valenza A., [2004]. Experimental and numerical evaluation of sandwich composite structures. *Composites Science and Technology*, 64:1709–1715.
- [15] Bruyneel M., Duysinx P., Fleury C., [2002]. A family of MMA approximations for structural optimization. *Structural and Multidisciplinary Optimization*, 24:263–276.
- [16] Buannic N., Cartraud P., Quesnel T., [2003]. Homogenization of corrugated core sandwich panels. *Composite Structures*, 59:299–312.
- [17] Burgueno R., Quagliata M.J., Mohanty A.K., Mehta G., Drzal L.T., Misra M., [2005]. Hierarchical cellular designs for load-bearing biocomposite beams and plates. *Materials Science and Engineering A*, 390:178–187.
- [18] Canfield S., Frecker M., [2000]. Topology optimization of compliant mechanical amplifiers for piezoelectric actuators. *Structural and Multidisciplinary Optimization*, 20:269–279.
- [19] Castanie B., Barrau J.J., Jaouen J.P., [2002]. Theoretical and experimental analysis of asymmetric sandwich structures. *Composite Structures*, 55:295–306.
- [20] Chang W.S., Ventsel E., Krauthammer T., John J., [2005]. Bending behavior of corrugated-core sandwich plates. *Composite Structures*, 70:81–89.
- [21] Chen C.P., Lakes R.S., [1989]. Dynamic wave dispersion and loss properties of conventional and negative Poisson's ratio polymeric cellular materials. *Cellular Polymers*, 8:343–369.
- [22] Chen C.P., Lakes R.S., [1996]. Micromechanical analysis of dynamic behavior of conventional and negative Poisson's ratio foams. *Journal of Engineering Materials and Technology (ASME)*, 118:285–288.
- [23] Choi J.B., Lakes R.S., [1992]. Nonlinear properties of metallic cellular materials with a negative Poisson's ratio. *Journal of Materials Science*, 27:5373–5381.
- [24] Cunningham P.R., White R.G., [2003a]. Dynamic response of doubly curved honeycomb sandwich panels to random acoustic excitation, Part 1: Experimental study. *Journal of Sound and vibration*, 264:579–603.

- [25] Cunningham P.R., Langley R.S., White R.G., [2003b]. Dynamic response of doubly curved honeycomb sandwich panels to random acoustic excitation, Part 2: Theoretical study. *Journal of Sound and vibration*, 264:605–637.
- [26] Dai G.M., Zhang W.H., [2008]. Size effects of basic cell in static analysis of sandwich beams. *International Journal of Solids and Structures*, 45:12512–2533.
- [27] Daniel I.M., Abot J.L., [2000]. Fabrication, testing and analysis of composite sandwich beams. *Composites Science and Technology*, 60:2455–2463.
- [28] De Boor R., [1998]. Theory of porous media—Past and present. *Z. Angew. Math. Mech*, 78:441–446.
- [29] Denli H., Sun J.Q., [2007]. Structural-acoustic optimization of sandwich structures with cellular cores for minimum sound radiation. *Journal of Sound and Vibration*, 301:93–105.
- [30] Di Sciuva M., Gherlone M., Lomario D., [2003]. Multiconstrained optimization of laminated and sandwich plates using evolutionary algorithms and higher-order plate theories, *Composite Structures*, 59:149–154.
- [31] Diaz A.R., Benard A., [2003]. Designing materials with prescribed elastic properties using polygonal cells. *International Journal for Numerical Methods in Engineering*, 57:301–314.
- [32] Duysinx P., [1996]. Layout optimization: a mathematical programming approach. LTAS-Report OA-41, University of Liege, Belgium.
- [33] Duysinx P., Bendsøe M.P., [1998]. Topology optimization of continuum structures with local stressconstraints. *International Journal for Numerical Method Engineering*, 43:1453-1478.
- [34] Duysinx P., Van Miegroet L., Lemaire E., Brüls O, Bruyneel M., [2007]. Topology and generalized shape optimization: Why stress constraints are so important? *International Workshop 2007: Advancements in Design Optimization of Materials, Structures and Mechanical Systems 17-20 December 2007 Xi'an, China*.
- [35] Eschenauer H.A., Kobelev V.V., Schumacher A., [1994]. Bubble method for topology and shape optimization of structures. *Structural Optimization*, 8:42–51.
- [36] Eschenauer H.A., Olhoff N., [2001]. Topology optimization of continuum structures: A review. *Applied Mechanics Reviews*, 54:331-390.
- [37] Evans A.G., Hutchinson J.W., Ashby M.F., [1999]. Multifunctionality of cellular

- metal systems. *Progress in Materials Science* 43:171–221.
- [38] Evans, A.G., Hutchinson, J.W., Fleck, N.A., Ashby, M.F., Wadley, H.N.G., [2001]. The Topological design of Multifunctional Cellular Metals. *Progress in Materials Science*, 46:309–327.
- [39] Fleury C., [1989]. Conlin: An efficient dual optimizer based on convex approximation concepts. *Structural and Multidisciplinary Optimization*, 1:81–89.
- [40] Frostig Y., Thomsen O.T., [2004]. High-order free vibration of sandwich panels with a flexible core. *International Journal of Solids and Structures*, 41:1697–1724.
- [41] Fu M.H., Yin J.R., [1999]. Equivalent elastic parameters of the honeycomb core. *ACTA MECHANICA SINICA*, 31:113–118.
- [42] Fujii D., Chen B.C., Kikuchi N., [2001]. Composites material design of two-dimensional structures using the homogenization method. *International Journal of Numerical Methods in Engineering*, 50: 2031–2051.
- [43] Fujii D., Kikuchi N., [2000]. Improvement of numerical instabilities in topology optimization using the SLP method. *Structural and Multidisciplinary Optimization*, 19:113–121.
- [44] Ghosh A.K., Biswal K.C., [1996]. Free-vibration analysis of stiffened laminated plates using higher-order shear deformation theory. *Finite Elements in Analysis and Design*, 22:143–161.
- [45] Gibiansky L.V., Sigmund O., [2000]. Multiphase composites with extremal bulk modulus. *Journal of the Mechanics and physics of solids*, 48:461–498.
- [46] Gibson L.J. [2005]. Biomechanics of cellular solids. *Journal of Biomechanics*, 38:377–399.
- [47] Gibson L.J., Ashby M.F., [1997]. *Cellular Solids: Structure and Properties*, 2nd edition, Cambridge University Press, Cambridge.
- [48] Gibson L.J., Ashby M.F., Schajer G.S., Robertson C.I., [1982]. The mechanics of two-dimensional cellular materials. *Proceedings of the Royal Society of London. Series A, Mathematical and Physical Sciences*, 382:25–42.
- [49] Glenn C.E., Hyer M.W., [2005]. Bending behavior of low-cost sandwich plates, *Composites: Part A*, 36:1449–1465.
- [50] Grenestedt J.L., [1998]. Influence of wavy imperfections in cell walls on elastic stiffness of cellular solids. *Journal of the Mechanics and Physics of Solids*, Vol. 46,

- No. 1: 29–50.
- [51] Grenestedt J.L., [1999a]. Influence of cell shape variations on elastic stiffness of closed cell cellular solids. *Scripta Materialia*, Vol. 40, No. 1: 71–77.
- [52] Grenestedt J.L., [1999b]. Effective elastic behavior of some models for ‘perfect’ cellular solids. *International Journal of Solids and Structures*, 36:1471–1501.
- [53] Grenestedt J.L., Reany J., [2007]. Wrinkling of corrugated skin sandwich panels. *Composites: Part A*, 38:576–589.
- [54] Guedes J.M., Kikuchi N., [1990]. Preprocessing and postprocessing for materials based on the homogenization method with adaptive finite element methods. *Computer Methods in Applied Mechanics and Engineering*, 83:143–198.
- [55] Guest J.K., Prevost J.H., [2006]. Optimizing multifunctional materials: Design of microstructures for maximized stiffness and fluid permeability. *International Journal of Solids and Structures*, 43:7028–7047.
- [56] Guest J.K., Prevost J.H., [2007]. Design of maximum permeability material structures. *Computer Methods in Applied Mechanics and Engineering*, 196:1006–1017.
- [57] Haber R.B., Jog C.S., Bendsøe M.P., [1994]. Variable-topology shape optimization with a control on perimeter, In: *Advances in Design Automation*, 69:261–272.
- [58] Haber R.B., Jog C.S., Bendsøe M.P. [1996]. A new approach to variable-topology design using a constraint on the perimeter. *Structural Optimization*, 11:1–12.
- [59] Hansen L.V., [2005]. Topology optimization of free vibrations of fiber laser packages. *Structural and Multidisciplinary Optimization*, 29:341–348.
- [60] Hassani B., [1996]. A direct method to derive the boundary conditions of the homogenization equation for symmetric cells. *Communications in Numerical in Engineering*, 12:185–196.
- [61] Hassani B., Hinton E., [1998a]. A review of homogenization and topology optimization I—Homogenization theory for media with periodic structure. *Computers and Structures*, 69:707–718.
- [62] Hassani B., Hinton E., [1998b]. A review of homogenization and topology optimization—Analytical and numerical solution of homogenization equations. *Computers and Structures*, 69:719–738.
- [63] Hassani B., Hinton E., [1998c]. A review of homogenization and topology

- optimization III—Topology optimization using optimality criteria. *Computers and Structures*, 69:739–756.
- [64] Hohe J., [2003]. A direct homogenization approach for determination of the stiffness matrix for microheterogeneous plates with application to sandwich panels. *Composites: Part B*, 34:615–626.
- [65] Hohe J., Becker W., [2000]. A mechanical model for two-dimensional cellular sandwich cores with general geometry. *Computational Materials Science*, 19:108–115.
- [66] Hohe J., Becker W., [2001a]. A refined analysis of the effective elasticity tensor for general cellular sandwich cores. *International Journal of Solids and Structures*, 38:3689–3717.
- [67] Hohe J., Becker W., [2001b]. An energetic homogenization procedure for the elastic properties of general cellular sandwich cores. *Composites: Part B*, 32:185–197.
- [68] Hori M., Nemat-Nasser S., [1999]. On two micromechanics theories for determining micro-macro relation in heterogeneous solids. *Mechanics of Materials*, 31:667–682.
- [69] Huang J.S., Chang F.M., [2005]. Effects of curved cell edges on the stiffness and strength of two-dimensional cellular solids. *Composite Structures*, 69:183–191.
- [70] Hutchinson J.W., He M.Y., [2000]. Buckling of cylindrical sandwich shells with metal foam cores. *International Journal of Solids and Structures*, 37:6777-6794.
- [71] Jakiela M.J., Chapman C., Duda J., Adewuya A., Saitou K., [2000]. Continuum structural topology design with genetic algorithms. *Computer Methods in Applied Mechanics and Engineering*, 186:339–356.
- [72] Jog C.S., [2002]. Topology design of structures using a dual algorithm and a constraint on the perimeter. *International journal for numerical methods in engineering*, 54:1007–1019.
- [73] Jung D., Gea H.C., [2004]. Design of negative Poisson's ratio materials using topology optimization. AIAA-2004-1969.
- [74] Kalamkarov A.L., Saha G.C., Georgiades A.V., [2007]. General micromechanical modeling of smart composite shells with application to smart honeycomb sandwich structures. *Composites: Part A*, 38:1533–1546.
- [75] Kam T.Y., Lai F.M., Chao T.M., [1999]. Optimum design of laminated composite foam-filled sandwich plates subjected to strength constraint. *International Journal of*

- Solids and Structures, 25:2865–2889.
- [76] Kamat M.P., [1993]. Structural optimization: Status and promise. Vol.150 Progress in Astronautics and aeronautics, published by American Institute of Astronautics and aeronautics, Inc., Washington DC.
- [77] Kikuchi N., Nishiwaki S., Ono Fonseca J.S., Nelli Silva E.C., [1998]. Design optimization method for compliant mechanisms and material microstructure. Computer Methods in Applied Mechanics and Engineering, 151:401–417.
- [78] Kim H., Querin O.M., Steven G.P., [2002]. On the development of structural optimisation and its relevance in engineering design. Design Studies, 23:85–102.
- [79] Kim H.S., Al-Hassani S.T.S, [2003]. Effective elastic constants of two-dimensional cellular materials with deep and thick cell walls. International Journal of Mechanical Sciences, 45:1999–2016.
- [80] Kim J.S., [2007]. Free vibration of laminated and sandwich plates using enhanced plate theories. Journal of Sound and Vibration, 308:268–286.
- [81] Kita E., Tanie H., [1999]. Topology and shape optimization of continuum structures using GA and BEM. Structural Optimization, 17:130–139.
- [82] Koissin V., Skvortsov V., Krahmalev S., Shilpsha A., [2004]. The elastic response of sandwich structures to local loading. Composite Structures 63:375–385.
- [83] Krog L.A., Olhoff N., [1999]. Optimum topology and reinforcement design of disk and plate structures with multiple stiffness and eigenfrequency objectives. Computers and Structures, 72:535–563.
- [84] Kruijff N., Zhou S., Li Q., Mai Y.W., [2007]. Topological design of structures and composite materials with multiobjectives. International Journal of Solids and Structures 44:7092–7109.
- [85] Lakes R., [1987]. Foam structures with negative Poisson's ratio. Science, 235:1038.
- [86] Lakes R.S., [1991]. Experimental micro mechanics methods for conventional and negative Poisson's ratio cellular solids as Cosserat continua. Journal of Engineering Materials and Technology, 113:148–155.
- [87] Lakes R., [1993]. Materials with structural hierarchy. Nature, 361:511–515.
- [88] Lakes R., [1996]. Cellular solid structures with unbounded thermal expansion. Journal of Materials Science Letters, 15:475–477.
- [89] Lakes R., [2001]. A broader view of membranes. Nature, 414, 29 November.

- [90] Lakes R., [2007]. Cellular solids with tunable positive or negative thermal expansion of unbounded magnitude. *Applied Physics Letters*, 90, 221905.
- [91] Lakes R.S., Witt R., [2002]. Making and characterizing negative Poisson's ratio materials. *International Journal of Mechanical Engineering Education*, 30:50–58.
- [92] Laschet G., [2002]. Homogenization of the thermal properties of transpiration cooled multi-layer plates. *Computer Methods in Applied Mechanics and Engineering*, 191: 4535–4554.
- [93] Li K., Gao X.L., Subhash G., [2005]. Effects of cell shape and cell wall thickness variations on the elastic properties of two-dimensional cellular solids. *International Journal of Solids and Structures*, 42:1777–1795.
- [94] Liu J.S., Parks G.T., Clarkson P.J., [2000]. Metamorphic development: A new topology optimization method for continuum structures. *Structural and Multidisciplinary Optimization*, 20:288–300.
- [95] Liu T., Deng Z.C., Lu T.J., [2006]. Design optimization of truss-cored sandwiches with homogenization. *International Journal of Solids and Structures*, 43:7891–7918.
- [96] Liu T., Deng Z.C., Lu T.J., [2007]. Minimum weights of pressurized hollow sandwich cylinders with ultralight cellular cores. *International Journal of Solids and Structures*, 44:3231–3266.
- [97] Lukkassen D., Meidell A., [2003]. *Advanced materials and structures and their fabrication processes*, Third edition, Narvik University College, HiN, October 13.
- [98] Luo Z., Chen L.P., Huang Y.Y., Zhang Y.Q., [2004]. Topological optimization design for continuum structures. *Advances in Mechanics*, 34:463–476.
- [99] Mai S.P., Fleck N.A., Lu T.J., [2007]. Optimal design of box-section sandwich beams in three-point bending. *International Journal of Solids and Structures*, 44:4742–4769.
- [100] Mamalis A.G., Spentzas K.N., Pantelelis N.G., Manolakos D.E., Ioannidis M.B., [2008]. A new hybrid concept for sandwich structures. *Composite Structure*, 83:335–340.
- [101] Meo M., Vignjevic R., Marengo G., [2005]. The response of honeycomb sandwich panels under low-velocity impact loading. *International Journal of Mechanical Sciences*, 47:1301–1325.
- [102] Meraghni F., Desrumaux F., Benzeggagh M.L., [1999]. Mechanical behavior of

- cellular core for structural sandwich panels. *Composites: Part A*, 30: 767–779.
- [103] Meunier M., Shenoi R.A., [1999]. Free vibration analysis of composite sandwich plates. *Proceedings of the Institution of Mechanical Engineers: Part C*, 213:715–727.
- [104] Min S., Nishiwaki S., Kikuchi N., [2000]. Unified topology design of static and vibrating structures using multiobjective optimization. *Computers and Structures*, 75:93–116.
- [105] Nakanishi Y., [2001]. Application of homology theory to topology optimization of three-dimensional structures using genetic algorithm. *Computer Methods in Applied Mechanics and Engineering*, 190(29):3849–3863.
- [106] Navarrina F., Muinos I., Colominas I., Casteleiro M., [2005]. Topology optimization of structures: A minimum weight approach with stress constraints. *Advances in Engineering Software*, 36:599–606.
- [107] Nayak A.K., Moy S.S.J., Shenoi R.A., [2002]. Free vibration analysis of composite sandwich plates based on Reddy's higher-order theory. *Composites: Part B*, 33: 505–519.
- [108] Nelli Silva E.C., Nishiwaki S., Ono Fonseca J.S., Kikuchi N., [1999]. Optimization methods applied to material and flextensional actuator design using the homogenization method. *Computer Methods in Applied Mechanics and Engineering*, 172:241–271.
- [109] Nelli Silva E.C., Ono Fonseca J.S., Kikuchi N., [1998]. Optimal design of periodic piezocomposites. *Computer Methods in Applied Mechanics and Engineering*, 159:49–77.
- [110] Neves M.M., Rodrigues H., Guedes J.M., [2000]. Optimal design of periodic linear elastic microstructures. *Computers and Structures*, 76:421–429.
- [111] Neves M.M., Sigmund O., Bendsøe M.P., [2002]. Topology optimization of periodic microstructures with a penalization of highly localized buckling modes. *International Journal for Numerical Methods in Engineering*, 54:809–834.
- [112] Olhoff N., Rønholt E., Scheel J., [1998]. Topology optimization of plate-like structures using 3D elasticity and optimum 3D microstructures. *AIAA-98-4947*:1853–1863.
- [113] Onck P.R., Andrews E.W., Gibson L.J., [2001]. Size effects in ductile cellular solids. Part I: modeling. *International Journal of Mechanical Sciences*, 43:681–699.

- [114] Paik J.K., Thayamballi, A.K. Kim G.S., [1999]. The strength characteristics of aluminum honeycomb sandwich panels. *Thin-Walled Structures*, 35:205–231.
- [115] Pan L., Du H.J., [2000]. Structural topology optimization for dynamics performance using SQP method. *AIAA-2000-4736*:1–10.
- [116] Pedersen N.L., [2000]. Maximization of eigenvalues using topology optimization. *Structural and Multidisciplinary Optimization*, 20:2–11.
- [117] Pedersen N.L., [2002]. Topology optimization of laminated plates with prestress. *Computers and Structures*, 80:559–570.
- [118] Peng X.Q., Cao J., [2002]. A dual homogenization and finite element approach for material characterization of textile composites. *Composites: Part B*, 33:45–56.
- [119] Petersson J., Sigmund O. [1998]. Slope constrained topology optimization. *International Journal for Numerical Methods in Engineering*, 41:1417–1434.
- [120] Petersson J., [1999]. Some convergence results in perimeter-controlled topology optimization. *Computer Methods in Applied Mechanics and Engineering*, 171:123–140.
- [121] Petras A., Sutcliffe M.P.F., [1999]. Failure mode maps for honeycomb sandwich panels. *Composite Structures*, 44:237–252.
- [122] Pokharel N., Mahendran M., [2004]. Finite element analysis and design of sandwich panels subject to local buckling effects. *Thin-Walled Structures*, 42:589–611.
- [123] Poulsen T.A., [2003]. A new scheme for imposing a minimum length scale in topology optimization. *International Journal for Numerical Methods in Engineering*, 57:741–760.
- [124] Prusty B.G., Satsangi S.K., [2001]. Finite element transient dynamic analysis of laminated stiffened shells. *Journal of Sound and Vibration*, 2:215–233.
- [125] Qatu M.S., [2002]. Recent research advances in the dynamic behavior of shells: 1989-2000, Part 1: Laminated composite shells. *Applied Mechanics Review*, 55: 325–350.
- [126] Querin O.M., Steven G.P., Xie Y.M., [1998]. Evolutionary structural optimization (ESO) using a bidirectional algorithm. *Engineering Computations*, 15:1031–1048.
- [127] Rabczuk T., Kim J.Y., Samaniego E., Belytschko T., [2004]. Homogenization of sandwich structures. *International Journal for Numerical Methods in Engineering*, 61:1009–1027.

- [128] Rao M.K., Desai Y.M., [2004]. Analytical solutions for vibrations of laminated and sandwich plates using mixed theory. *Composite Structures*, 63: 361–373.
- [129] Reddy J.N., [1984]. *Energy and variational methods in applied mechanics*. A Wiley-Interscience publication.
- [130] Rietz A., [2001]. Sufficiency of a finite exponent in SIMP (power law) methods. *Structural and Multidisciplinary Optimization*, 21:159–163.
- [131] Rodrigues H., Guedes J.M., Bendsøe M.P., [2002]. Hierarchical optimization of material and structure. *Structural and Multidisciplinary Optimization*, 24:1–10.
- [132] Romanoff J., Varsta P., [2007]. Bending response of web-core sandwich plates. *Composite Structures*, 81:292–302.
- [133] Rozvany G.I.N., Bendsøe M.P., Kirsch U., [1995]. Layout optimization of structures. *Applied Mechanics Reviews*, 48:41–119.
- [134] Rozvany G.I.N., Zhou M., Birker T., [1992]. Generalized shape optimization without homogenization. *Structural Optimization*, 4:250–252.
- [135] Saha G.C., Kalamkarov A.L., Georgiades A.V., [2007a]. Effective elastic characteristics of honeycomb sandwich composite shells made of generally orthotropic materials. *Composites: Part A*, 80:1533–1546.
- [136] Saha G.C., Kalamkarov A.L., Georgiades A.V., [2007b]. Asymptotic homogenization modeling and analysis of effective properties of smart composite reinforced and sandwich shells. *International Journal of Mechanical Sciences*, 49:138–150.
- [137] Sanchez-Palencia E., [1980]. *Non-homogeneous Media and Vibration Theory*. Lecture Notes in Physics, vol. 127. Springer-Verlag, Berlin.
- [138] Sigmund O., [1994]. Materials with prescribed constitutive parameters: An inverse homogenization problem. *International Journal of Solids and Structures*, 31:2313–2329.
- [139] Sigmund O., [1995]. Tailoring materials with prescribed elastic properties. *Mechanics of Materials*, 20:351–368.
- [140] Sigmund O., [2001]. A 99 line topology optimization code written in Matlab. *Structural and Multidisciplinary Optimization*, 21:120–127.
- [141] Sigmund O., [2001a]. Design of multiphysics actuators using topology optimization – Part I: One-material structures. *Computer Methods in Applied Mechanics and*

- Engineering, 190:6577–6604.
- [142] Sigmund O., [2001b]. Design of multiphysics actuators using topology optimization – Part II: Two-material structures. *Computer Methods in Applied Mechanics and Engineering*, 190:6605–6627.
- [143] Sigmund O., Petersson J., [1998]. Numerical instabilities in topology optimization: A survey on procedures dealing with checkerboards, mesh-dependencies and local minima. *Structural Optimization*, 16:68–75.
- [144] Sigmund O., Torquato S., [1997]. Design of materials with extreme thermal expansion using a three-phase topology optimization method. *Journal of the Mechanics and physics of solids*, 45:1037–1067.
- [145] Sigmund O., [2000]. A new class of Extremal Composites. *Journal of the Mechanics and Physics of Solids*, 48:397–428.
- [146] Soto C.A., [2000]. Simultaneous design of structural topology and material properties. AIAA-2000-4913:1–9.
- [147] Styles M., Compston P., Kalyanasundaram S., [2007]. The effect of core thickness on the flexural behaviour of aluminium foam sandwich structures. *Composite Structures*, 80:532–538.
- [148] Stolpe M., Svanberg K., [2001]. An alternative interpolation scheme for minimum compliance topology optimization. *Structural and Multidisciplinary Optimization*, 22:116–124.
- [149] Sun S.P., [2006]. Investigation on the key Theory and Methods of Topology Optimization of Materials and Structures. PhD thesis, Northwestern Polytechnical University.
- [150] Takano N., Zako M., [2000]. Integrated design of graded microstructures of heterogeneous materials. *Archive of Applied Mechanics*, 70:585–596.
- [151] Tan X.H., Soh A.K., [2007]. Multi-objective optimization of the sandwich panels with prismatic cores using genetic algorithms. *International Journal of Solids and Structures*, 44:5466–5480.
- [152] Tanov R., [2000]. A contribution to the finite element formulation for the analysis of composite sandwich shells. PhD thesis, University of Cincinnati.
- [153] Tekoğlu C., [2007]. Size effects in cellular solids. PhD thesis, University of Groningen.

- [154] Tekoglu C., Onck P.R., [2005]. Size effects in the mechanical behavior of cellular materials. *Journal of Materials Science*, 40:5911–5917.
- [155] Thamburaj P., Sun J.Q., [2002]. Optimization of anisotropic sandwich beams for higher sound transmission loss. *Journal of Sound and vibration*, 254:23–36.
- [156] Tian Y.S., Lu T.J., [2005]. Optimal design of compression corrugated panels. *Thin-Walled Structures*, 43:477–498.
- [157] Valdevit L., Wei Z., Mercer C., Zok F.W., Evans A.G., [2006]. Structural performance of near-optimal sandwich panels with corrugated cores. *International Journal of Solids and Structures*, 43:4888–4905.
- [158] Vinson J.R., Sierakowski R.L., [1987]. *The behavior of structure composed of composite materials*. Martinus Nijhoff Publishers.
- [159] Wang A.J., McDowell D.L., [2003]. Optimization of a metal honeycomb sandwich beam-bar subjected to torsion and bending. *International Journal of Solids and Structures*, 40:2085–2099.
- [160] Wang B., Yang M., [2000]. Damping of honeycomb sandwich beams. *Journal of Materials Processing Technology*, 105:67–72.
- [161] Wang M.Y., Wang X.M., Guo D.M., [2003]. A level set method for structural topology optimization. *Computer Methods in Applied Mechanics and Engineering*, 192:227–246
- [162] Wen T., Xu F., Lu T.J., [2007]. Structural optimization of two-dimensional cellular metals cooled by forced convection. *International Journal of Heat and Mass Transfer*, 50:2590–2604.
- [163] Wicks N., Hutchinson J.W., [2004]. Performance of sandwich plates with truss cores. *Mechanics of Materials*, 36:739–751.
- [164] Wo D.Z., [2000]. *A Complete Collection of Composites*. Beijing: Chemical Industry Press.
- [165] Xia Q., Wang M.Y., [2008]. Simultaneous Optimization of Material Property and Topology of Functionally Graded Structures. *Computer-Aided Design (2008)*, doi:10.1016/j.cad.2008.01.014.
- [166] Xu X.F., Qiao P.Zh., [2002]. Homogenized elastic properties of honeycomb sandwich with skin effect. *International Journal of Solids and Structures*, 39:2153–2188.
- [167] Xue Z., Hutchinson J.W., [2004]. Constitutive model for quasi-static deformation of

- metallic sandwich cores. *International Journal for Numerical Methods in Engineering*, 61:2205–2238.
- [168] Yang R. J., Lu C. M., [1996]. Topology optimization with superelements. *AIAA Journal*, 34(7):1533–1535.
- [169] Yi Y.M., Park S.H., Youn S.K., [2000]. Design of microstructures of viscoelastic composites for optimal damping characteristics. *International Journal of Solids and Structures*, 37:4791–4810.
- [170] Yin L.Z., Ananthasuresh G.K., [2002]. A novel topology design scheme for the multi-physics problems of electro-thermally actuated compliant micromechanisms. *Sensors and Actuators*, A97-98:599–609.
- [171] Yoo J., Hong H., [2004]. A modified density approach for topology optimization in magnetic fields. *International Journal of Solids and Structures*, 41:2461–2477.
- [172] Yoon G.H., Heo S., Kim Y.Y., [2005]. Minimum thickness control at various levels for topology optimization using the wavelet method. *International Journal of Solids and Structures*, 42:5945–5970.
- [173] Young V., Querin O.M., Steven G.P., Xie Y.M., [1999]. 3D and multiple load case bi-directional evolutionary structural optimization (BESO). *Structural Optimization*, 18:183–192.
- [174] Yu J.L., Li J.R., Hu S.S., [2006]. Strain-rate effect and micro-structural optimization of cellular metals. *Mechanics of Materials*, 38:160–170.
- [175] Yuan W.X., Dawe D.J., [2002]. Free vibration of sandwich plates with laminated faces. *International Journal for Numerical Methods in Engineering*, 54:195–217.
- [176] Yuan W.X., Dawe D.J., [2004]. Free vibration and stability analysis of stiffened sandwich plates. *Composite Structures*, 63: 123–137.
- [177] Zenkour A.M., [2005a]. A comprehensive analysis of functionally graded sandwich plates: Part 1–Deflection and stresses. *International Journal of Solids and Structures*, 43:5224–5242.
- [178] Zenkour A.M., [2005b]. A comprehensive analysis of functionally graded sandwich plates: Part 2–Buckling and free vibration. *International Journal of Solids and Structures*, 43:5243–5258.
- [179] Zhang W.H., [2003]. A compromise programming method using multibounds formulation and dual approach for multicriteria structural optimization. *International*

- Journal for Numerical Methods in Engineering, 58:661–678.
- [180]Zhang W.H., Duysinx P., [2003]. Dual approach using a variant perimeter constraint and efficient sub-iteration scheme for topology optimization. *Computers and structures*, 81:2173–2181.
- [181]Zhang W.H., Fleury C. [1997]. A modification of convex approximation methods for structural optimization. *Computers & Structures*, 64:89–95.
- [182]Zhang W.H., Sun S.P., [2006]. Scale-related topology optimization of cellular materials and structures. *International Journal for Numerical Methods in Engineering*, 68:993–1011.
- [183]Zhang W.H., Wang F.W, Dai G.M., Sun S.P., [2007]. Topology Optimal Design of Material Microstructures Using Strain Energy-based Method. *Chinese Journal of Aeronautics*, 20:321–328.
- [184]Zhou M., Shyy Y.K., Thomas H.L., [2001]. Checkerboard and minimum member size control in topology optimization. *Structural and Multidisciplinary Optimization*, 21:152–158.
- [185]Zhou M., [2004]. Topology Optimization for Shell Structures with Linear Buckling Responses. *Computational Mechanics, WCCM VI in conjunction with APCOM'04*, Sept. 5–10, 2004, Beijing, China.
- [186]Zhu H., Sankar B.V., [2007]. Analysis of sandwich TPS panel with functionally graded foam core by Galerkin method. *Composite Structures*, 77:280–287.
- [187]Zok F.W., Rathbun H.J., Wei Z., Evans A.G., [2003]. Design of metallic textile core sandwich panels. *International Journal of Solids and Structures*, 40:5707–5722.

Acknowledgements

Firstly, I want to thank Sino-French doctoral college and China Scholarship Council for the financial support during the study in France.

Next, I am most grateful to my supervisors, Professor Matthieu DOMASZEWSKI and Professor Weihong ZHANG, for their guidance, patience, encouragement and support throughout my doctoral program of study.

Then, I specially thank Professor Pierre DUYSINX for his kind support and help in finishing this thesis and the defense.

I would like to thank Dr. Dominique CHAMORET for her careful modifications and good suggestions to this thesis.

I would also like to thank Professor Yingqiao GUO and Professor Xiaolu GONG for the time they spent on reading and evaluating my thesis.

I also wish to thank staff of M3M in UTBM and Sino-French Laboratory of Concurrent Engineering in NWPU for their beneficial discussion and help.

Finally, but certainly not least, I sincerely appreciate my family for their endless love and support at all stage of my life.